(12)

FLIGHT MODEL DISCHARGE SYSTEM

R.R. Robson, W.S. Williamson, and J. Santoru

Hughes Research Laboratories
3011 Malibu Canyon Road
Malibu, CA 90265

AD-A169 423

/

Air Force Geophysics Laboratory
Air Force Systems Command
United States Air Force
Hanscom AFB, MA 01731

DTIC FILE COPY

86   7   1   072

"This technical report has been reviewed and is approved for publication"

B.M. SHUMAN
Contractor Manager
Space Systems Technology
Space Physics Division

EDWARD C. JONSON, LT COL, USAF
Space Systems Technology
Space Physics Division

FOR THE COMMANDER

RITA C. SAGALYN, Director
Space Physics Division

This report has been reviewed by the ESD Public Affairs Office (PA) and is releasable to the National Technical Information Service (NTIS).

Qualified requestors may obtain additional copies from the Defense Technical Information Center. All others should apply to the National Technical Information Service.

If your address has changed, or if you wish to be removed from the mailing list, or if the addressee is no longer employed by your organization, please notify AFGL/DAA, Hanscom AFB, MA 01731. This will assist us in maintaining a current mailing list.

Do not return copies of this report unless contractual obligations or notices on a specific document requires that it be returned.

AD-A169 423

REPORT DOCUMENTATION PAGE

1a. REPORT SECURITY CLASSIFICATION Unclassified	1b. RESTRICTIVE MARKINGS
2a. SECURITY CLASSIFICATION AUTHORITY	3. DISTRIBUTION/AVAILABILITY OF REPORT Approved for public release; distribution unlimited.
2b. DECLASSIFICATION/DOWNGRADING SCHEDULE	
4. PERFORMING ORGANIZATION REPORT NUMBER(S)	5. MONITORING ORGANIZATION REPORT NUMBER(S) AFGL-TR-86-0036

6a. NAME OF PERFORMING ORGANIZATION Hughes Research Laboratories	6b. OFFICE SYMBOL (If applicable)	7a. NAME OF MONITORING ORGANIZATION Air Force Geophysics Laboratory
6c. ADDRESS (City, State and ZIP Code) 3011 Malibu Canyon Rd. Malibu, CA 90265		7b. ADDRESS (City, State and ZIP Code) Hanscom AFB Massachusetts 01731

8a. NAME OF FUNDING/SPONSORING ORGANIZATION Air Force Geophysics Lab.	8b. OFFICE SYMBOL (If applicable) AFGL/PHE	9. PROCUREMENT INSTRUMENT IDENTIFICATION NUMBER F19628-83-C-0143

8c. ADDRESS (City, State and ZIP Code) Hanscom AFB Massachusetts 01731	10. SOURCE OF FUNDING NOS			
	PROGRAM ELEMENT NO	PROJECT NO	TASK NO	WORK UNIT NO
11. TITLE (Include Security Classification) Flight Model Discharge System	63410F	2823	01	A

12. PERSONAL AUTHOR(S)
R.R. Robson, W.S. Williamson, and J. Santoru

13a. TYPE OF REPORT Scientific Report No.2	13b. TIME COVERED FROM 11/84 TO 12/85	14. DATE OF REPORT (Yr., Mo., Day) Feburary 1986	15. PAGE COUNT 178

16. SUPPLEMENTARY NOTATION

17	COSATI CODES		18 SUBJECT TERMS (Continue on reverse if necessary and identify by block number)
FIELD	GROUP	SUB GR	Spacecraft Charging, FMDS, Flight Model Discharge System, Spacecraft Automatic Active Discharge System

19. ABSTRACT (Continue on reverse if necessary and identify by block number)

The viability of the Flight Model Discharge System (FMDS) concept has been demonstrated by the successful fabrication and testing of a breadboard system. The FMDS is a spacecraft charge-control system designed to overcome the problem of charge buildup on a space vehicle which occurs during periods of adverse space-environmental conditions. Operational characteristics of the entire system are presented, including the electrostatic analyzers, surface potential monitors, transient pulse monitor, plasma source, and microprocessor-based controller, including its software. Results of the breadboard demonstration testing and the preliminary flight hardware design are also included.

20. DISTRIBUTION/AVAILABILITY OF ABSTRACT UNCLASSIFIED/UNLIMITED X SAME AS RPT DTIC USERS ☐	21. ABSTRACT SECURITY CLASSIFICATION Unclassified	
22a. NAME OF RESPONSIBLE INDIVIDUAL Bert Sinman	22b. TELEPHONE NUMBER (Include Area Code) (617) 377-3991	22c. OFFICE SYMBOL AFGL/PHE

DD FORM 1473, 83 APR   EDITION OF 1 JAN 73 IS OBSOLETE

TABLE OF CONTENTS

LIST OF ILLUSTRATIONS

LIST OF TABLES

SECTION 1

INTRODUCTION

The objectives of the Flight Model Discharge System (FMDS) program are the design, development, fabrication, test and delivery of two flight units of a satellite FMDS. The FMDS is a stand-alone system capable of autonomous operation (except for power) that will monitor spacecraft potential, determine when spacecraft charging is present, and operate a discharge device to eliminate potentials and maintain the spacecraft in a neutral charge state. The FMDS is designed to be incorporated into the "housekeeping" function of any spacecraft that may be subject to spacecraft charging. While full ground-command capability is retained for redundancy, only a "power on" command is required to activate the system. In addition to the capability for remote command override of its autonomous operation, the FMDS also provides telemetry signals to monitor such functions as sensor outputs, controller "commands," plasma source operation, gas supply in the reservoir tank, and system state-of-health diagnostics (i.e., temperature, voltages, and currents).

The technical discussion which follows presents the results of the second year's effort on the FMDS contractual program which is being carried out by Hughes Research Laboratories (HRL) in Malibu, California. An overview of the FMDS system is presented, followed by an in-depth treatment of the FMDS components and the results of the breadboard demonstration tests.

SECTION 2

FLIGHT MODEL DISCHARGE SYSTEM TOTAL SYSTEM

The FMDS is a stand-alone system capable of autonomous operation (except for power) that monitors space-vehicle potential, determines when charging is present, and operates a discharge device to eliminate charge buildup and maintain the vehicle in a neutral charge state. The FMDS is designed to be incorporated into the "housekeeping" functions of any vehicle which may be subject to spacecraft charging. While full ground-command capability is retained for redundancy, only a "power on" command is required to activate the system. It detects charging, operates to neutralize the charging, and returns to the passive mode when the charging hazard is no longer present.

The FMDS consists of three types of components:

(1) Charging sensors:

- Electrostatic Analyzers (ESAs). These sensors detect absolute charging relative to the ambient plasma in space.

- Surface Potential Monitors (SPMs). These sensors determine differential charging relative to spacecraft ground.

- Transient Pulse Monitor (TPM). This sensor detects the electromagnetic pulses generated by the onset of arcing.

(2) An active discharge device (plasma source).

(3) A control unit to interpret the sensor outputs, determine when and if charging is occurring, and control the discharge device.

A block diagram of the system is shown in Figure 2-1.

The controller incorporates comprehensive charging-detection algorithms which contain ground-alterable parameters to allow in-space refinement of FMDS operation. The controller incorporates redundant and fault-tolerant software to permit the FMDS to
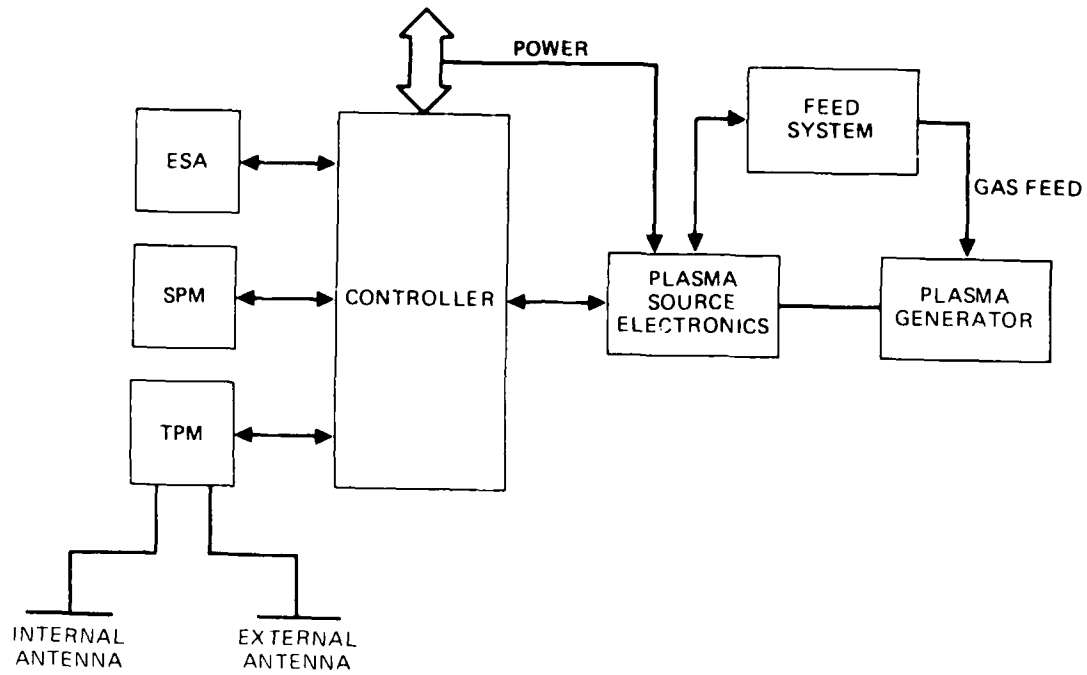
Figure 2 1. Block diagram of the FMDS.

continue operation in the face of specific faults or failures. In addition, it is capable of ground or remote-command override of its autonomous operation, and also provides telemetry signals to monitor such functions as sensor outputs, controller status flags, plasma source operation, gas supply pressure in the reservoir tank, temperatures, voltages, currents, etc.

The FMDS is ultimately intended for extended satellite operation in stationary orbit; however, it is designed to withstand the launch and operating environments of both geostationary and Shuttle orbits. While the primary emphases are safety and reliability, low operating and transient voltages are also considered.

2.1 OVERALL SYSTEM

The general FMDS configuration is depicted in Figures 2-2 and 2-3. All components of the system are attached to a common honeycomb-structure mounting-plate to provide a simple lightweight and structurally sturdy interface with the host spacecraft. No attempt is made in this model to indicate the exact interface of the FMDS with the host spacecraft since at this time a specific ride has not been determined. Because of this uncertainty, the FMDS has been designed to function independently of the characteristics of the host spacecraft. The structurally integrated design approach will also facilitate system testing in both laboratory vacuum chambers and environmental test fixtures (vibration, thermal/vacuum, etc.).

The layout of the system has been slightly modified from the model shown in Figures 2-2 and 2-3; the new layout is shown in Figure 2-4. Alterations include an exchange of the ion and electron electrostatic analyzers (ESAs) and one surface potential monitor (SPM); an increase in the size of the xenon tank from 1 to 2 liters; and the moving of the plasma generator outside the cover. The ESAs and the SPM have been interchanged to move the entrance apertures on the ESAs farther from the plasma generator, the size of the xenon tank has been increased to handle the

PLASMA
GENERATOR

ELECTROSTATIC
ANALYZER

SURFACE
POTENTIAL
MONITORS

HUGHES

TRANSIENT PULSE
MONITOR EXTERNAL
ANTENNA (INTERNAL
ANTENNA ON
UNDERSIDE OF UNIT)

Figure 2 2. Model of the FMDS with its cover in place.

14315 1R2

PLASMA
GENERATOR
ELECTRONICS

VALVE

CONTROLLER

TRANSIENT
PULSE
MONITOR

ELECTROSTATIC
ANALYZER

HUGHES

PRESSURE
REGULATOR

HUGHES

PLASMA
GENERATOR

HONEYCOMB
MOUNTING
PLATE

XENON
TANK

VALVE

SURFACE
POTENTIAL
MONITORS
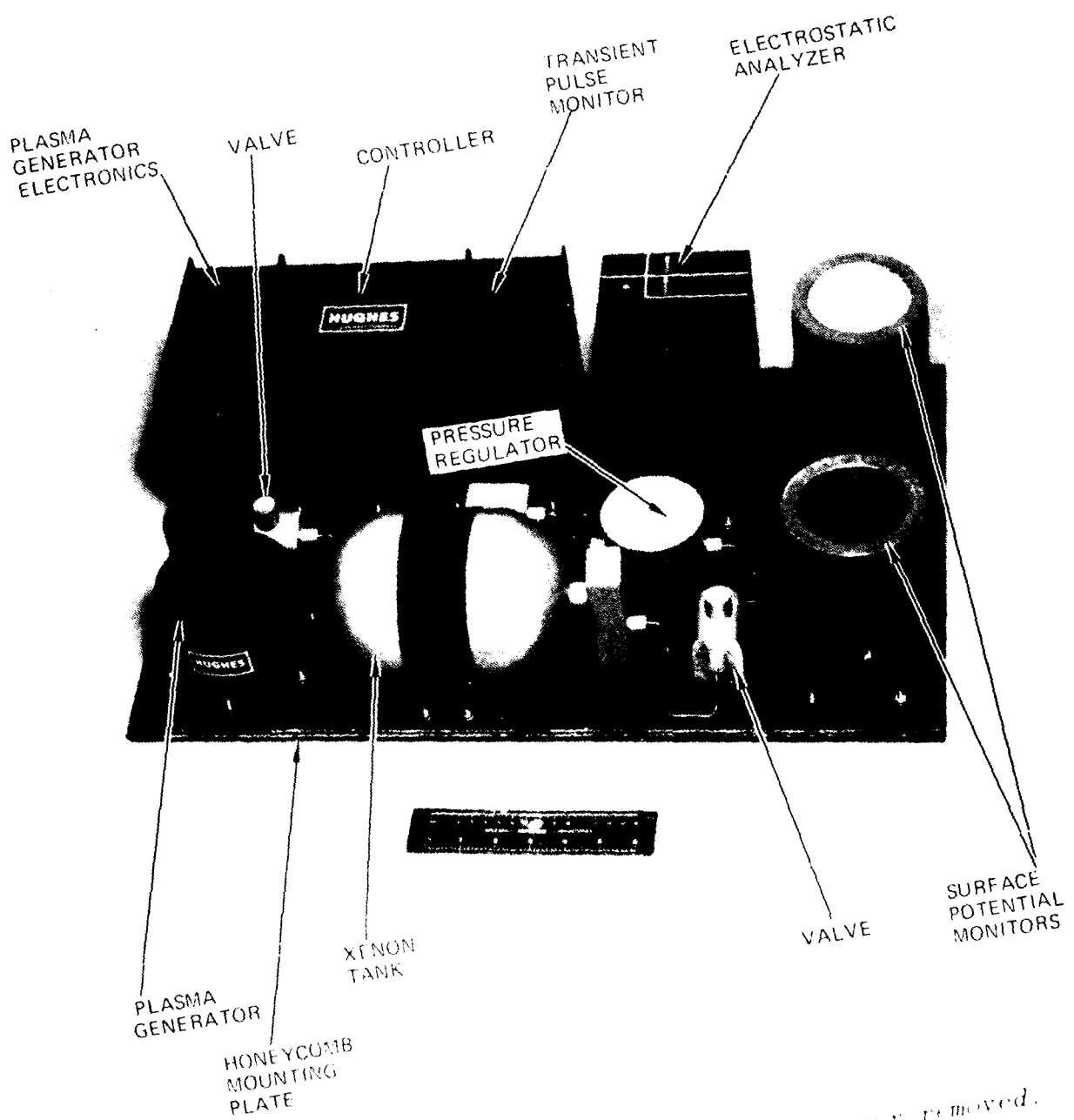
Figure 2-3. Model of the PDS with the cover removed.

15866-47

PLASMA SOURCE ELECTRONICS

CONTROLLER

TPM

SPM

ESA

PLASMA SOURCE

HONEYCOMB MOUNTING PLATE

5.5 in.

1 in.

24 in.

XENON TANK

TPM ANTENNA

15 in.

SPM
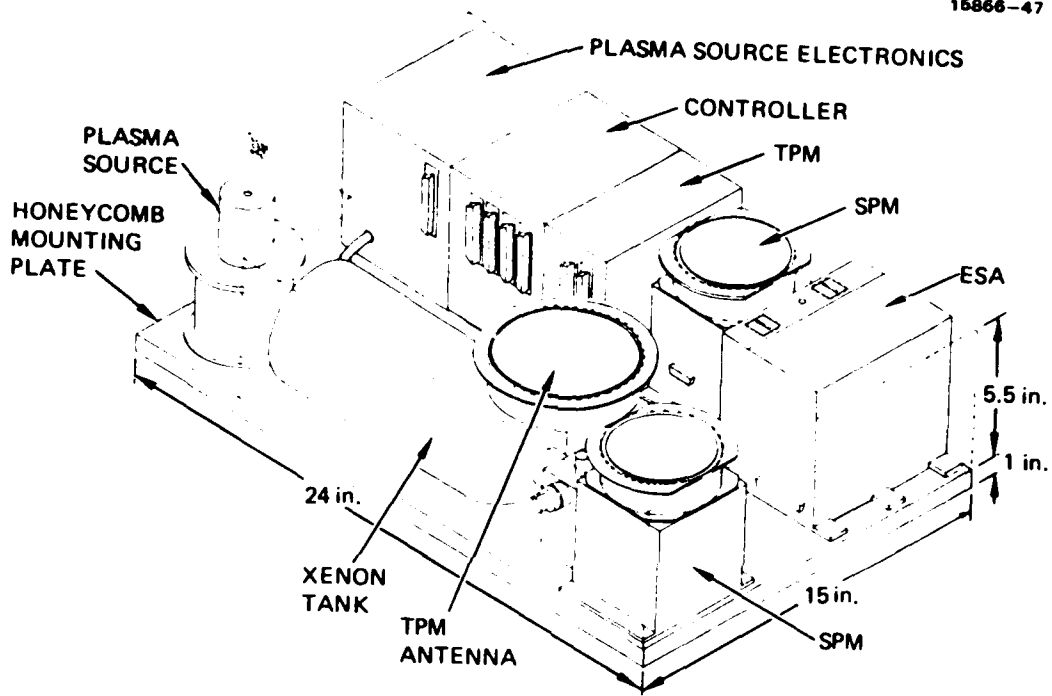
Figure 2 4. Flight design layout of the FMDS.

2-6

quantity of expellant required, and the plasma generator has been removed from inside the cover to prevent it from radiating heat to the electronics boxes.

Because of the diversity of functions required of the various FMDS components, each element is packaged separately and attached separately to the common mounting plate. Maintaining separation between each of the components has the added advantage of substituting of upgraded component designs if such upgrades become available in the future.

The two SPMs and the ESAs are mounted on one end of the FMDS mounting plate to provide both maximal and similar exposure of the sensors to incoming particle flux while avoiding (as much as possible) any local distortions of electrostatic equipotentials which might be caused by other devices such as the plasma source.

The plasma source is located at the end of the FMDS where it is farthest from the charged-particle entrance apertures of the ESAs; this will minimize the introduction of plasma-source-generated particles. In this location, the source is reasonably remote from both the ESAs and the SPMs.

The electronics packages for the plasma-generator, TPM, and controller; the SPMs; the ESAs; and the plasma generator are all at the same height. This allows a cover to be added to the FMDS to form a ground plane and to provide a mounting surface for the TPM external antenna. Thermal control surfaces and/or thermal blankets will also be attached to the cover.

Inasmuch as the FMDS is intended for satellite use, minimizing weight, volume, and power is of utmost concern. The overall FMDS is expected to weigh less than 19.4 kg (42.4 lb.), and consume less than 13.7 W when the plasma source is not activated, and less than 28.1 W when it is activated. FMDS weights and power consumption are summarized in Tables 2-1 and 2-2, respectively. The overall dimensions are 16.5 x 38.1 x 61 cm (6.5 x 15 x 24 in.).

Table 2-1. Summary of FMDS Weights

15866—46

UNIT	MASS, kg	WEIGHT, lbs	CONTRACT SPEC, lbs
ESA	2.7	6.0	6.0
SPM (2 UNITS)	1.4	3.0	3.0
TPM	1.6	3.5	3.0
CONTROLLER	1.7	3.7	—
PLASMA SOURCE	1.4	3.0	} 15.0
SOURCE ELECTRONICS	2.0	4.4	
FEED SYSTEM	4.2	9.2	
HARNESS	0.7	1.5	—
THERMAL CONTROL	0.9	2.0	—
ENCLOSURE	2.2	4.8	—
FMDS DRY MASS	18.8	41.1	—
XENON	0.6	1.3	—
FMDS AT LAUNCH	19.4	42.4	35.0

Table 2-2. Summary of FMDS Power Consumption

15866—45

UNIT	SOURCE OFF, W	SOURCE ON, W	CONTRACT SPEC, W
ESA	1.25	1.25	1.25
SPM (2 UNITS)	1.0	1.0	2.0
TPM	4.0	4.0	3.0
CONTROLLER	4.0	4.0	(4.0)
PLASMA SOURCE	0.0	13.7	(25.0)
HOUSEKEEPING INVERTER	3.4	4.1	—
FMDS	13.7	28.1	
FMDS CONTRACT SPEC	10.0	35.0	

( ) = INFERRED

2.2 COMPONENTS

The ESAs will measure the energy distribution (from 50 eV to 20 keV) of the particles incident upon the satellite. There will be a shift in this energy distribution when the environmental conditions are conducive to spacecraft charging (caused by a change in the environmental conditions), and another shift directly related to the potential of the satellite frame relative to the space potential. Since the ESAs are referenced to the satellite frame and the particles originate with energies relative to space potential, any change in the potential of the satellite frame will appear as a change in the particle-energy distributions. Algorithms in the controller will detect the shift in the particle-energy distributions (Figure 2-5) in order to (1) provide an early warning that the environmental conditions are conducive to spacecraft charging (by detection of electrons), and (2) detect that charging of the satellite frame has exceeded a threshold level (by ion detection) and provide a signal to turn on the plasma source.

The SPMs will detect the onset of differential charging of the satellite dielectric surfaces. When the satellite is in sunlight and charging conditions exist, the isolated dielectric surfaces that are shaded will charge much faster than the satellite frame because of the lack of photoemission from these shaded surfaces (Figure 2-6). Therefore, by measuring the potential on the surface of a shaded dielectric sensor, differential charging can be detected quickly and prior to the detection of satellite-frame charging by the ESA. When the satellite is in eclipse, however, satellite-frame charging occurs faster than differential charging (Figure 2-6). In this circumstance the ESA will be the prime detector.

The TPM will detect electrical discharges that occur on the surface of the satellite resulting from differential charging. A floating-plate sensor is employed to pick up radiated electric fields caused by these discharges. If electrical discharges are occurring, it implies that the satellite is charged up, that the

2-9
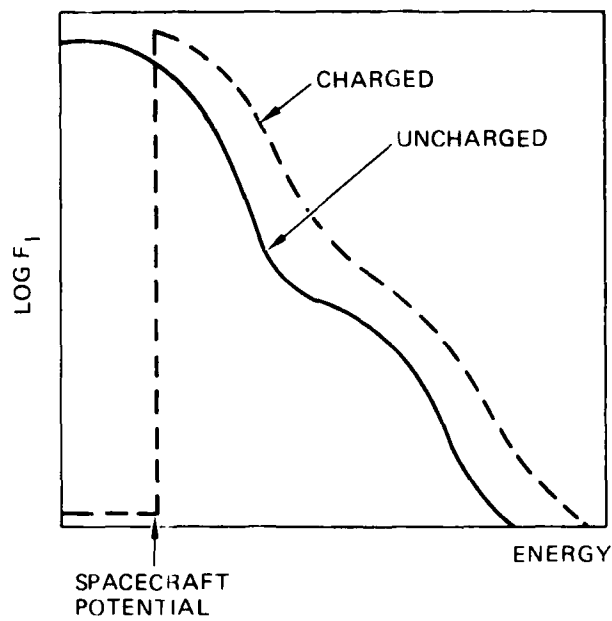
ION SPECTRUM

ELECTRON SPECTRUM
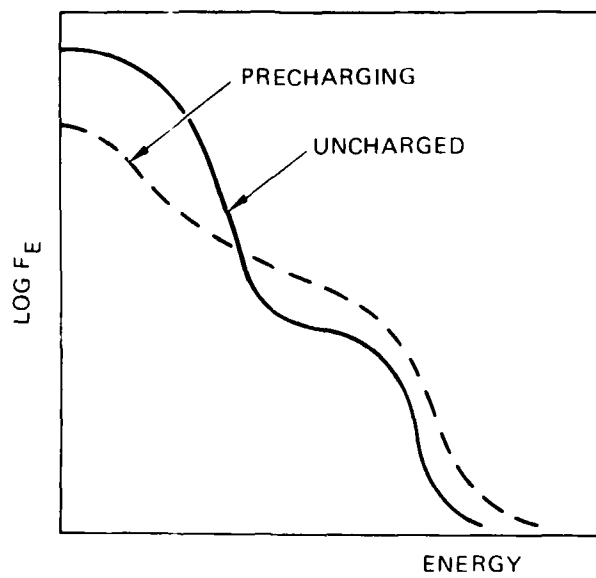
Figure 2 5.
Shift in the observed ion and
electron spectra caused by
environmental conditions con
ducive to charging and by actual
charging of the spacecraft.

SUNLIGHT CHARGING

ECLIPSE CHARGING
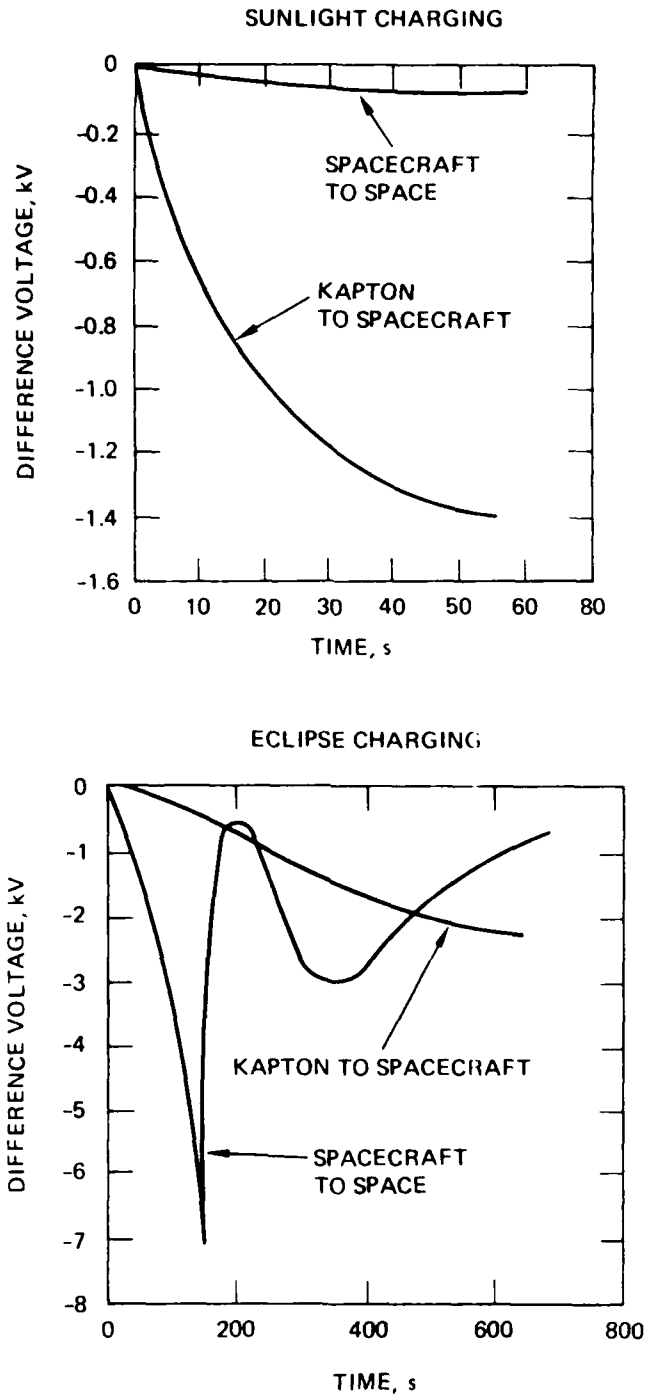
Figure 2 6.
Charging characteristics of a shaded
dielectric sensor.

2-11

plasma generator should be turned on, and that the other sensors have failed to detect the charging. The TPM has ground-adjustable parameters and can be commanded to ignore transients which occur within 1 s following receipt of a command by the spacecraft. The TPM is designed to avoid false arc-discharging alarms.

The controller provides for autonomous control of the FMDS relative to the remainder of the satellite. It is also the device which ties the other units of the FMDS together. The brain of the controller is a microprocessor which contains the algorithms necessary to interpret the data from the sensors and command the plasma generator to turn ON when spacecraft charging is occurring, and then turn OFF when it is no longer required. The plasma generator is turned OFF after a programmable time-out (when the emission current from the plasma generator has been less than a threshold value for a specified period of time) and when the ambient electron environment returns to a quiescent condition. The controller also provides the command and telemetry interface with the satellite.

The plasma generator emits xenon ions and electrons in sufficient quantity (>1 mA) to bathe the satellite in a conductive low-energy (<50 eV) plasma. This conductive plasma will drain the charge from dielectric surfaces and also form a "plasma bridge" to the surrounding natural space-plasma environment. The plasma generator is capable of igniting in less than 1 s, operating for 1,200 h, and executing 1,000 ON/OFF cycles. It requires three power supplies and a gas-feed system consisting of a xenon storage tank, a pressure regulator, valves, and a flow regulator.

Tables 2-3 through 2-8 list the major contractual specifications for the ESAs, SPMs, TPM, controller, plasma source, and system, respectively. The respective parameters of the flight design are also listed in these tables.

Table 2-3. *Electrostatic Analyzer Contractual Specifications and Respective Flight Design Parameters*

CONTRACTUAL SPECS	DESIGN
ION AND ELECTRON SPECTRA $<100\ eV$ TO 20 keV	50 eV TO 20 keV
GEOMETRIC FACTOR $\approx 10^{-5}$ TO $10^{-4}\ cm^2$ - SR	$6 \times 10^{-4}\ cm^2$ - SR
$\geqslant$ 8 ENERGY CHANNELS	16 CHANNELS
$\leqslant$ 2% OVERLAP AT FWHM	2% OVERLAP - NO GAPS
SWEEPS OF 2, 5, AND 10 s	SWEEPS OF 2, 4, 8, AND 16 s
VOLTAGES SETTLED TO 95% BEFORE COUNTING	VOLTAGES SETTLED TO $\geqslant$ 95% BEFORE COUNTING
GRID TO REPEL PLASMA SOURCE IONS AND ELECTRONS ($<$ 50 eV)	GRID BIASED AT 50 V
SUN SENSOR TO PROTECT CEM	SUN SENSOR
CMD OVERRIDE OF SUN SENSOR	CMD OVERRIDE
REDUCE UV SCATTERING	SANDBLASTED PLATES
COMMANDABLE CEM BIAS	COMMANDABLE BIAS (8 LEVELS)
THREE-YEAR ON ORBIT LIFE	DESIGNED FOR THREE-YEAR OPERATIONAL LIFE
TELEMETRY	ACCUMULATED COUNTS, ENERGY CHANNEL, STATUS, AND DIAGNOSTICS
1.25 W	1.25 W
6 lb	6 lb

Table 2 4. *Surface Potential Monitor Contractual*
Specifications and Respective Flight
Design Parameters

CONTRACTUAL SPECS	DESIGN
DIELECTRIC SURFACE POTENTIAL MEASURED WITH ELECTRIC FIELD SENSOR	VIBRATING ELECTRODE ELECTROSTATIC VOLTMETER
POTENTIAL AND POLARITY FROM 100 V TO 20 kV	DUAL RANGE: ± 2 kV ± 20 kV
TWO DIFFERENT DIELECTRICS IN FLIGHT	TWO INSTRUMENTS WITH DIFFERENT DIELECTRICS
CHOICE OF SIX DIFFERENT DIELECTRICS	CHANGE SENSING PLATE TO CHANGE DIELECTRICS
TELEMETRY	SURFACE POTENTIAL, RANGE, DIAGNOSTICS
· 2 W	$\leqslant 1$ W (2 UNITS)
· 3 lb	$\leqslant 3.5$ lb (2 UNITS)

Table 2 5. *Transient Pulse Monitor Contractual Specifications and Respective Flight Design Parameters*

CONTRACTUAL SPECS	DESIGN
DIPOLE SENSOR	MONOPOLE (123 cm^2 PLATE)
MEASURE RADIATED ELECTROMAGNETIC PULSES	MEASURE ELECTROSTATIC PULSES
MULTIPLE THRESHOLD LEVELS	8-BIT DAC
PARAMETERS MEASURED 1s	PARAMETERS MEASURED/1s
MAX POSITIVE PEAK AMPLITUDE	POSITIVE PEAK AMPLITUDE/PULSE
MAX NEGATIVE PEAK AMPLITUDE	NEGATIVE PEAK AMPLITUDE/PULSE
POSITIVE INTEGRAL	INTEGRALS NOT MEASURED
NEGATIVE INTEGRAL	
PULSE WIDTH	PULSE WIDTH PULSE
NUMBER OF PULSES	PULSES s
10 V/M TO 10 kV/m FIELD STRENGTH	10 V/m TO 10 kV/m
10 ns TO 10 μs PULSE WIDTHS	20 ns TO 10 μs
1 COUNT/ms MAX	1 COUNT/5ns
TELEMETRY	PARAMETERS MEASURED AND DIAGNOSTICS
3 W	4 W
3 lb	4 lb

Table 2 6. *Controller Contractual Specifications and Respective Flight Design Parameters*

CONTRACT SPECS	DESIGN
PROVIDE AUTONOMOUS OPERATION OF FMDS	AUTONOMOUS OPERATION
DETERMINE IF THRESHOLD LEVELS OF CHARGING HAVE BEEN EXCEEDED	CHARGING ABOVE THRESHOLD WILL BE DETECTED
TURN-ON PLASMA SOURCE AND OPERATE FOR 5, 10, 30, OR 60 min	TURN-ON AND CONTROL PLASMA SOURCE TURN-OFF BASED ON TIME, EMISSION CURRENT, AND/OR ENVIRONMENTAL CONDITIONS
DETECT WITH 98% RELIABILITY 95% OF CASES FOR CHARGING · 500 V 100% OF CASES FOR CHARGING · 1000 V	DESIGNED TO MEET BASED ON SC9 DATA
COMMANDABLE THRESHOLD CHARGING LEVELS OF 200, 500, 1000, AND 2000 V	SAME
SPACECRAFT ARCING TO ACTIVATE PLASMA SOURCE	ARCING WILL ACTIVATE PLASMA SOURCE
EMI PULSES WITHING 1s OF SPACECRAFT COMMAND TO BE IGNORED	ABILITY TO BLANK TPM FOR 1s (RE-QUIRES SIGNAL FROM SPACECRAFT)
EXTERNAL COMMAND ADJUSTMENT OF TPM ALGORITHM	ALL ALGORITHMS WILL BE ADJUSTABLE VIA EXTERNAL COMMAND
EXTERNAL COMMANDING OF PLASMA SOURCE	MANUAL OPERATION OF COMPLETE FMDS
TELEMETRY	STATUS AND DIAGNOSTICS
DESIGN TO INCLUDE CONSIDERATIONS OF RADIATION HARDENING	HARDENED TO 5×10^5 RADS (FLIGHT)
REDUNDANCY	CRITICAL PARAMETERS STORED IN THREE LOCATIONS (MAJORITY VOTING)
EXCESS CAPACITY	EXCESS MEMORY AND I O

Table 2-7.   Plasma Source Contractual Specifications
and Respective Flight Design Parameters

CONTRACTUAL SPECS	DESIGN
< 50 eV NEUTRAL PLASMA	~ 40 eV
IONS FROM A NOBLE GAS	XENON
10 μA, 100 μA, AND 1 mA ION CURRENT LEVELS (SELECTABLE)	< 200 μA TO > 1 mA, 4 SETPOINTS FOR DISCHARGE AND KEEPER
≤ 10s IGNITION	~ 1s
1200 HOURS OPERATION	> 1200 hr
1000 ON-OFF CYCLES	> 1000 CYCLES
< 25 W	≤ 10 W OPERATING ≤ 20 W CONDITIONING
< 15 lb	< 17 lb DRY
BLOW-OFF COVER	REMOVE-BEFORE-LAUNCH COVER
TELEMETRY	EMISSION CURRENT AND DIAGNOSTICS

Table 2 8. FMDS System Contractual Specifications and
Respective Flight Design Parameters

CONTRACTUAL SPECS	DESIGN
LOW-ENERGY PLASMA WITHIN 30s OF EXCEEDING A CHARGING THRESHOLD	SAME EXCEPT FOR ESA 16-s SWEEP WHICH REQUIRES 38s
ANALOG TELEMETRY OUTPUTS BETWEEN 0.00 AND 5.10V	NO ANALOG SIGNALS TO SATELLITE
DIGITAL COMMANDS AND TELEMETRY TTL COMPATIBLE	TTL COMPATIBLE AND OPTICALLY ISOLATED
ALL GROUND RETURNS SELF CONTAINED AND ISOLATED BY $\geqslant$1 MEGOHM	DESIGNED TO MEET – SINGLE GROUND POINT PHILOSOPHY
PERMANENT MAGNETIC FIELDS $\leqslant$100 nT AT 1 METER IN ANY DIRECTION	DESIGNED TO MEET
MATING CONNECTORS TO BE FURNISHED	MATING CONNECTORS WILL BE FURNISHED
NO CADMIUM-PLATED CONNECTORS OR OTHER HARDWARE	NO CADMIUM ANYWHERE
$<$35 LBS	41.1 LBS DRY 42.2 LBS AT LAUNCH
$<$10W WITH PLASMA SOURCE OFF	13.7W WITH SOURCE OFF 28.1W WITH SOURCE ON
POWER PROFILE TO BE PROVIDED	POWER PROFILE WILL BE MEASURED AND PROVIDED
HIGH-REL PARTS FOR $>$3 YR LIFE IN DEEP SPACE ORBIT	RAD-HARD CLASS-B PARTS
THERMAL MODELS TO BE PROVIDED	ANALYTICAL THERMAL MODELS WILL BE PROVIDED
MASS MODELS TO BE PROVIDED – BOTH ANALYTICAL MODELS AND HARDWARE SIMULATORS	ANALYTICAL MASS MODELS AND HARDWARE MASS SIMULATORS WILL BE PROVIDED
ELECTRICAL SIMULATORS TO BE PROVIDED	ELECTRICAL SIMULATORS WILL BE PROVIDED
GROUND SUPPORT EQUIPMENT TO BE PROVIDED – COMMAND/TELEMETRY AND POWER SOURCE	GROUND SUPPORT EQUIPMENT WILL BE PROVIDED – COMMAND/ TELEMETRY, POWER SOURCE, AND VACUUM PUMP
EMI: DESIGNED TO MEET MIL-STD-461B AND MIL-STD-1541	DESIGNED TO MEET
SHALL MEET SHUTTLE SAFETY REQUIREMENTS – NASA HANDBOOK 1700.7A, JSC 11123 AND JSC 13830	DESIGNED TO MEET
ACCEPTANCE TESTS TO BE PERFORMED IN ACCORDANCE WITH MIL-STD-1540A	DESIGNED TO MEET
RANDOM VIBRATION: FREQUENCY (Hz) PSD (q^2/Hz) 20 0.004 20-37.5 +12 dB/OCTAVE 37.5-90 0.050 90 200 +4 dB/OCTAVE	DESIGNED TO MEET

Table 2 8.   Continued

15866—44B

CONTRACTUAL SPECS	DESIGN

RANDOM VIBRATION (cont):
   FREQUENCY (Hz)   PSD (g^2/Hz)
   200-2000   -4 dB/OCTAVE
   COMPOSITE   13.7g RMS
   DURATION OF 2 MINUTES ALONG EACH OF
   3 ORTHOGONAL AXES	

SINE SURVEY:
   0.5 TO 1.0g,
   15 TO 100 Hz,
   ONE SWEEP UP AND DOWN IN EACH AXIS AT
   2 OCTAVES/MINUTE
	DESIGNED TO MEET

TRANSIENT SHOCK:
   25g, 11 ms, HALF-SINE PULSE ALONG EACH
   AXIS
	DESIGNED TO MEET

THERMAL VACUUM:
   $\leq$10^{-5} TORR,
   -24°C TO +61°C,
   12 HRS AT THE LOW AND HIGH TEMPERATURE
   LEVELS
	DESIGNED TO MEET

THERMAL CYCLING:
   AMBIENT PRESSURE
   -24°C TO +61°C
   $\geq$8 CYCLES WITH 2 HR DWELL AT LOW AND
   HIGH TEMPERATURE, TRANSITIONS AT
   $\geq$3°C/MIN
	DESIGNED TO MEET

BURN-IN:
   AMBIENT PRESSURE,
   -24°C TO +61°C,
   $\geq$18 TOTAL CYCLES INCLUDING THOSE
   ABOVE
	DESIGNED TO MEET

DEPRESSURIZATION/REPRESSURIZATION:
   SHUTTLE PROFILE,
   JSC 07700 VOL XIV,
   ATTACHMENT 1, REV G
	DESIGNED TO MEET

SECTION 3

ELECTROSTATIC ANALYZERS

The FMDS incorporates ESAs to measure the distribution of ion and electron energies which are incident on the spacecraft. The ESAs are important to the FMDS charging-detection function because they are the only instruments of those specified for FMDS that can detect the onset of eclipse charging. (The SPMs respond too slowly when the spacecraft is in darkness.) The data can be analyzed to determine the actual vehicle potential (i.e., frame potential relative to space potential) rather than the dielectric-surface potentials monitored by the SPMs. In addition to these important charging-detection attributes, the ESAs provide valuable scientific information.

The ESAs that are employed on the FMDS are configured with short-cylindrical section sensors. Instruments of this type have been used in physics experiments since the turn of the century, and similar devices have been used on many spacecraft. The FMDS instrument incorporates 16 channels and fast sweep times in order to provide the rapid reaction time that is required in the FMDS mission.

The ESAs for the FMDS are being provided by Panametrics Inc. of Waltham, Massachusetts under subcontract.

3.1 ESA DESIGN

The ESA design is for 15 energy channels covering the range of 50 eV to 20 keV, plus a background channel, for a total of 16 channels. The background channel is included to allow for subtraction of the scattered electron background in the lower energy channels. Table 3-1 lists the basic specifications for the ESA, along with the corresponding flight design values; Table 3-2 lists the energy detection characteristics of the ESA. The following sections describe the design in more detail.

Table 3 1. Basic Specifications for the ESAs and the Corresponding Flight Design Values

PARAMETER	SPECIFICATION	DESIGN
PARTICLES DETECTED	IONS AND ELECTRONS	IONS AND ELECTRONS
GEOMETRIC FACTOR	BETWEEN 10^{-5} AND 10^{-4} CM^2-SR	6×10^{-4} CM^2-SR
NUMBER OF ENERGY CHANNELS	MINIMUM OF EIGHT	16 CHANNELS
NOMINAL UPPER EDGES AT FWHM	100 eV, 200 eV, 500 eV, 1 keV, 2 keV, 5 keV, 10 keV, AND 20 keV	75 eV, 111 eV, 166 eV, 247 eV, 368 eV, 549 eV, 819 eV, 1.22 keV, 1.82 keV, 2.71 keV, 4.05 keV, 6.03 keV, 9.0 keV, 13.4 keV, AND 20 keV
ADJACENT CHANNEL OVERLAP	0 TO 2% AT FWHM	<2% OVERLAP — NO GAPS
TIME PERIOD FOR FULL ENERGY SWEEP	MINIMUM OF 1s, 5s, AND 10s. CHANGE OF SWEEP RESULTS IN RESET TO FIRST CHANNEL	SWEEPS OF 2, 4, 8, AND 16s. RESET TO FIRST CHANNEL
SETTLING TIME BETWEEN CHANNELS	VOLTAGES TO AT LEAST 95% OF OPERATING VALUE	VOLTAGES SETTLED TO ≥95% BEFORE COUNTING
LOW ENERGY ION CUT-OFF	50 eV TO AVOID COUNTING PLASMA SOURCE IONS	GRID BIASED AT 50V
SUN SENSOR TO PROTECT CEM	REDUCE ELECTRON MULTI-PLIER GAIN WHEN VIEWING THE SUN. CAN BE OVER-RIDDEN BY COMMAND	SUN SENSOR WITH COM-MAND OVERRIDE
ELECTRON MULTIPLIER GAIN CONTROL	BIAS VOLTAGE TO BE CON-TROLLABLE TO OFFSET EFFECTS OF DEGRADATION	COMMANDABLE BIAS (8 LEVELS)
DESIGN LIFETIME	MINIMUM OF THREE YEARS IN FMDS APPLICATION	DESIGNED FOR THREE YEAR OPERATIONAL LIFE
DIGITAL (BILEVEL) OUTPUTS TO CONTROLLER	ACCUMULATED COUNTS, ENERGY CHANNEL	ACCUMULATED COUNTS, ENERGY CHANNEL, SWEEP PERIOD, SUN SENSOR, DETECTOR VOLTAGE LEVEL
DIGITAL (BILEVEL) OUTPUTS TO TELEMETRY	ACCUMULATED COUNTS, ENERGY CHANNEL, SWEEP PERIOD, SUN SENSOR, DETECTOR VOLTAGE LEVEL	ACCUMULATED COUNTS, ENERGY CHANNEL, SWEEP PERIOD, SUN SENSOR, DETECTOR VOLTAGE LEVEL
ANALOG OUTPUTS TO TELEMETRY	APPROPRIATE DIAGNOSTICS	HOUSEKEEPING VOLTAGES AND TEMPERATURE
POWER CONSUMPTION	1.25W MAX	≤1.25W
WEIGHT	6 LBS MAX	≤6 LBS

Table 3 2.   *Energy Detection Characteristics of the ESAs*

14881 25R2

CHANNEL NUMBER	ENERGIES IN eV		
	E (LOW)	E (HIGH)	E (AVERAGE)
0	BACKGROUND CHANNEL		
1	50	75	62
2	75	111	93
3	111	166	138
4	166	247	206
5	247	368	308
6	368	549	459
7	549	819	684
8	819	1221	1020
9	1221	1821	1521
10	1821	2714	2267
11	2714	4047	3381
12	4047	6034	5041
13	6034	8997	7516
14	8997	13414	11205
15	13414	20000	16707

GEOMETRIC FACTOR 6×10^{-4} cm^2 – sr (CAN BE MADE SMALLER)

INTRINSIC ENERGY RESOLUTION Δ E (FWHM) E (AVERAGE) = 39%

3.1.1 Detection Assembly Design

The basic design of the ESA detection assembly is shown in Figure 3-1. The assembly is similar to several that have been constructed by Panametrics, so it is a proven design with well-known detection characteristics. The unit has been designed for satellite use, and can withstand the shock, vibration, and other environmental aspects of launch and orbital operations. The major characteristics of the detection assembly are described below.

- The analyzer plates have a narrow separation, and the surfaces are treated to reduce particle and light scattering. This is important to reduce electron background from the scattering of the intense high energy (tens of kilo-electron-volt) electron fluxes present during spacecraft charging events. This unit should readily detect the ion charging peak in the presence of intense electron fluxes. The plate design also strongly reduces the intensity of scattered solar UV rays reaching the channel electron multiplier (CEM) detector.

- The CEM and associated electronics are mounted on a ceramic circuit board. This reduces the level of organic vapors near the CEM, which helps to prolong its life. Since the CEM is the component most likely to degrade, considerable care must be used to minimize organic contamination, which tends to hasten CEM gain degradation.

- The CEM ceramic board is easily replaced so that routine refurbishing of the FMDS can easily include replacement of a partially degraded CEM. Since CEM exposure to organic vapor occurs primarily during exposure to the atmosphere in the prelaunch and postreturn environments, a CEM in an FMDS which has experienced several launch/recovery cycles will degrade faster than one that remains in orbit.

- The ESA has a geometric factor of about 6×10^{-4} cm^2-sr, which is appropriate for geostationary orbit applications; it can be readily reduced, if desired, for low earth orbit applications. The geometry of the detection head is shown in Figure 3-2 where

14881 12R1

CHANNELTRON
COLLIMATOR
AND 50 V BIAS

CYLINDRICAL PLATE
ANALYZER SECTION

INCIDENT
PARTICLES

CURVED CHANNELTRON
DETECTOR (CEM)

ESA HOUSING AND
ELECTROSTATIC SHIELD
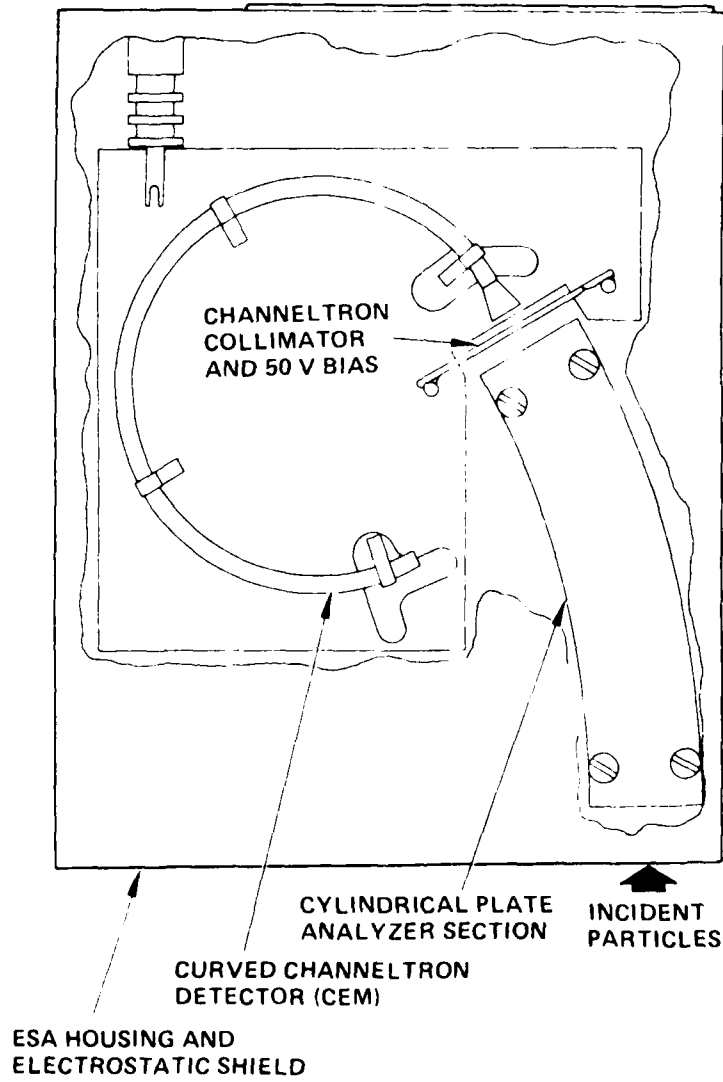
Figure 3-1.   Basic design of the electrostatic
analyzer detection assembly.

3-5
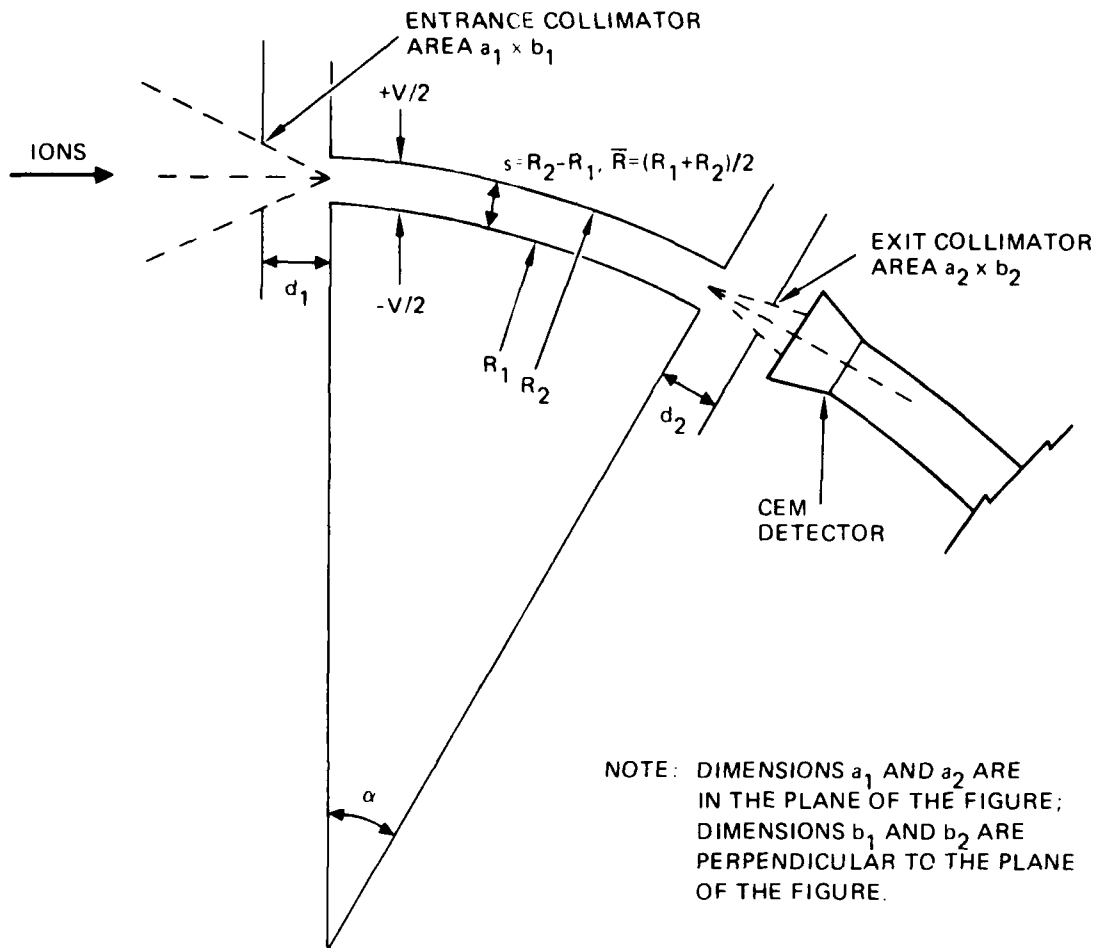
Figure 3 2. Basic geometry of the cylindrical plate electrostatic analyzer.

$$a_1 = 0.25 \text{ cm}$$

$$b_1 = 2 \text{ cm}$$

$$d_1 = 1 \text{ cm}$$

$$a_2 = 0.25 \text{ cm}$$

$$b_2 = 2 \text{ cm}$$

$$d_2 = 1 \text{ cm}$$

$$R_1 = 15.000 \text{ cm}$$

$$R_2 = 15.112 \text{ cm}$$

$$s = 0.112 \text{ cm}$$

$$\alpha = 20°$$

$$V/2 = 200 \text{ V maximum}$$

$$\text{Geometric factor} = 6 \times 10^{-4} \text{ cm}^2\text{-sr}$$

$$\text{Energy resolution} = 39\%.$$

A normalized curve for the detection characteristics of this design is shown in Figure 3-3. Adjacent energy bins are spaced such that their curves overlap from 0 to 2% at FWHM.

The physical design of the complete ESA unit is shown in Figure 3-4. The ESA detection assembly, photodiode, and electronics are all contained in a 4.5 x 6 x 5.5-in. housing. The ESA entrance apertures and the photodiode must have a clear view of the external particle fluxes. The housing also contains connectors for power and information flow to/from the controller and for access to test points.

3.1.2 Electronics Design

The basic electronics design for the ESA is shown in Figure 3-5, which indicates how the basic required operational characteristics are met. Significant features of the design for ions (electrons) include:
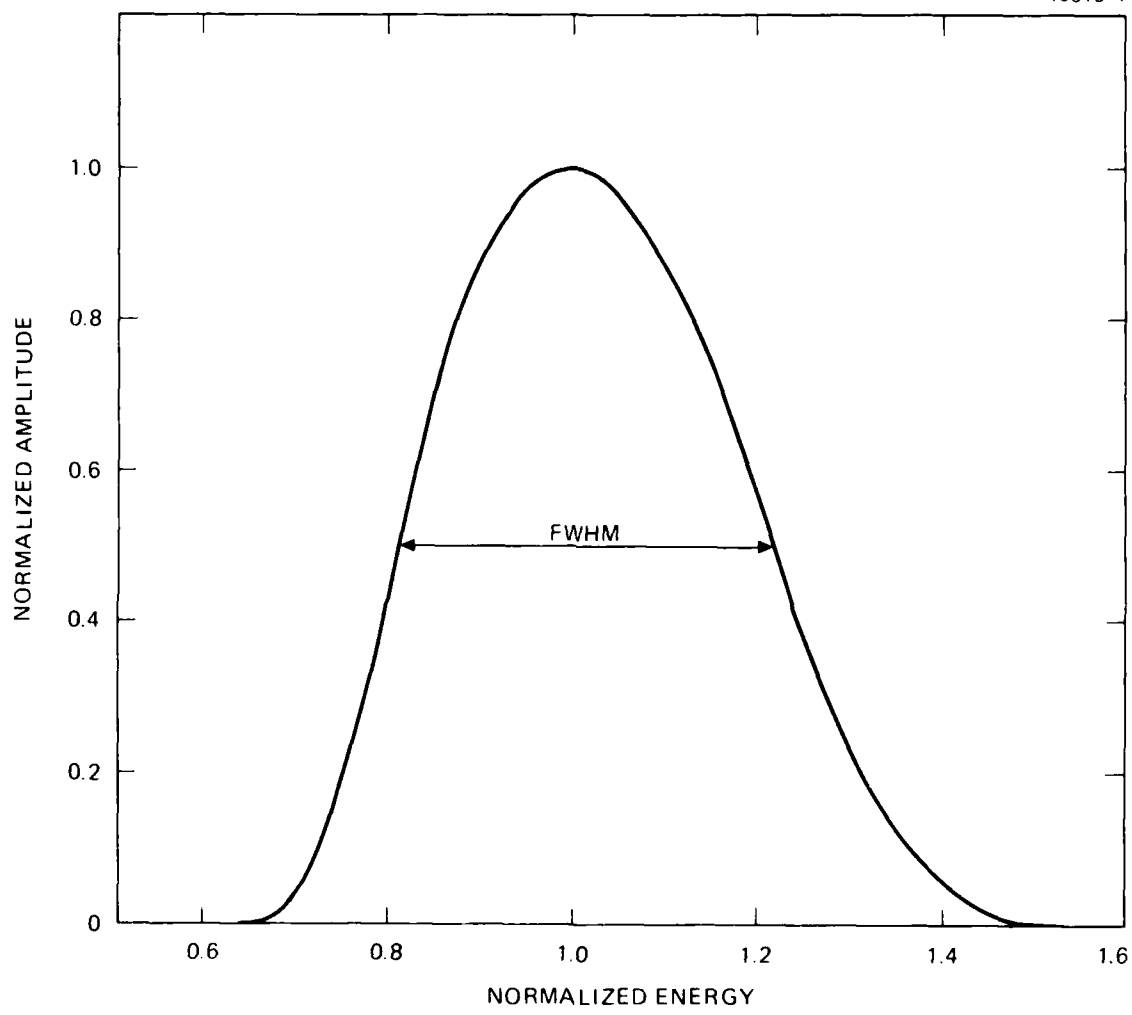
*Figure 3 3.   Normalized detection characteristic
of a single energy bin.*
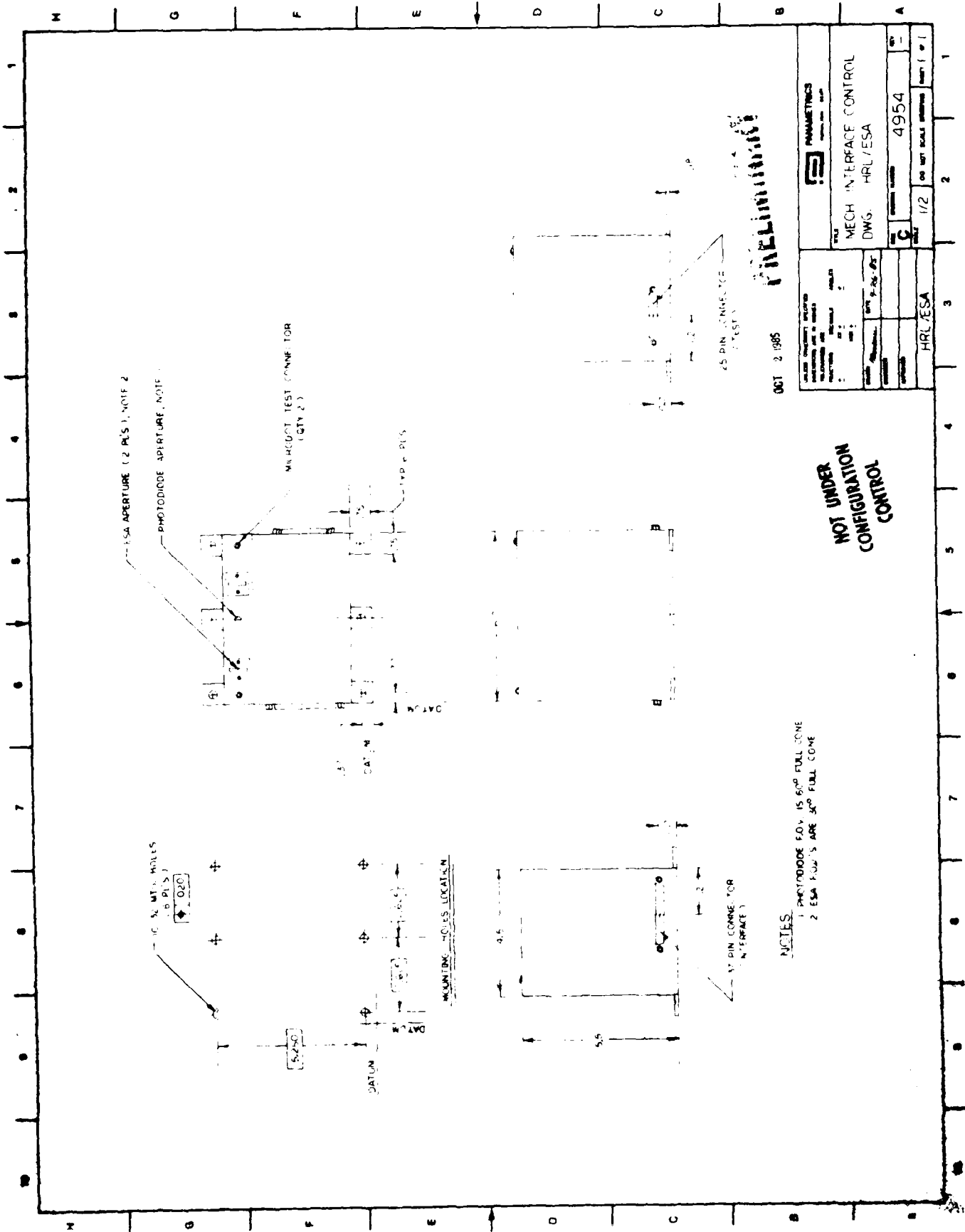
Figure 3.4. Physical design of the complete ESA.
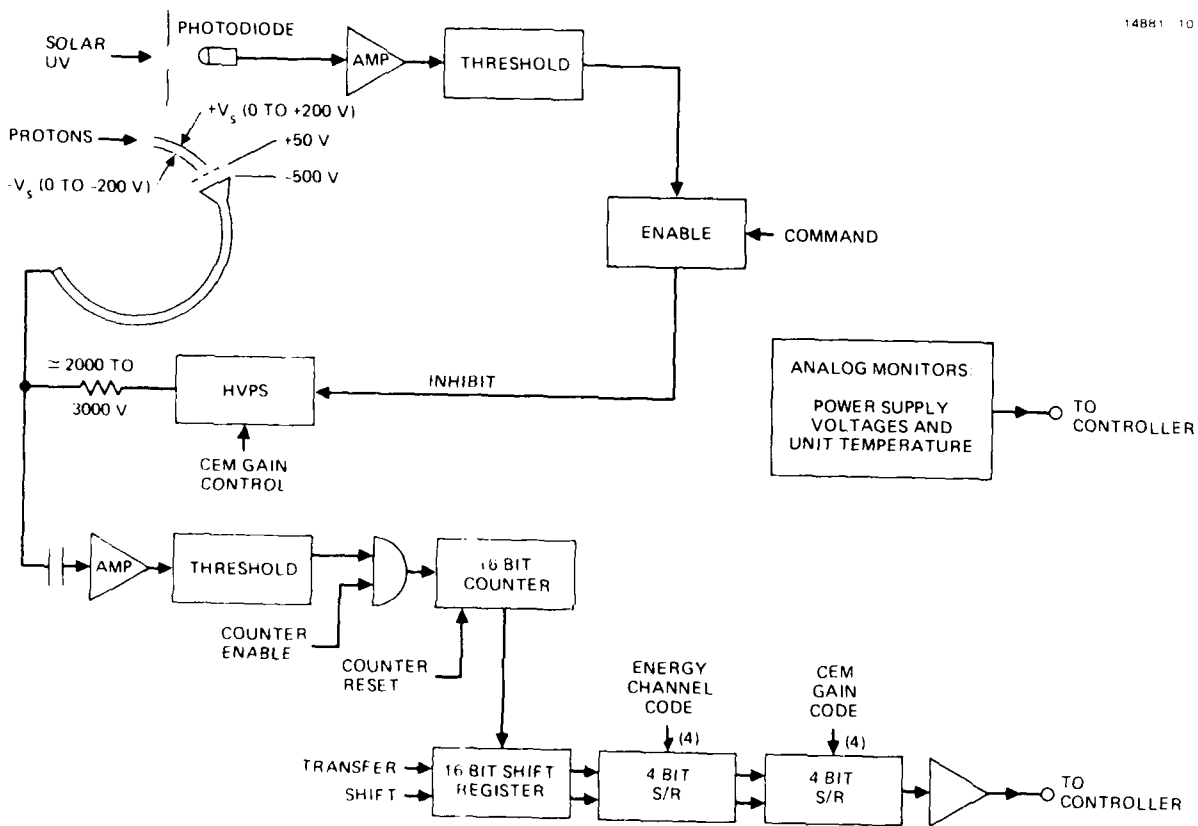
Figure 3-5. Block diagram of the ESA electronics for the ion detection head. Electron detection electronics are similar except for the polarity of some voltages.

- A +50 V (-50 V) grid in front of the CEM to eliminate ions (electrons) below 50 eV, thus protecting the CEM from the plasma source ions (electrons).

- A CEM aperature biasing of -500 V (500 V) to increase the detection efficiency for low energy ions (electrons). This voltage is held fixed to avoid efficiency changes with CEM gain-voltage changes.

- Adjustable CEM gain by command using a controlled high voltage power supply (HVPS).

- Reducible CEM gain when the unit is turned toward the sun, by means of the photodiode. This operation can be enabled or disabled by command.

- CEM counts which are accumulated in a 16-bit counter (65,535 maximum, after which the counter rolls over). This allows the CEM to operate at 524 kHz for the 2-s accumulation time, and at 65.5 kHz for the 16-s accumulation time, based on 16 channels.

- The ESA-plate voltage-sweep control block diagram is shown in Figure 3-6. The control voltage drives a bipolar supply to provide the $V/2$ and $-V/2$ in Figure 3-2. The ESA is designed so that for 20-keV ions or electrons, $\pm V/2 = \pm 200$ V. The sequencing in Figure 3-6 is such that R_1 through R_{16} set up the central energy of each energy channel. The value of R_1 is set so that channel 0 measures background, with no direct ion (electron) response. The circuitry can be readily set to provide the energy channels of Table 3-2.

The remainder of the electronics design is straightforward digital control circuitry, timing circuitry, power supplies, and interface buffers. The schematics for all the electronics are presented in Figures 3-7 through 3-11.

3.1.3 CEM lifetime

Channel electron multipliers (CEMs) are typically quoted as having a lifetime in excess of 10^{11} total counts before their gain starts to decrease. However, their lifetime is a strong function of the contaminants they are exposed to, particularly complex hydrocarbons such as vacuum pump oil. A typical lifetime curve for a CEM is shown in Figure 3-12. The initial high gain is attributed to the sputtering of contaminants from the CEM

14881-9
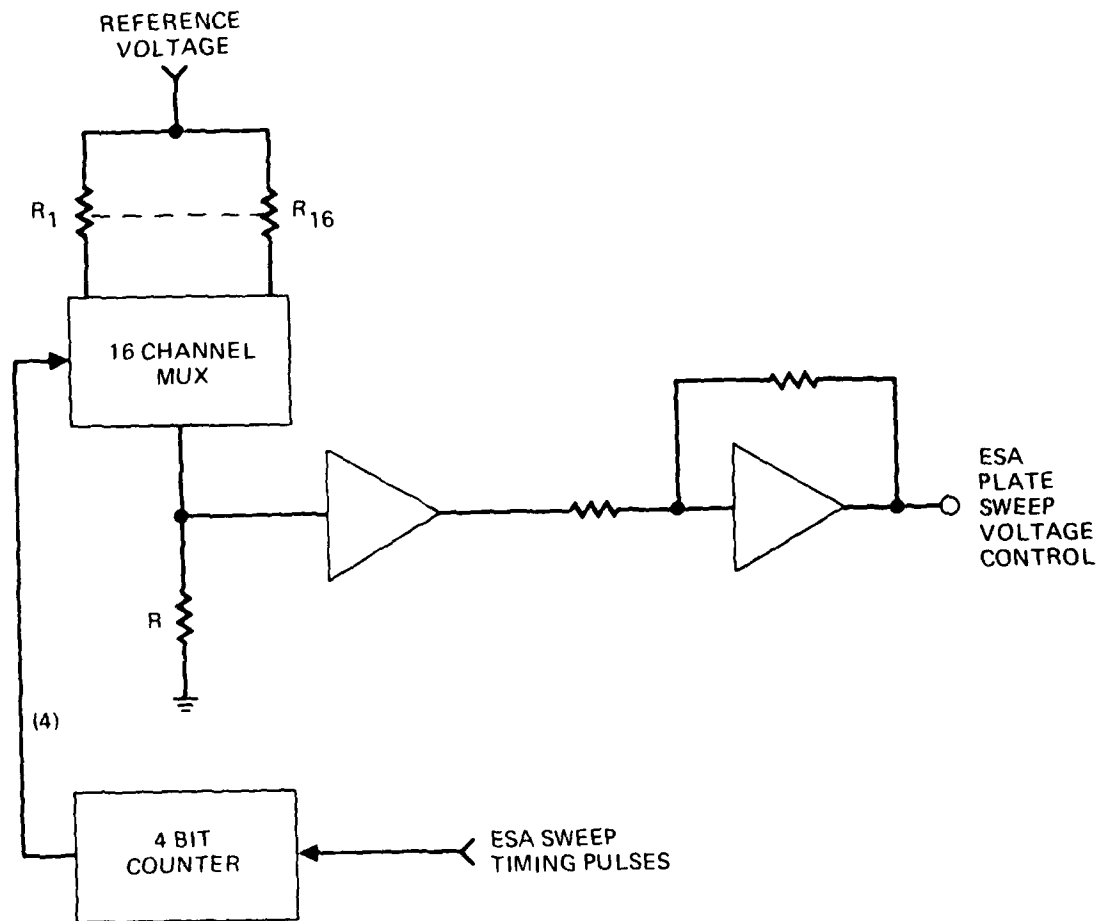
Figure 3 6. *Block diagram of the ESA-plate voltage sweep control.*
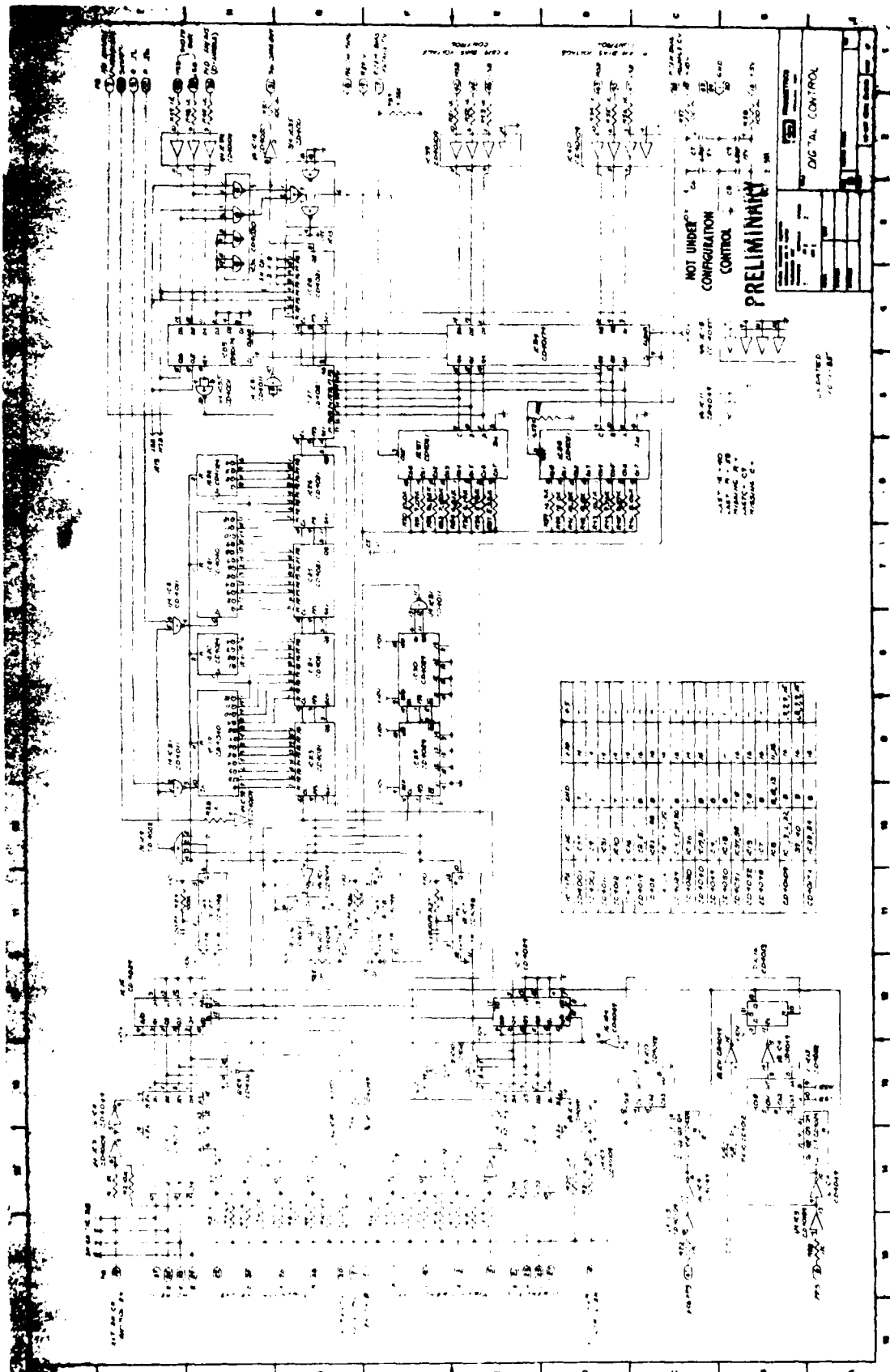
Figure 3-7. Schematic of the ESA digital control electronics.

Figure 3-8. Schematic of the ESA voltage-sweep generator and ±500 V dc-to-dc converter.

Figure 3.9. Schematic of the ESA low voltage power supply
and high voltage inhibit circuitry.
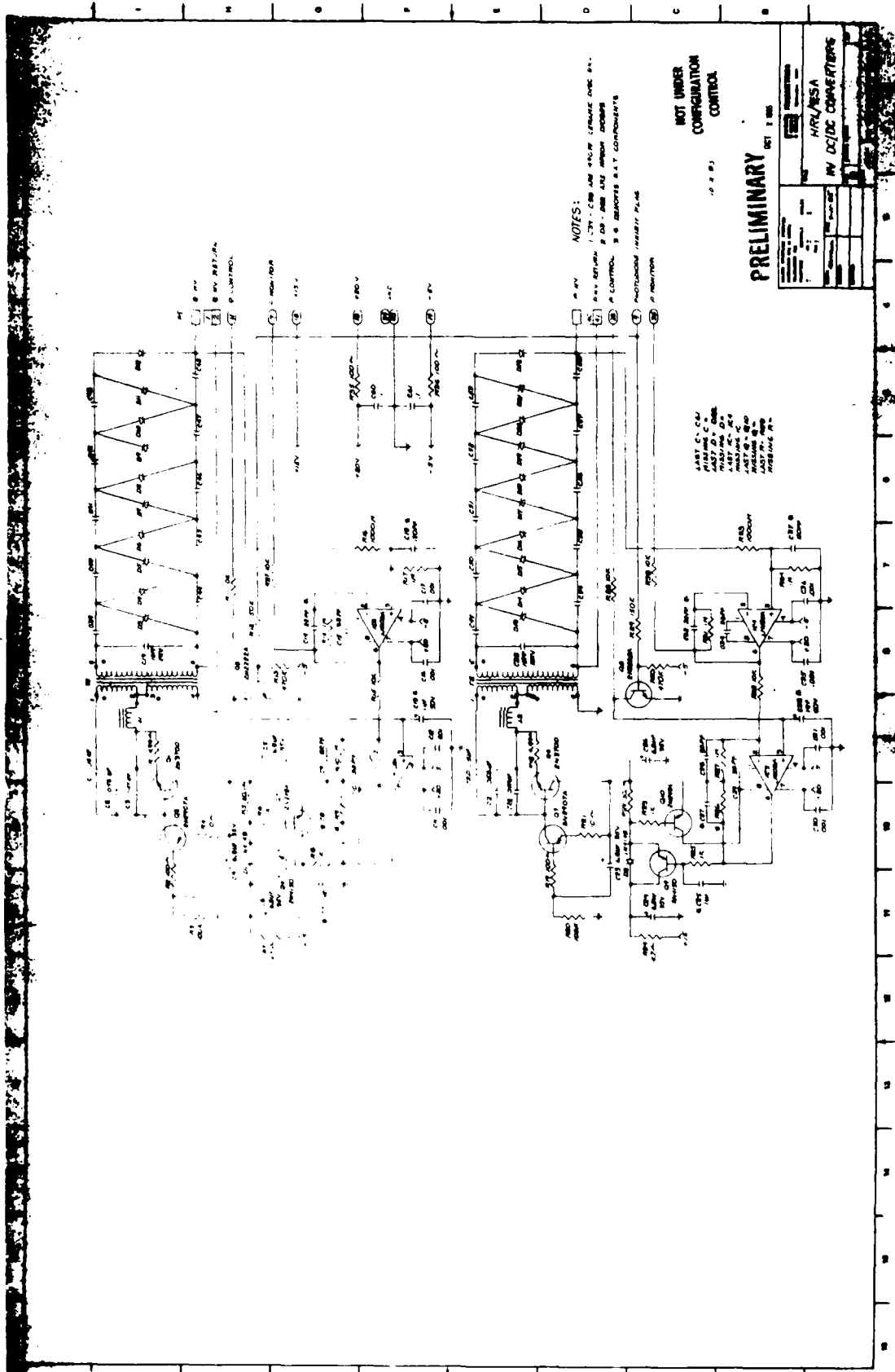
Figure 3-10. Schematic of the ESA high voltage dc-to-dc converter.
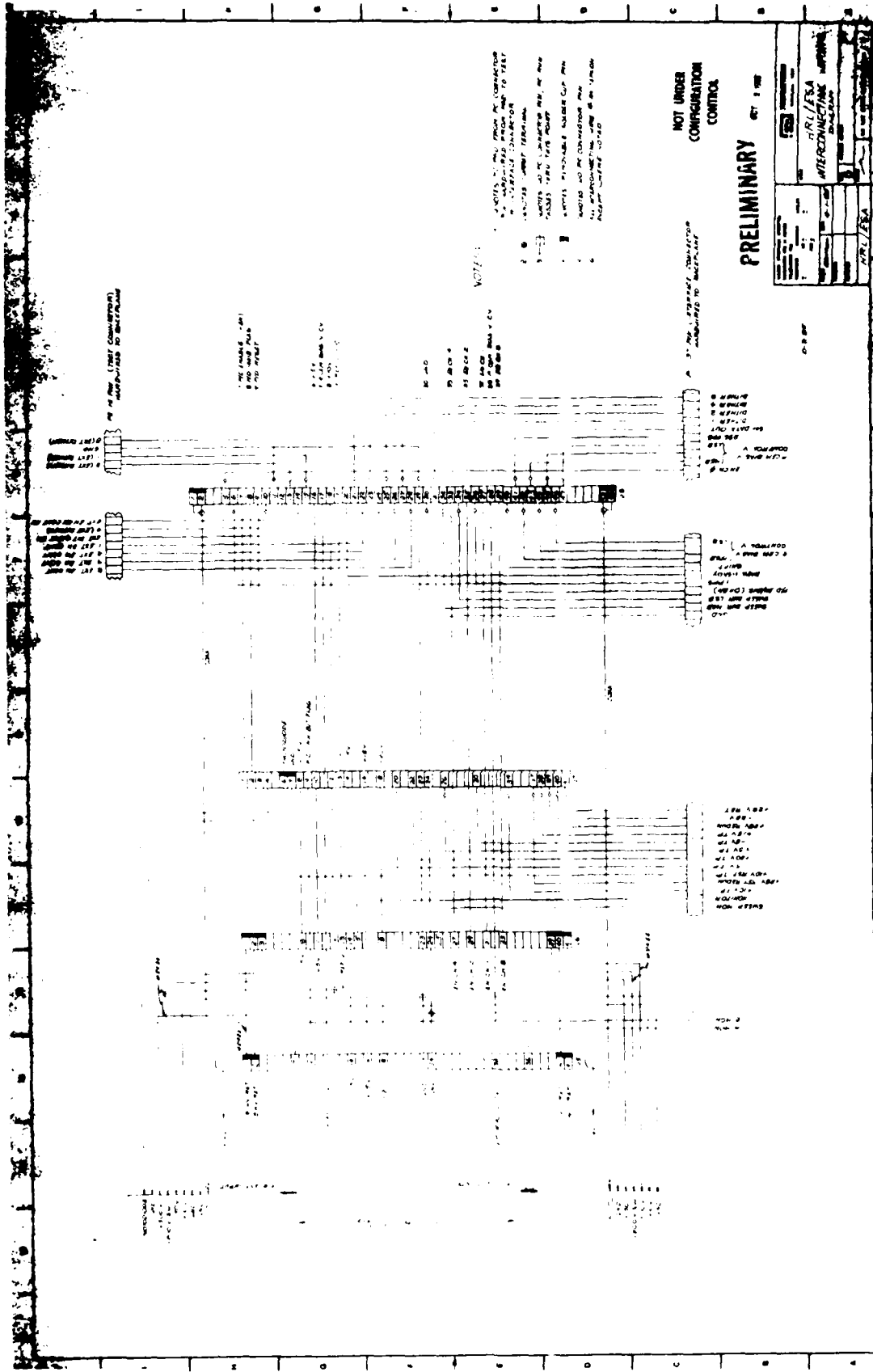
Figure 3-11. Interconnection wiring diagram for the ESA.

15816-3
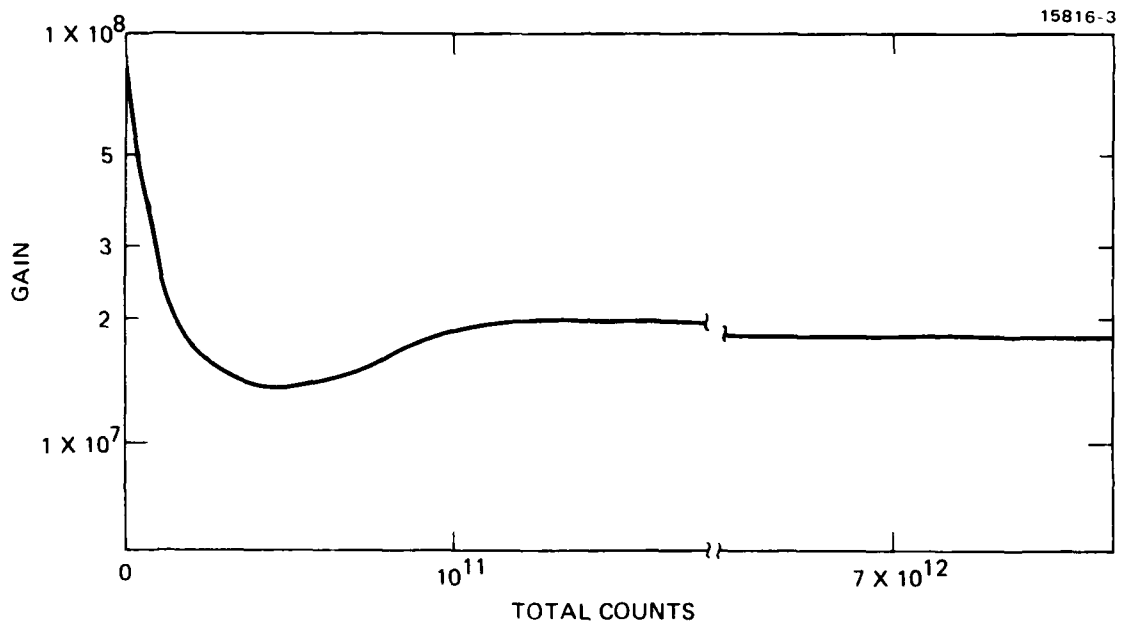
Figure 3-12.   Typical gain versus total
count curve for a CEM.

3-18

surface. Electron avalanches produce ions from the contaminants; these ions produce additional electron avalanches which account for the high gain. As the surface is cleaned by the sputtering process, the gain falls to a minimum value and then increases slighty. This increase in gain is attributed to a further cleaning of the CEM surface. The gain then levels off and remains at this level to greater than 10^{11} counts, provided the CEM environment is and has been free of heavy hydrocarbons. Tests have been performed that show the gain is flat to at least $2x10^{11}$ counts[1]; one test showed $7x10^{12}$ counts.[2]

Assuming a conservative lifetime estimate of 10^{11} counts for the CEM, and a counting rate for ions of about 60 counts/s at GEO with our geometric factor of $6x10^{-4}$ cm^2-sr the lifetime of a CEM should be at least 53 years. The estimated electron counting rate is expected to be about 13,300 counts/s, yielding a lifetime of only 0.25 years. Therefore, the entrance aperture of the electron ESA should be reduced by a factor of 40 using a plate with many small pin holes to provide a 10 year lifetime. Numerous small pin holes as opposed to a single smaller aperture will reduce the counting rate without changing the field-of-view of the ESA.

A counting rate of 60 counts/s, or an average of 3.75 counts/channel/s, would be marginal for the ESA algorithms on a system cycle of 1 s. The minimum system cycle time now being considered is 4 s, which gives an average of 15 counts/channel/ cycle; this is still marginal from a statistical standpoint. The ESA 16-s sweep will give an average of 60 counts/channel/sweep, which is statistically significant.

3.1.4 Commands and Telemetry

The ESA accepts a parallel digital command to set the ion detector CEM bias, the electron detector CEM bias, and the sweep time, and to enable or disable the sun sensor. The digital bit patterns for these commands are listed in Table 3-3 and the digital interface is defined in Figure 3-13.

Table 3-3. Digital Bit Patterns for the ESA Commands

ESA COMMANDS

ION OR ELECTRON CEM BIAS	MSB BIT 2	BIT 1	LSB BIT 0
LOWEST BIAS	0	0	0
	0	0	1
	0	1	0
MONOTONICALLY INCREASING	0	1	1
	1	0	0
	1	0	1
	1	1	0
HIGHEST BIAS	1	1	1

SWEEP TIME (s)	MSB BIT 1	LSB BIT 0
2	0	0
4	0	1
8	1	0
16	1	1

PHOTO DIODE	1 BIT
ENABLED	0
DISABLED	1

NOTE: ALL SIGNALS ARE POSITIVE TRUE ("1").

Figure 3-13. ESA digital command interface.

The ESA provides serial digital telemetry data for the energy channel, the sweep time, the ion detector CEM bias, the electron detector CEM bias, the sun sensor status, the sweep time reset flag, the sun sensor inhibit flag, the data overrun flag, the ion detector count, and the electron detector count. The digital bit patterns associated with these data are shown in Table 3-4 and the serial digital interface is defined in Figure 3-14. The ESA also provides analog telemetry (0 to 5 V) for the electron-CEM bias voltage, the ion-CEM bias voltage, the sweep voltage, the reference voltage, the bias voltage monitor (±50, ±300, and ±500 bias voltages), the temperature, and the 5-V and 10-V housekeeping voltages.

3.2 BREADBOARD TEST RESULTS

The breadboard instrument fabricated by Panametrics was part of the breadboard demonstration and exhibited its ability to detect both ions and electrons and provide suitable data to the ion-ESA and electron-ESA algorithms. Operation of the ESA was not affected by the presence of the xenon plasma emitted by the plasma source.

The ion ESA was calibrated at Hughes using a monoenergetic proton beam and a gimbal to vary the direction of the beam relative to the ESA entrance aperture. A typical calibration curve is shown in Figure 3-15. The response curves for several angles are shown, along with the envelope of these response curves, and the theoretical envelope for the instrument. The ratio of the high and low energies at FWHM (1.504) is very close to the theoretical value of 1.491. The center energy of 4.35 kV, however, is approximately 12% lower than the theoretical value of 4.94 kV. This can be corrected by slightly increasing the voltage on the detection plates. All of the energy bins exhibited similar responses except for the low energies (50 to 200 eV) where the Earth's magnetic field was affecting the trajectory of the proton beam.

Table 3-4. ESA Digital Telemetry Bit Patterns

ESA DATA   14881-27R1

ENERGY CHANNEL	MSB BIT 3	BIT 2	BIT 1	LSB BIT 0
0 – LOWEST ENERGY	0	0	0	0
1	0	0	0	1
2	0	0	1	0
3	0	0	1	1
4	0	1	0	0
5	0	1	0	1
6	0	1	1	0
7	0	1	1	1
8	1	0	0	0
9	1	0	0	1
10	1	0	1	0
11	1	0	1	1
12	1	1	0	0
13	1	1	0	1
14	1	1	1	0
15 – HIGHEST ENERGY	1	1	1	1

SWEEP TIME (s)	MSB BIT 1	LSB BIT 0
2	0	0
4	0	1
8	1	0
16	1	1

Table 3-4. *(Continued)*

14881—28

ION OR ELECTRON CEM BIAS	MSB BIT 2	BIT 1	LSB BIT 0
LOWEST BIAS	0	0	0
	0	0	1
	0	1	0
	0	1	1
MONOTONICALLY INCREASING	1	0	0
	1	0	1
	1	1	0
HIGHEST BIAS	1	1	1

PHOTODIODE STATUS	1 BIT
ENABLED	0
DISABLED	1

SWEEP TIME RESET FLAG	1 BIT
NORMAL	0
RESET OCCURRED	1

PHOTODIODE INHIBIT FLAG	1 BIT
NORMAL	0
INHIBIT OCCURRED	1

Table 3-4. (Continued)

DATA OVERRUN FLAG	1 BIT
NORMAL	0
OVERRUN OCCURRED	1

ION OR ELECTRON COUNT HIGH BYTE	
BIT WEIGHT	BIT
256	0 - LSB
512	1
1,024	2
2,048	3
4,096	4
8,192	5
16,384	6
32,768	7 - MSB

ION OR ELECTRON COUNT LOW BYTE	
BIT WEIGHT	BIT
1	0 - LSB
2	1
4	2
8	3
16	4
32	5
64	6
128	7 - MSB

NOTE: ALL SIGNALS ARE POSITIVE TRUE ("1").

Figure 3 14. ESA digital data interface.
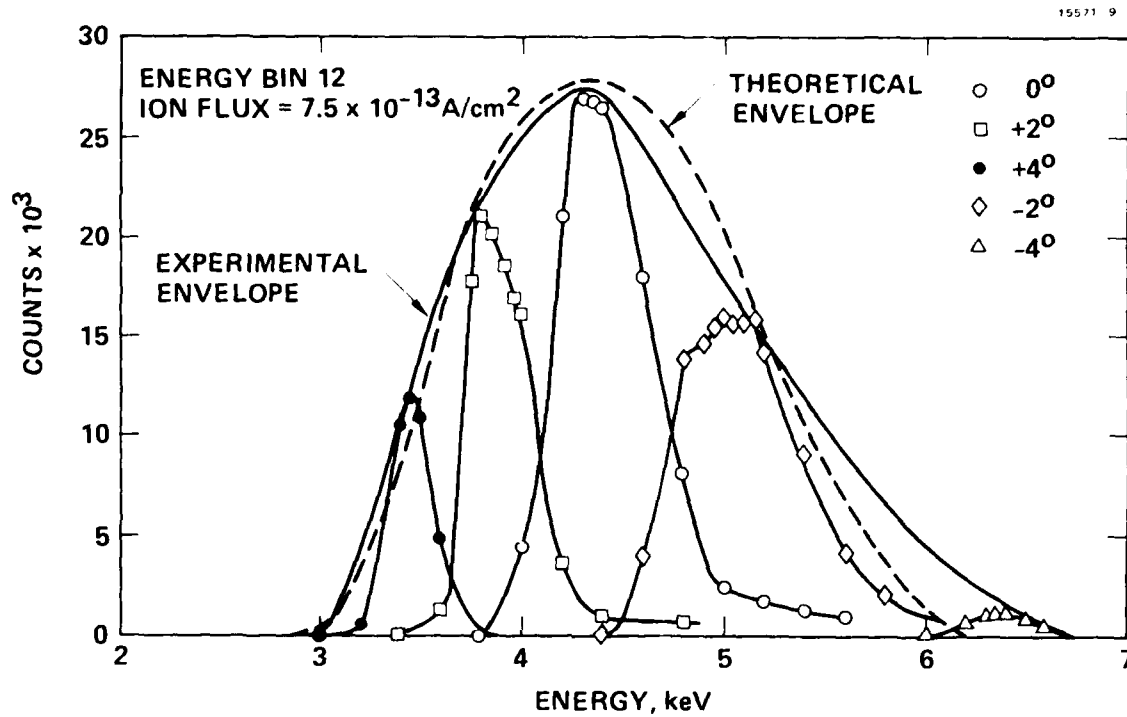
Figure 3-15. *Calibration curve for energy bin 12 of the ion ESA.*

The electron ESA could not be calibrated at Hughes because of the effect of the Earth's magnetic field on the electron beam. The instrument was returned to Panametrics for performance of this calibration; preliminary data indicate characteristics very similar to the ion ESA.

SECTION 4

SURFACE POTENTIAL MONITORS

Two surface potential monitors (SPMs) are included as part of the FMDS to detect the charging of dielectric surfaces on the satellite. Since two different dielectric materials are to be used in flight, and since it is desirable to have them physically separated (to minimize their effect on each other), the best approach was to use two instruments, with the dielectric material being the only difference (see Figure 2-2).

One of the main factors in the design of the SPMs is the requirement of not altering the charge buildup of ions or electrons on the dielectric material due to the measurement. This dictates that some type of electric-field-sensing device be used.

Most electrostatic voltmeters that have sufficient accuracy and resolution use a field-sensing probe that is closed-loop controlled to the same potential as the surface being measured. In this way the field sensor need only detect a null. To use this approach in this application a "servo-amplifier" with an output of ±20 kV would be required, which is not practical within the weight and power limitations for this instrument. We have chosen, therefore, to use the approach that was adopted by the NASA Lewis Research Center for their surface-voltage sensor (SVS).[3] NASA's approach retains most of the advantages of a feedback sensing system, yet does not require high voltage. This system uses a combination of electrodes that attenuate the field produced by the sensing surface and allows it to be nulled with a low-voltage (±10 V) feedback signal.

We have slightly modified the specifications for the SPMs from those called out in the original RFQ issued by AFGL. The RFQ called for measurement over a range of 100 V to 20 kV, and a determination of the polarity. If 8-bit digital data are used, then the resolution for a 20-kV full scale range is 78 V, which is rather coarse when looking for surface potentials of 200 V.

Therefore, we are using a dual-range instrument with nominal ranges of 0 to ±2 kV and 0 to ±20 kV. These ranges provide a resolution of 16 V and measure potentials to ±20 kV.

4.1 SPM SENSOR HEAD DESIGN

Since the SPMs will be required to survive vibration and shock experienced during launch, an ideal design would be all solid state; i.e., no moving parts as are present in a tuning fork. Therefore, several potentially feasible design principles were investigated such as modulation of a light beam within a fiber-optic bundle by the E-field, and semiconductor-conductivity modulation by the E-field similar to the operation of field effect transistors. However, these ideas would have required considerable development and testing to achieve the level of flight readiness required by the FMDS program. We therefore decided to utilize the most mature technology available at this time: the NASA LeRC vibrating electrode approach.

The functional operation of this approach is best understood with reference to Figure 4-1. If the dielectric surface is covered by a surface charge (represented in Figure 4-1(a) as negative), then the dielectric surface will assume some voltage, V_S, as indicated in Figure 4-1(b). The electric field associated with voltage V_S penetrates the entrance aperture of the electrically grounded sensor head so that the value of the field drops off precipitously within the sensor head. If we assume (for the sake of explanation) that the feedback-aperture plate is grounded (i.e., $V_A = 0$), the electric potential along the centerline of the sensor head would vary according to the curve marked "feedback aperture grounded."

In actual operation, however, the feedback-aperture plate is not grounded, but is set at a chosen potential, V_A. If we instead imagine that the dielectric surface is grounded (i.e., $V_S = 0$), the electric potential along the centerline of the sensor head would vary according to the curve marked "dielectric surface grounded." In practice, the potential varies as the net
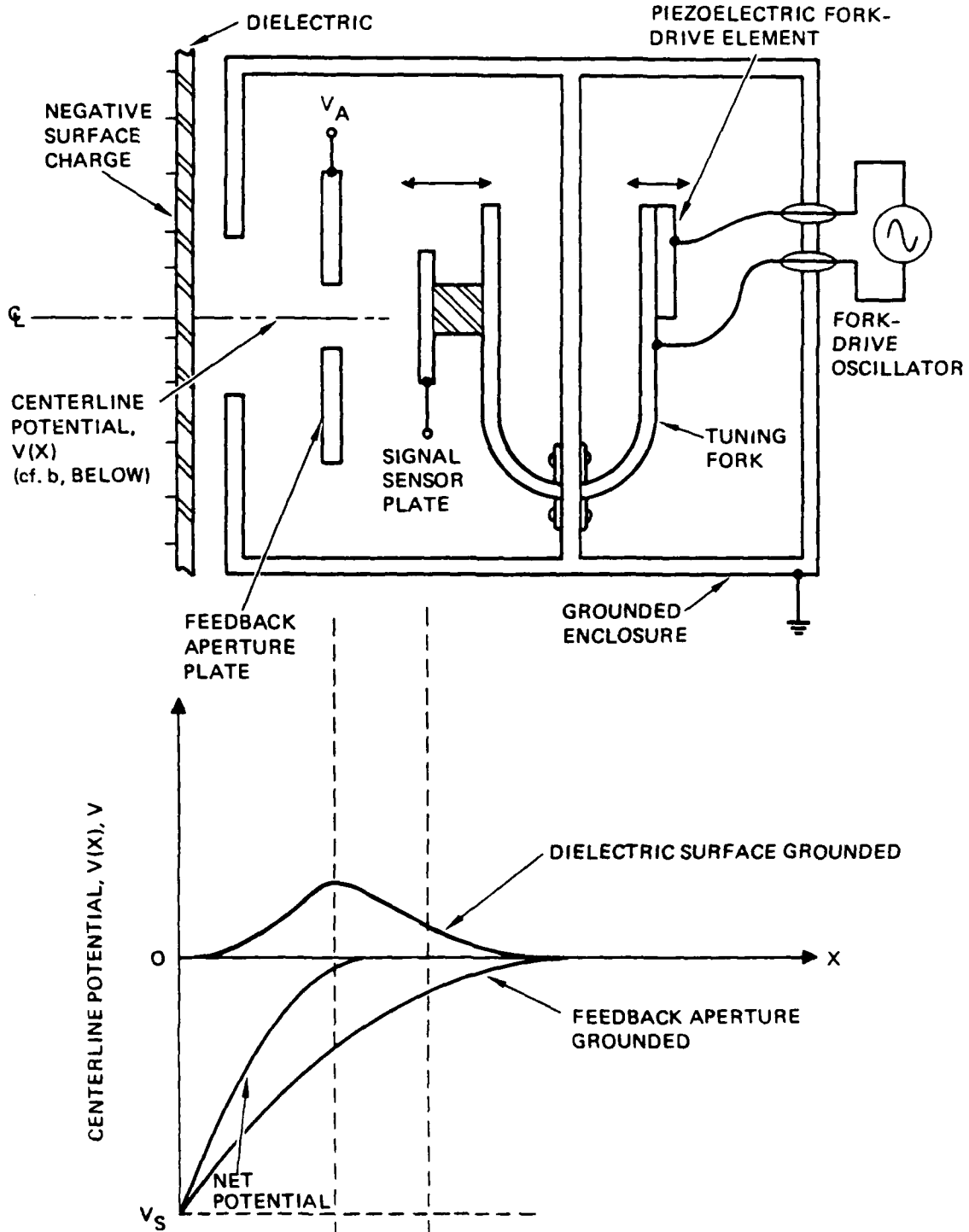
Figure 4-1. Functional operation of the vibrating
electrode surface potential monitor.

potential curve which is influenced both by the potential on the dielectric surface and by the potential on the aperture plate. The associated electronics varies V_A in a manner that maintains the potential at the signal sensor plate location equal to zero.

A cross section of the breadboard sensing head is shown in Figure 4-2. The input electrode with the dielectric material on its surface (a and b) is insulated from the rest of the instrument by a ring of G-10 glass epoxy. No electrical connection is made to this electrode. The potential of the front surface of the dielectric is transferred to the input electrode by capacitive coupling. Therefore, if the input electrode is to closely track the dielectric front surface, the capacitance from the input electrode to ground must be much smaller than the capacitance between the dielectric front surface and the input electrode. Creepage paths must also be kept long to support the 20 kV that may appear on the input electrode without bleeding the charge from it.

Sensing of the field is done using a vibrating electrode driven by a tuning fork (g). Above the sensing electrodes are two compensating electrodes (d and e) with holes of appropriate size for controlled penetration of the electrostatic field created by the charge on the collector plate. As it vibrates, the sensing electrode generates a displacement current that is proportional to the net field and at the vibration frequency. The phase of this signal is determined by the polarity of the net field. The field at the sensing electrode is nulled to zero by driving the first compensating electrode (d) for the low range or both compensating electrodes (d and e) for the high range to a voltage inversely proportional to that producing the field. By proper selection of the geometry, particularly the hole sizes in the compensating electrodes, the electrostatic field created by the charge on the collector plate can be tailored to permit nulling the maximum field with a maximum of 10 V applied to the compensating electrode(s).

14881-8
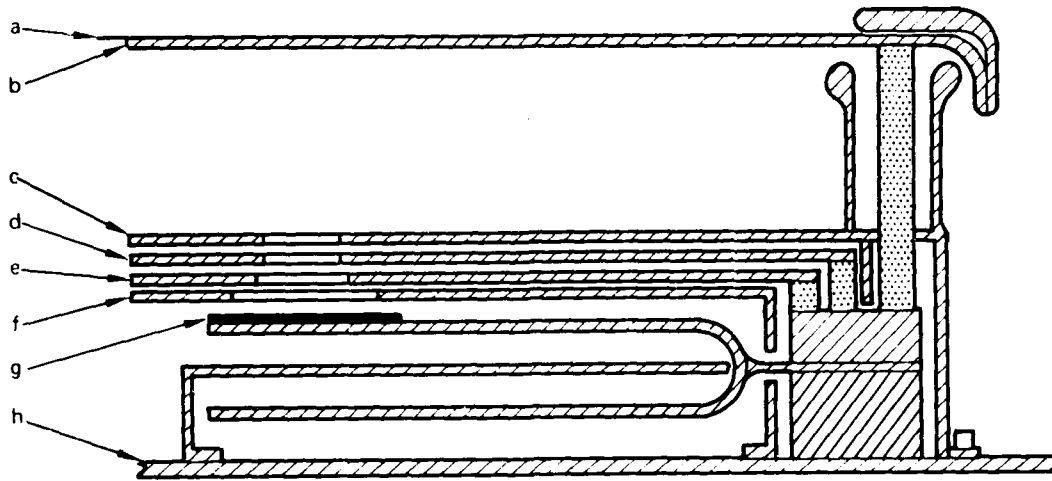
a = DIELECTRIC SAMPLE

b = INPUT ELECTRODE

c = GROUNDED SHIELD

d = 1ST COMPENSATING ELECTRODE

e = 2ND COMPENSATING ELECTRODE
    (GROUND FOR LOW RANGE)

f = GROUNDED SHIELD

g = SENSING ELECTRODE (BONDED TO TUNING FORK)

h = GROUNDED MOUNTING PLATE

Figure 4-2.   Schematic cross section of the breadboard SPM
              sensor head design (not to scale).

To provide compensating-voltage multiplication factors of 200 in the low range and 2,000 in the high range, typical values of the crucial parameters (aperture/electrode diameter d and separation s) for this design are as follows (see Figure 4-2 for notation): d(c) = 8.4 mm, d(d) = 8.7 mm, d(e) = 11.9 mm, d(f) = 20 mm, d(g) = 22 mm, and s(b-d) = 27.6 mm.

4.2 SPM ELECTRONICS DESIGN

A block diagram of the SPM is shown in Figure 4-3. The circuit is basically a servo-amplifier providing an output of 0- to ±10 V which is used to drive the sensed signal to a null. The signal from the sensing electrode is buffered by a high-input-impedance amplifier, amplified in two stages (preamplifier and voltage amplifier), demodulated by a phase sensitive demodulator, and fed back to the compensating electrode(s) through the integrating feedback amplifier and the autorange circuit. The output of the instrument is derived directly from the ±10-V feedback signal through the output buffer where it is attenuated by a factor of 4 and offset by 2.5 V to provide a 0- to 5-V telemetry signal corresponding to -2 kV to 2 kV or -20 kV to 20 kV. The range output from the autorange circuit indicates on which range the instrument is set.

A means of driving the tuning fork is also required. To get the maximum amplitude of oscillation with minimum power, the fork is driven at its self-resonant frequency. This is accomplished by deriving a feedback signal from the motion of the fork and using it to generate the drive. A pair of piezoelectric crystals are used as both the drive and feedback elements, and are mounted on the bottom tine of the fork. Piezoelectric drive, as opposed to magnetic drive, has the advantages of ease of shielding and the absence of external magnetic fields that might influence other spacecraft instruments. The limiting amplifier and the power amplifier comprise the remainder of the tuning fork drive oscillator.
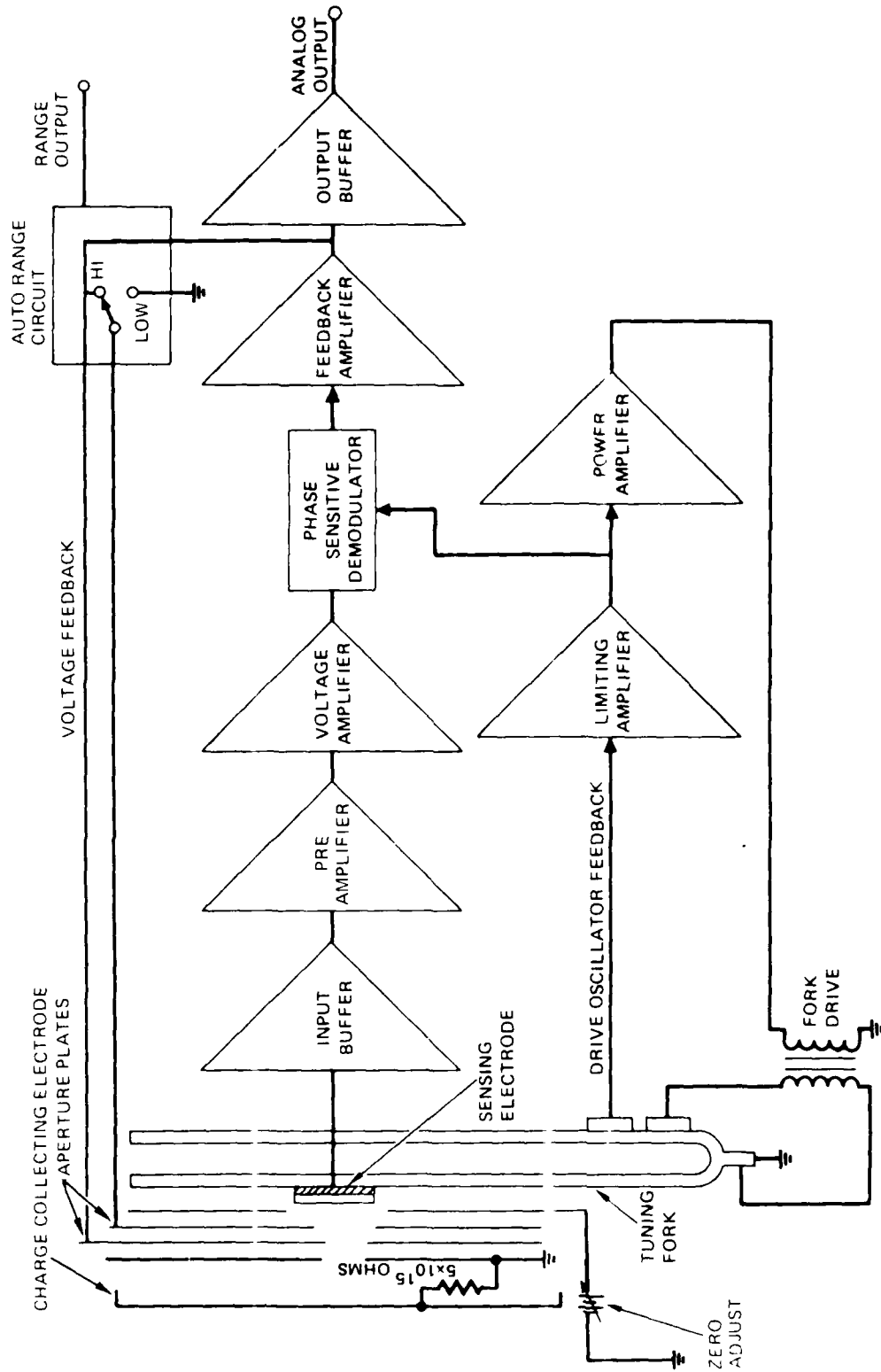
Figure 4-3. SPM block diagram.

13006-40R4

The schematic diagram of the SPM electronics is shown in Figure 4-4. Q4 is the input buffer; U2 is the preamplifier; U4 is the voltage amplifier; U5 is the phase-sensitive demodulator; U6 is the feedback amplifier; U7 is the output buffer; U3, U10, and U11 form the autorange circuit; U8 is the limiting amplifier; and U9 is the power amplifier.

4.3 BREADBOARD TEST RESULTS

The initial design of the breadboard SPM hardware was an open type of construction where the tuning fork and compensating electrodes were open to the environment. Vacuum chamber tests of this design showed a large and rapid zero shift whenever the electron gun, proton gun, or plasma source was operated. This zero shift would then gradually disappear over a period of hours, provided that none of the charged particle sources were operated. This zero drift was attributed to the buildup of charged particles within the sensing head.

The sensing head was redesigned so that the tuning fork and attenuation plates are completely enclosed. Any openings in the sensing head are smaller than the Debye length of the highest density plasma environment expected. This design did not experience the zero drift described above. However, when it was operated in the configuration shown in Figure 4-5(a), the output of the SPM reached a plateau above which it would not go as shown in Figure 4-6. This was attributed to scattered or secondary particles impinging on the input electrode, causing secondary emission, and preventing the electrode potential from increasing above the plateau value (even though the Kapton dielectric front surface was above the plateau value). The configuration in Figure 4-5(b) did not experience this problem since scattered or secondary particles or local plasma cannot get to the input electrode.

Figure 4.4. Schematic of the SPM electronics.

15816-2
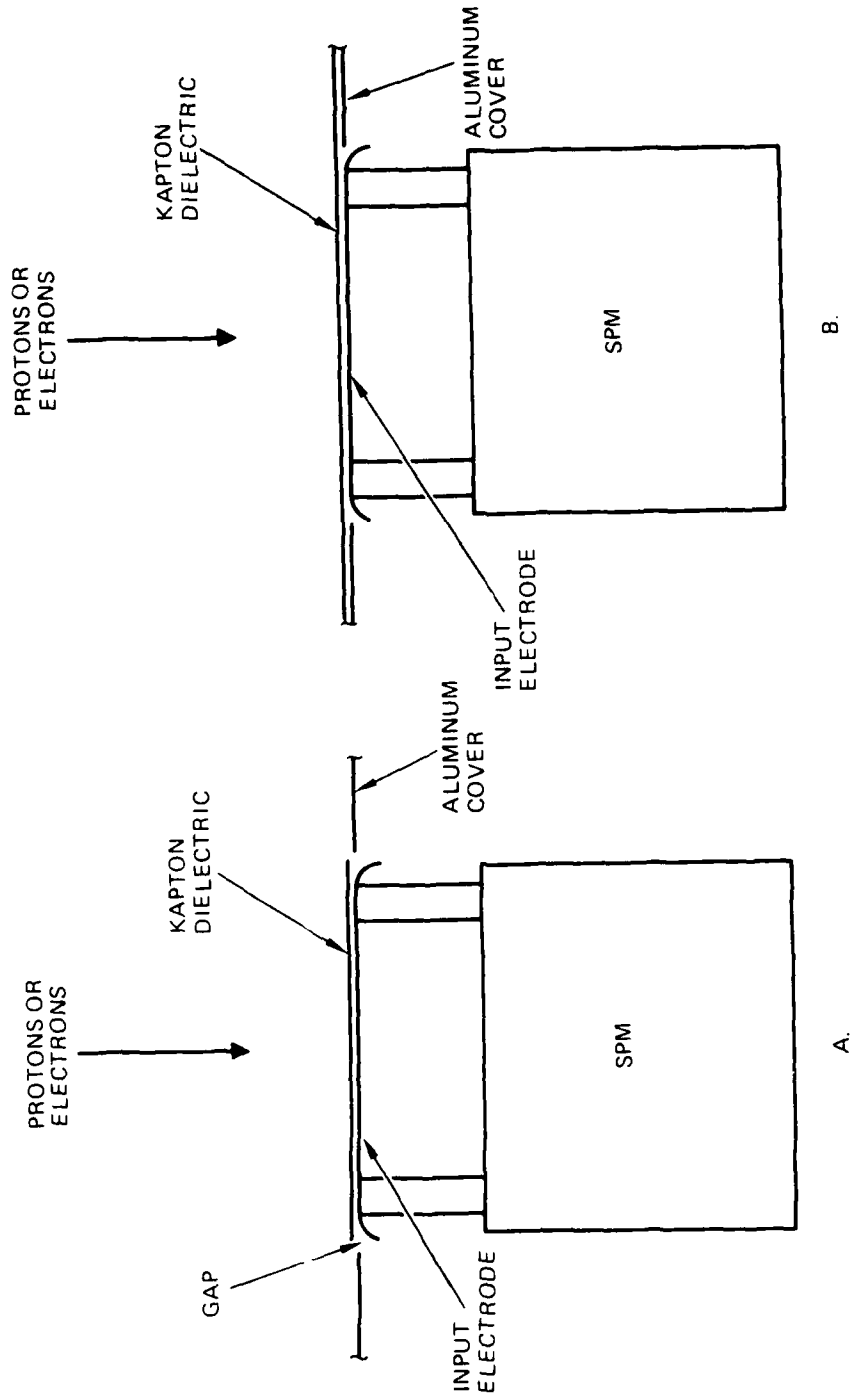
Figure 4-5. Test configurations for the breadboard SPM.
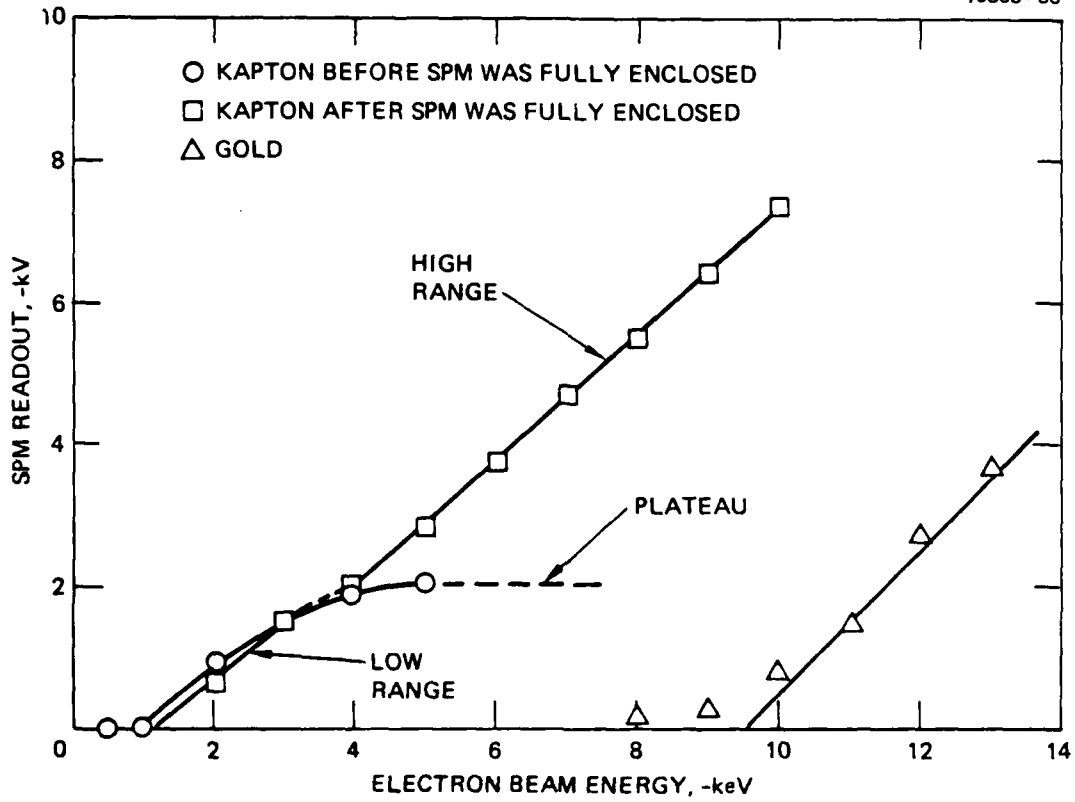
Figure 4 6.   Calibration data for the breadboard SPM.

On separate occasions, the SPM was exposed to a monoenergetic electron beam with two types of material on its input electrode; gold and Kapton. As is typical, the gold did not start to charge until the energy of the electron beam was between -9 and -10 keV (Figure 4-6); it linearly increased with increasing energy thereafter. The Kapton started to charge when the electron energy reached -1.1 keV, and then linearly increased with increasing energy. Activation of the plasma source returned the Kapton surface to near zero potential with the electron beam ON or OFF. The plasma source was not available at the time the gold surface was tested; however, other tests have shown that a plasma source will discharge a gold surface.

4.4 FLIGHT SPM DESIGN

The flight SPM has been designed to simulate the configuration of Figure 4-5(b) since this is the only configuration that responded properly under all of the conditions tested. Figure 4-7 shows the flight design where the input electrode is now supported by an annular insulating ring from the side rather than from below, as in the breadboard design. This allows the dielectric sample to extend past the input electrode onto the annular insulating ring, thereby shielding it from any particles or plasma that are in the immediate area. The compensating electrodes and tuning fork are mounted in a manner similar to the breadboard and the electronics are contained on two printed circuit cards mounted in the lower portion of the housing. The flight electronics design is the same as the breadboard design.

The flight SPMs are to be delivered with a choice of six different front-surface materials. The front-surface material will be changed by replacing the annular insulating ring, input electrode, and front-surface material as an assembly. Six assemblies will be manufactured which can be easily installed at any time. The present selection of front-surface materials is pure Kapton, Kapton with conductive black paint, Kapton with white paint, solar cells, front-surface radiator mirrors, and a floating conductor (material to be determined).
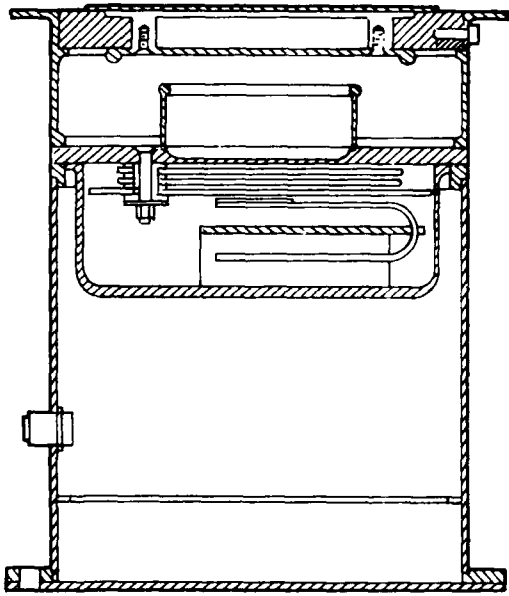
15866-02
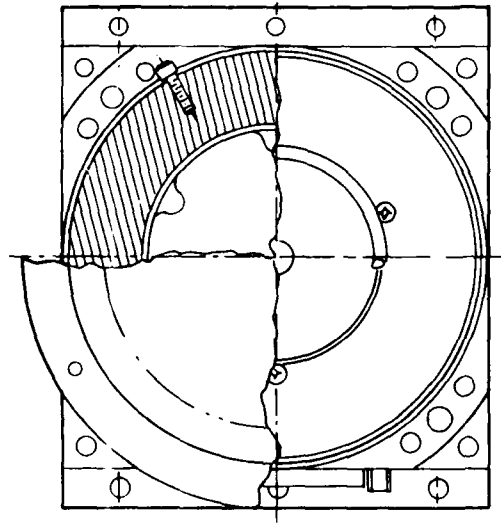
Figure 4 7. Flight package des'gn for the SPM.

A possible problem with the SPMs is that the input electrode could gather some charge not related to the potential of the dielectric front surface. This charge would then introduce a zero offset into the SPM. The breadboard design called for a shorting relay and software routine that would connect the input electrode to ground when the SPM was in full sunlight. Under full sunlight conditions, the dielectric front-surface should be within 100 V of ground; therefore, the SPM would be zeroed to within 100 V. This scheme required that the spacecraft periodically rotate the SPMs into full sunlight; a small, lightweight 20-kV relay turned out to be a significant engineering problem.

The flight design calls for deleting the relay and using a 2-h time constant to discharge the input electrode. A 2-h time constant requires about 5×10^{15} Ω from the input electrode to ground, which can be the leakage of the annular insulating ring. A normal operating scenario will be that differential charging exists which will charge the front surface of the dielectric, and the input electrode will go to the same potential. The 2-h time constant will start to bleed the charge from the input electrode; however, differential charging normally occurs in minutes, and if it is of any significant level, the plasma source will be turned ON. The plasma source will immediately remove the charge from the front surface of the dielectric and return it to ground. The 2-h time constant will then reset the input electrode to ground. The problem with this approach is that very slow differential charging will not be detected by the SPMs.

SECTION 5

TRANSIENT PULSE MONITOR

The transient pulse monitor (TPM) is included as part of the FMDS to detect the onset of arcing on spacecraft surfaces. The main criterion for the selection of the TPM sensor design is the requirement to maximize the ability for discrimination between signals generated by arcing events and signals resulting from "legitimate" spacecraft circuit transients. A secondary consideration is the necessity to register arcs occurring anywhere on the spacecraft surface with a minimum number of sensing elements.

A review of the literature revealed the main types of effects caused by arcing on a spacecraft:

(1) The arc causes "blowoff" of a cloud of electrons which rapidly disperses. This geometrical change causes a pulse of electrostatic field which can be detected by capacitive coupling to an electrometer plate. This electrostatic field can be detected, weakly perhaps, beyond the line of sight.

(2) The arc creates a plasma which radiates at high frequency, causing a pulse of wideband rf energy to appear, with its source in the plasma cloud and randomly polarized. This energy can be detected by antennas (horns, dipoles, monopoles, etc.); for the most part, the radiation can be sensed in line of sight only.

(3) During the pre-arc stage an increasing electrostatic potential appears (probably at the surface) of dielectric materials. The arc causes a substantial collapse of this potential, which can be detected by capacitive coupling to an electrometer plate. The width of the detected pulse is determined by the low frequency response of the detection equipment rather than by any characteristic of the arc signature itself. The collapse of the potential can be detected beyond the line of sight.

(4) The arc causes replacement currents, which can be detected by current sensors, to flow in the conducting skin of the satellite.

Effect (4) has been employed on several satellites (e.g., SCATHA and Canadian Technology Satellite) as a means of detecting arcs. The major problem encountered with this technique is the inability to differentiate between arcs and legitimate spacecraft transients, particularly in real time. Therefore, it was not seriously considered for this application.

The remaining effects can be classified by the type of detector required. Effects (1) and (3) utilize an electrometer plate (E-field antenna) which is broadband, while effect (2) requires an rf antenna, which is narrowband. The relative merits of these two detection methods are as follows:

- If only a single detector with a single antenna outside the Faraday cage of the spacecraft is used, the ability to discriminate correctly between arcs and transients appears to be equally limited for both detection methods.

- A single broadband antenna is more likely than a single rf antenna to pick up a detectable signal from an arcing event occurring at a location that is far below the horizon of the antenna; i.e, far from having a line of sight connection with it.

- Regardless of the detection method, the addition of a second antenna inside the spacecraft Faraday cage, in conjunction with a simple pulse-analysis circuit, offers a much increased probability of correct discrimination between arcs and transients by permitting a comparison between the signals received inside and outside of the Faraday cage.

- It is more likely for the signals received by two broadband antennas, rather than for those received by two rf antennas, that their amplitude ratios will characterize arcs and transients properly, irrespective of the location of the event relative to that of the antennas.

- Additional practical points in favor of the broadband approach are the ease of protection from destructive overloads resulting from arcs adjacent to the antenna, and the lower power consumption.

The TPM design for FMDS is based on the broadband detection approach utilizing a 123 cm^2 E-field antenna outside of the spacecraft Faraday cage connected to a 250-Hz to 75-MHz broadband amplifier and pulse analysis circuitry, and a second 123-cm^2 E-field antenna with greatly simplified pulse analysis capabilities inside the Faraday cage. The design is discussed in more detail in the following sections, along with some test results.

5.1 TPM DESIGN

The TPM consists of two remote signal sensors and microprocessor-based pulse analysis circuitry, as shown in Figure 5-1. The remote signal sensors each consist of a 123-cm^2 plate driving a buffer amplifier (U1 of Figure 5-2). These remote sensors are connected to the TPM electronics unit via a coaxial signal cable and wires for ±5-V power. The sensors act as capacitive potential dividers from the electrostatic field of the arc to the spacecraft frame. The scaling input capacitors of 45 pF (parasitic capacitance of the wiring and U1) or 1,400 pF (C4) to ground are selected by a relay (K1) to provide two dynamic ranges of 10 to 300 V/m and 300 to 10,000 V/m. The input signal to the buffer has a dynamic range of ±0.025 to ±0.75 V. The mechanical design of the sensor is shown in Figure 5-3.

The TPM electronics unit contains the circuitry to detect positive and negative pulses above a commandable threshold setpoint, the pulse width of signals above threshold, and the positive and negative peak amplitudes. D/A converters set the threshold levels, a multiplexed A/D converter is used to convert analog signals to digital, and a dedicated microprocessor controls the TPM and exercises the transient pulse algorithms for arc discrimination.

The threshold detectors are fast comparators (AR10 or AR12 of Figure 5-4) that compare the positive and negative pulses with the commanded threshold setpoints and produce an "above-threshold" logic signal. The comparators each drive an RS latch (U11 or U12) which provides a 5 ms lockout before another pulse
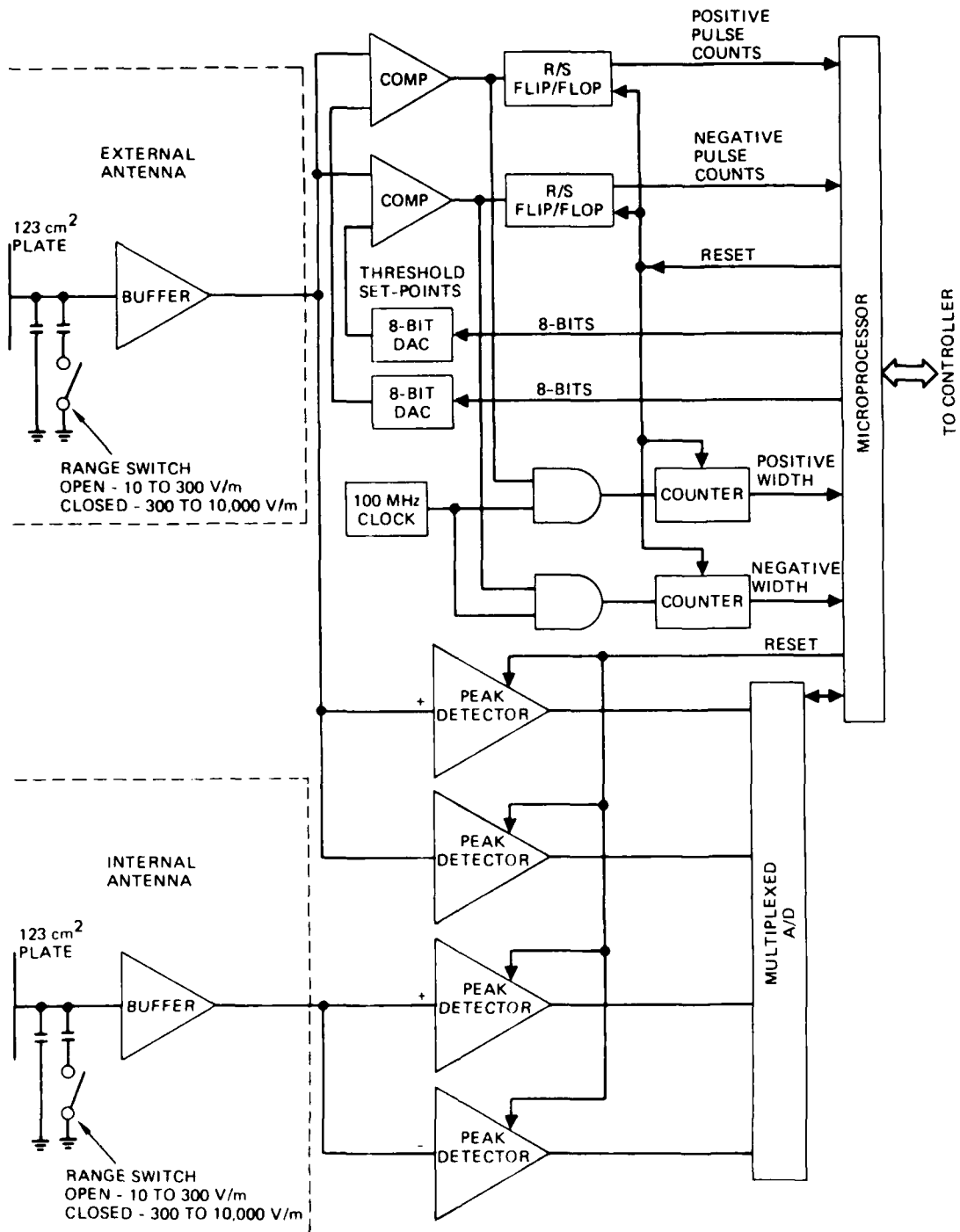
Figure 5-1. Block diagram of the TPM.

Figure 5.2. Schematic of the TPM input buffer.

15866—30

123 cm^2 SENSING PLATE

GROUNDED
SHIELD

PC CARD WITH BUFFER
AMP AND RANGE SWITCHING

CONNECTOR
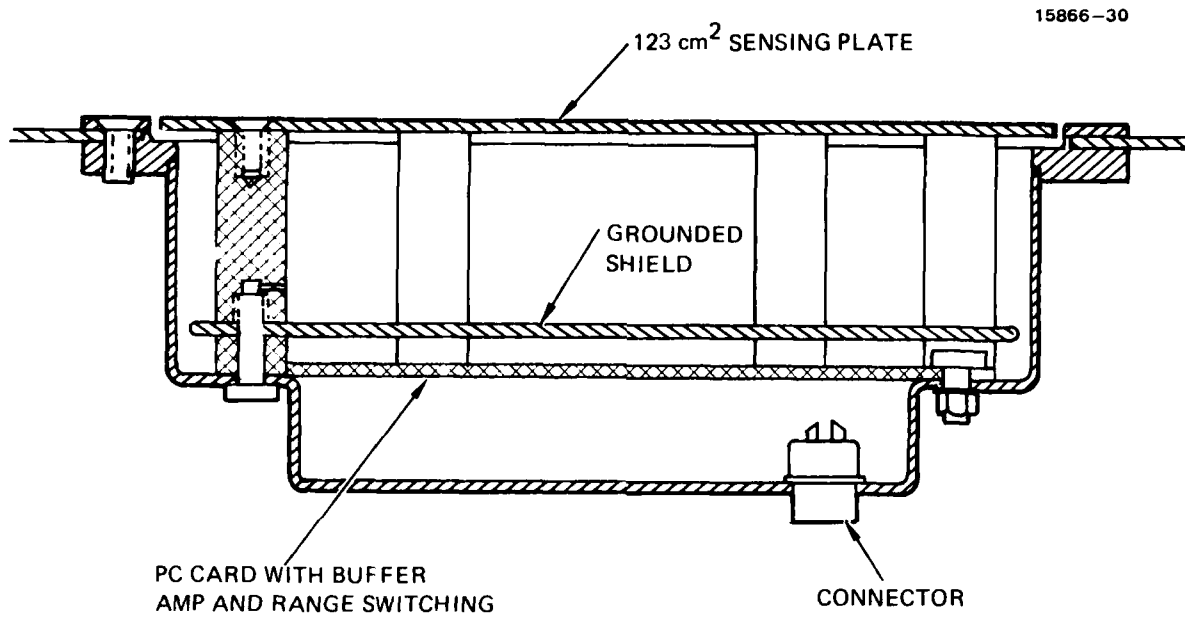
Figure 5 3.   Cross section of the TPM sensor head.
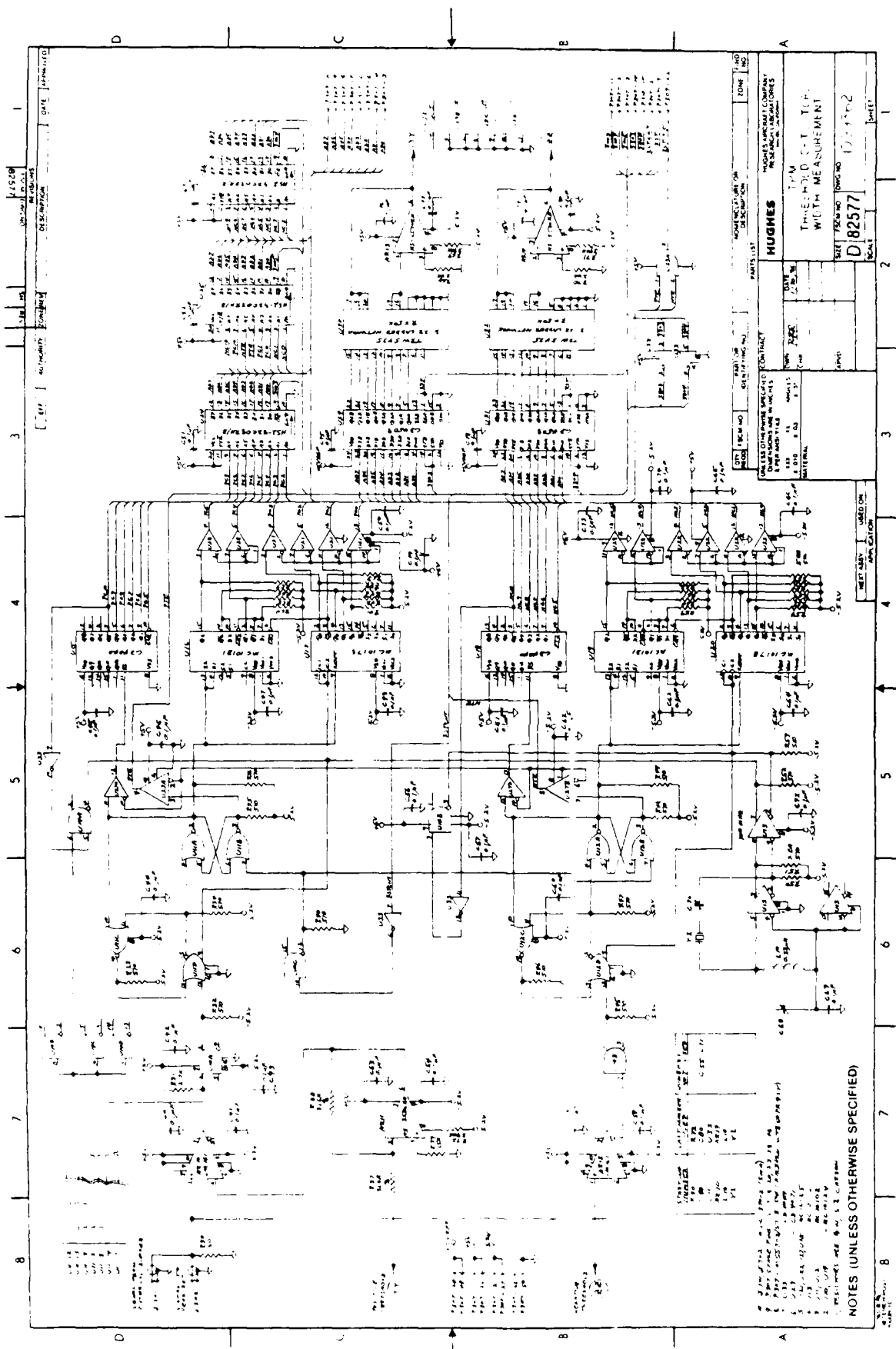
Figure 5-4. Schematic of the TPM threshold detectors and width measurement circuitry.

can be detected. The microprocessor resets the RS latch after 5-ms and also stores the pulse count in memory. The positive and negative threshold levels are set by digital-to-analog converters (U29, U30, and AR13, or U31, U32, and AR14).

The pulse width detectors use the "above-threshold" logic signal to gate a 100-MHz clock (U13) into a counter (U15, U16, and U17, or U18, U19, and U20). The counter then counts until the signal pulse drops back below the threshold setpoint at which time the 100-MHz clock is gated OFF. The width of the pulse is then the counts in the counter times 10 ns. The microprocessor stores the counts in memory (via bus buffers U24, U25, and U26) and resets the counter at the end of the 5-ms lockout.

The peak-amplitude detectors each consist of three stages of peak amplitude detection where the first stage (AR1 and C2, or AR4 and C12 of Figure 5-5) has a very fast risetime and consequently a rather fast decay time. The second stage (AR2 and C6, or AR5 and C16) has a slower rise time and hence a slower decay time, but is fast enough to detect the peak amplitude reached by the first stage. The third stage (AR3 and C7, or AR6 and C17) is slower yet, and has a decay time which is slow enough to allow the microprocessor to read the peak amplitude by means of the A/D converter. The peak amplitude detectors are really three stages of a peak-reading voltmeter which allow the amplitudes of 20-ns to 10-μs pulses to be read by the microprocessor. The output signals of the four peak detectors are multiplexed (U1 and U2) and sent to an analog-to-digital converter. The detectors are reset to zero at the end of the 5-ms lockout.

The microprocessor and its interfaces consist of a radhard 80C85 (U40 of Figure 5-6) with 2K of CMOS RAM (U53), 2K of CMOS EEPROM (U52), 2K of CMOS PROM (U48, U49, U50, and U51), an 8-bit A/D converter (U60, AR20, U61, and U62), and a parallel interface to the system controller (U55, U56, U57, and U58).
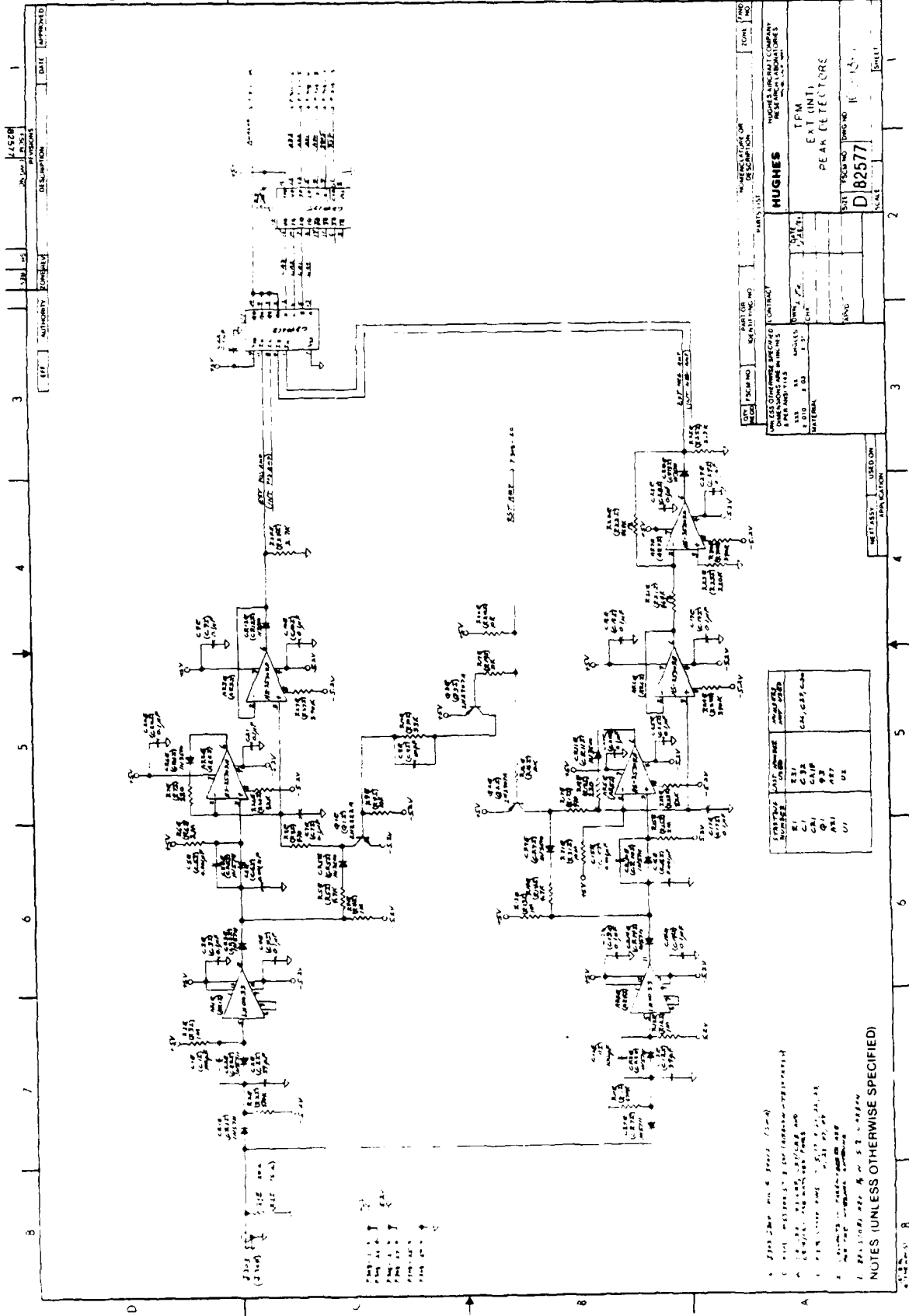
Figure 5.5. Schematic of the TPM peak amplitude detectors.
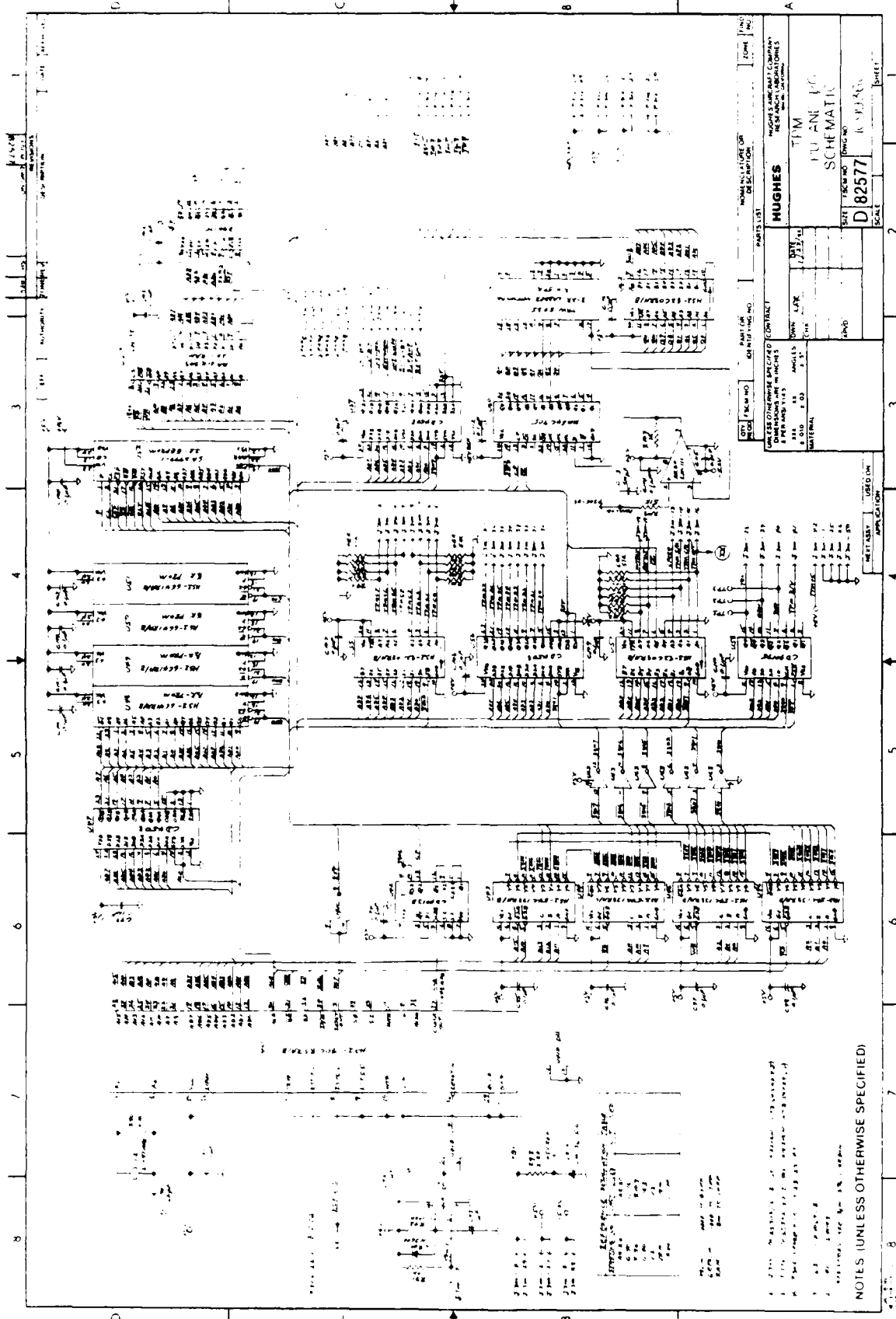
Figure 5.6. Schematic of the TPM microprocessor.

Telemetry data provided by the TPM is measured any time that the external signal is above the threshold setpoint (whether caused by an arc or a spacecraft transient) and is accumulated over a 4-s time period. The data provided by the TPM are as follows;

Data from the external antenna:

- Number of positive pulses above threshold

- Number of negative pulses above threshold

- Amplitude of the largest-amplitude positive pulse

- Amplitude of the largest-amplitude negative pulse

- Width of the largest-amplitude positive pulse

- Width of the largest-amplitude negative pulse

- Amplitude of the widest positive pulse

- Amplitude of the widest negative pulse

- Width of the widest positive pulse

- Width of the widest negative pulse.

Data from the internal antenna:

- Amplitude of the internal pulse corresponing to the largest-amplitude external positive pulse

- Amplitude of the internal pulse corresponding to the largest-amplitude external negative pulse

- Amplitude of the internal pulse corresponding to the widest external positive pulse

- Amplitude of the internal pulse corresponding to the widest external negative pulse.

General data:

- Relay status (readback of relay setting command).

5.2 BREADBOARD TEST RESULTS

The TPM was tested in a metallic vacuum chamber using real arcs from a dielectric sample. The test setup for performing this test is shown in Figure 5-7. The dielectric sample was irradiated with a 15-kV monoenergetic electron beam, causing it to charge up and arc approximately every 15 s. The external antenna had full view of the vacuum chamber interior while the internal antenna was mounted behind a grounded plate. The replacement current to the dielectric sample and the output of the external antenna's buffer amplifier were viewed on an oscilloscope.

Typical waveforms and data produced by an arc are shown in Figure 5-8. The replacement current rings for approximately 1 μs and is zero from then on (Figure 5-8(a)). The buffer-amplifier output goes negative and then positive within 1 μs (Figure 5-8(a)), after which it rings out at a low frequency (Figure 5-8(b)). The initial negative and then positive signal is in response to the radiated E-field generated by the arc, and the low-frequency ring-out is the response of the flat-plate antenna and the buffer amplifier settling out to a lower steady-state E-field (the arc lowers the voltage on the dielectric sample and therefore lowers the E-field that it generates). We do not have enough data to determine if the low-frequency ring-out is associated with all arcs. If it is, then this might be a characteristic that could distinguish arcs from other spacecraft transients. Spacecraft transients would not be expected to change the steady-state E-field seen by the antenna.

The pulse-characterization circuitry interpreted the signal from the buffer amplifier as a negative pulse of 2.1 V and 100 ns, and a positive pulse of 1.11 V and 180 ns. Since the pulse-characterization circuitry is blanked for 5 ms after a pulse occurs, the low-frequency ring-out is ignored. The internal antenna picked up a signal that was lower in amplitude by a factor of >3 and therefore the algorithm of "external > internal" would have interpreted this data as an arc.

5-12
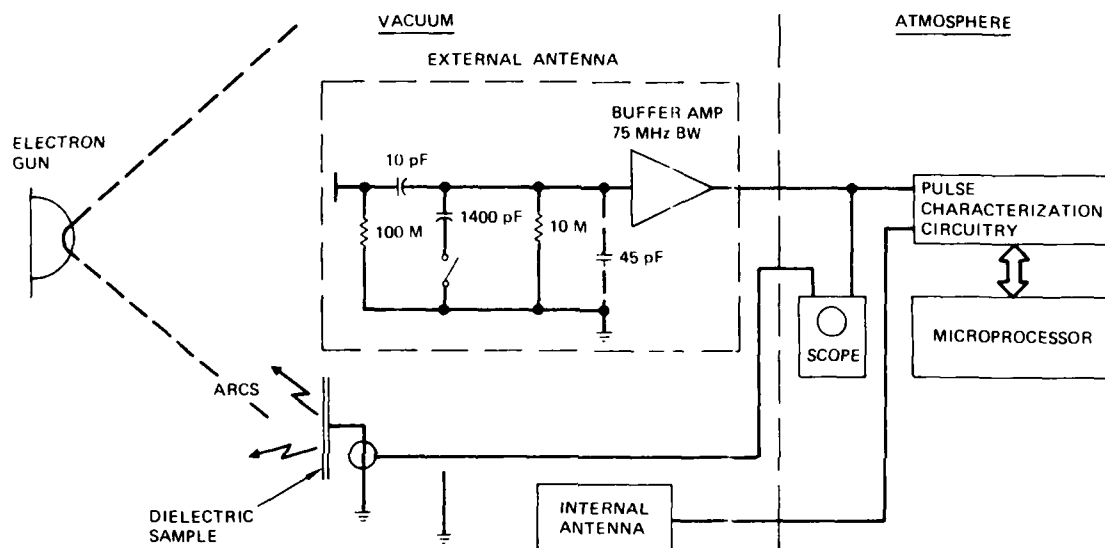
Figure 5-7. Test setup for testing the breadboard TPM in a
metallic vacuum chamber.
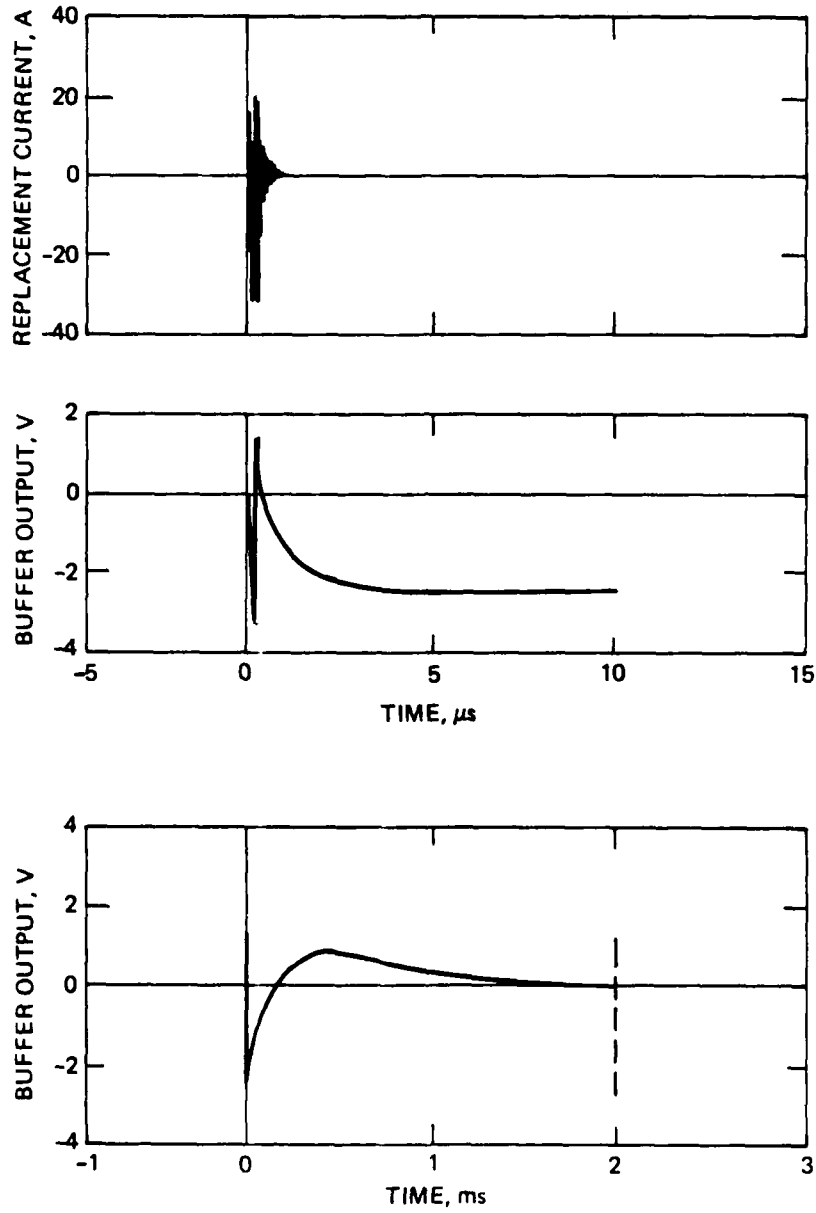
Figure 5-8. Typical waveforms produced by an arc.

5-14

A test was made to simulate a normal spacecraft transient where a 28-V dc relay coil was actuated. The TPM responded to this transient and the output of the buffer amplifier showed 1 to 2 μs of high-frequency noise, after which it was zero. The low-frequency ring was not present. This particular test was not performed in a manner suitable to evaluate the "external > internal" algorithm.

The TPM was also tested with pulses of known polarity, amplitude, and width injected into the pulse characterization circuitry, and with arcs created inside the vacuum chamber as part of the breadboard demonstration. The telemetry data read out on the GSE correlates closely with the injected pulses. When arcs were created inside the vacuum chamber, both the internal and external antennas detected the arcs. The amplitude detected by the external antenna was ~1.5 times higher than the amplitude detected by the internal antenna; therefore, the "external > internal" algorithm determined that it was an arc.

The cables between the two antennas and the electronics were interchanged so that the electronics for the internal antenna would receive the larger of the signals when an arc occured. The algorithm determined that it was "not an arc" since the internal signal was larger than the external signal. In this configuration the TPM never detected what was interpreted as an arc.

SECTION 6

CONTROLLER

The controller provides for autonomous control of the FMDS relative to the remainder of the satellite and also ties the other units of the FMDS together. The "brain" of the controller is a microprocessor which contains the algorithms necessary to interpret the data from the sensors and command the plasma source to turn ON when spacecraft charging is occurring. It then monitors the operation of the plasma source and maintains it in stable operation. The controller turns the plasma source OFF after either a programmable time-out, when the emission current from the plasma source has been less than a threshold value for a specified period of time, and/or the ambient electron environment returns to a quiescent condition. The controller has the ability to accommodate certain instrumental faults and failures and to adjust instrument parameters. It is also the command and telemetry interface with the satellite.

In this section we describe the hardware design and software architecture for the FMDS Controller. Flow charts of the major software routines and algorithms are also presented.

6.1 CONTROLLER HARDWARE DESIGN

Figure 6-1 shows the hardware architecture of the FMDS controller. It is designed to survive 10 years at geosynchronous orbit from both a reliability and radiation standpoint. It contains a watchdog timer for CPU errors; redundant storage, error checking, and correction for RAM bitflips; instrument mask, powerdown, and subroutine timer for instrument failures; EEPROM write capability for algorithm faults; and redundant command checking and command interlock for command errors or bitflips during transmission. It does not contain any hardware redundancy.

The design employs two separate HS80C85RH microprocessors: one microprocessor ("ESA") services the ESA, producing a "vehicle
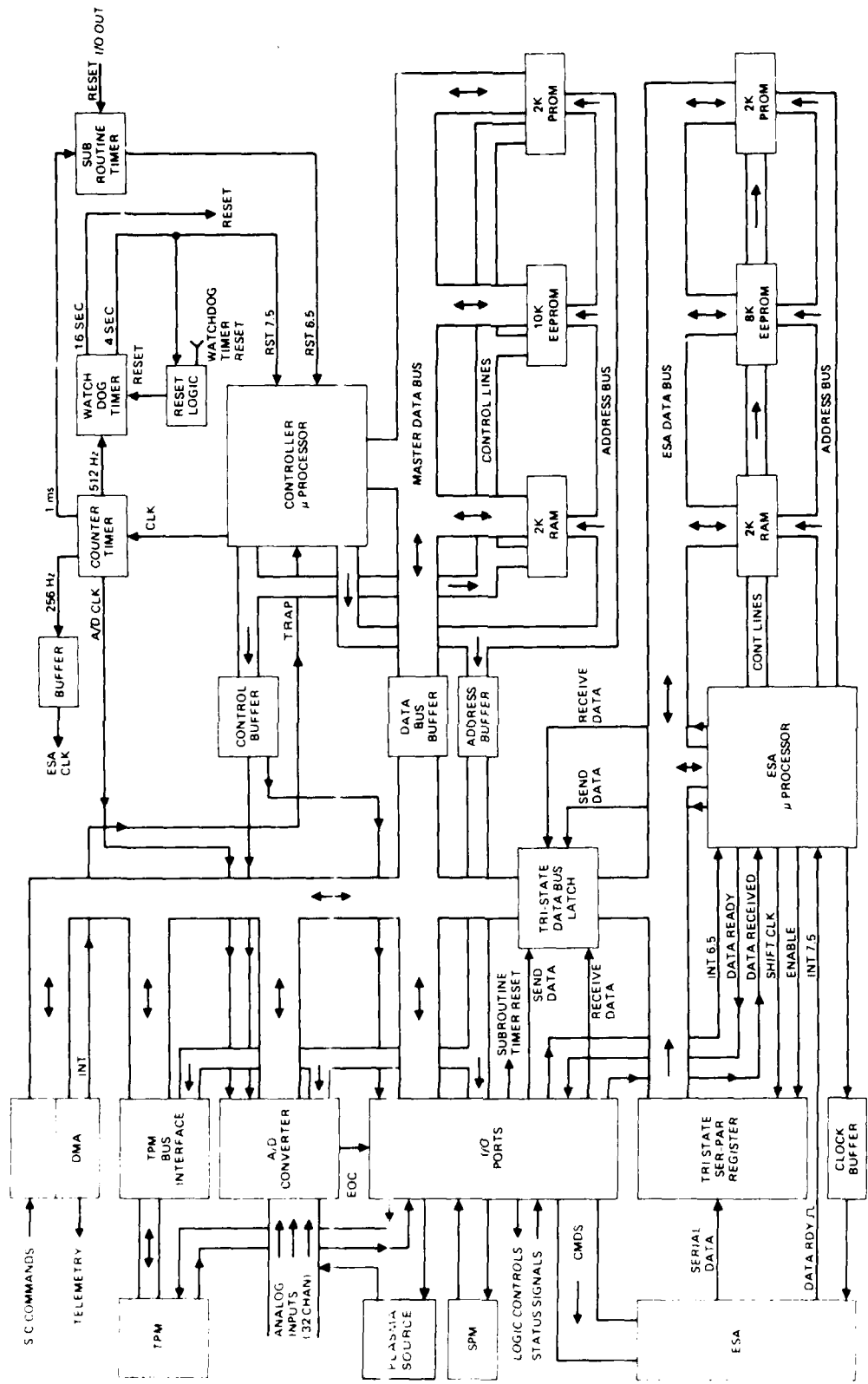
Figure 6-1. Block diagram of the FMDS controller.

potential" signal; the second microprocessor ("master") serves the functions of operating the plasma source, maintaining command and telemetry contact with the spacecraft, and determining when to activate the plasma generator based on inputs from the ESA processor, SPMs, and TPM. This two-processor approach was chosen because the comparatively heavy total computational requirement (which is dominated by processing ESA spectra to determine the vehicle potential) makes it unlikely that a single microprocessor can handle the job. The use of one processor for the single activity of processing ESA data is a logically desirable approach which avoids excessive interrupts of the multitasking executive routine.

EEPROM (Electrically Erasable Programmable Read Only Memory) is used instead of the combination of PROM (Programmable Read Only Memory) and RAM (Random Access Memory) that we have used in previous spaceborne systems such as the IAPS (Hughes/NASA-LeRC Ion Auxiliary Propulsion System). In these previous systems, default setpoints and logic decision thresholds were contained in PROM and were copied into RAM on system powerup. The RAM values were the ones that were actually used by the system, thus permitting new values to be uploaded into RAM from the ground (with a RAM-write command). Because of the extent of this RAM and the critical nature of its contents, separate error-correcting hardware was required to avoid system errors which could result from cosmic-ray-induced bitflips. The approach for the FMDS controller exploits the availability of the new radiation-hardened CMOS EEPROM from Sandia (SA2999). Both the FMDS operating algorithms and the default setpoints are housed in the EEPROM. This approach has several substantial advantages: (1) the amount of RAM is minimized; (2) the probability of bitflip-generated hazards to the system is small enough that separate error-correcting hardware is not required, and a simpler measure provides more than adequate protection (i.e., storing critical parameters in three locations and using majority voting); (3) virtually all parts of the software can be rewritten from the ground, rather than just selected setpoints; and (4) a

system reset or power outage will not cause unwanted default set points to reappear (as is the case with the IAPS controller). The Sandia EEPROM is specified for 10,000 erase/write cycles and a 10-year retention period. These are entirely adequate to fullfill FMDS objectives.

The PROM contains routines that are very basic and critical to operation of the system (initial boot up, commands and telemetry, and EEPROM rewrite). If these routines were in EEPROM and the wrong location was accidentally written to, it could very well be a catastrophic mistake.

Telemetry data to the spacecraft is provided when it is requested by the spacecraft. This is done with DMA (Direct Memory Access). The DMA approach offers a simple interface with flexible timing to the spacecraft. The controller will accept one command byte every cycle (every 4 s). If commands are sent at a faster rate, then some of the command bytes will be lost.

The controller also contains I/O ports for the transfer of digital data between itself and the other units (ESA, SPMs, TPM, and plasma source) and a multiplexed analog-to-digital converter for digitizing analog parameters from the other units.

The master micropocessor schematic is shown in Figure 6-2, where U1 is the radiation-hard 80C85 microprocessor; U2 is the lower 8-bit address latch; U3 and U4 are the RAM; U8, U9, U10, and U11 are the PROM; and U13, U14, U15, U16, U17, and U18 are the EEPROM. In addition, U19, U20, and U21 are memory chip select decoders, U12 is a latch that controls the erase/write of the EEPROM; U22 forces the correct address bits and control signals onto the bus for DMA; and U23 is a bidirectional address/data bus buffer.

Figure 6-3 shows the ESA microprocessor schematic, where U40 is the microprocessor; U48 is the RAM; U41, U42, U43, and U44 are the PROM; and U45, U46, and U47 are the EEPROM. The U52 is a latch controlling the EEPROM erase/write; U53 is the lower 8-bit address latch; U54, U55, and U56 are address decoders; and U60, U61, U62, and U63 are I/O ports to the master microprocessor. The serial to parallel shift register, U57, inputs data from the

Figure 6.2. Schematic of the master microprocessor.

Figure 6-3.   Schematic of the ESA microprocessor.
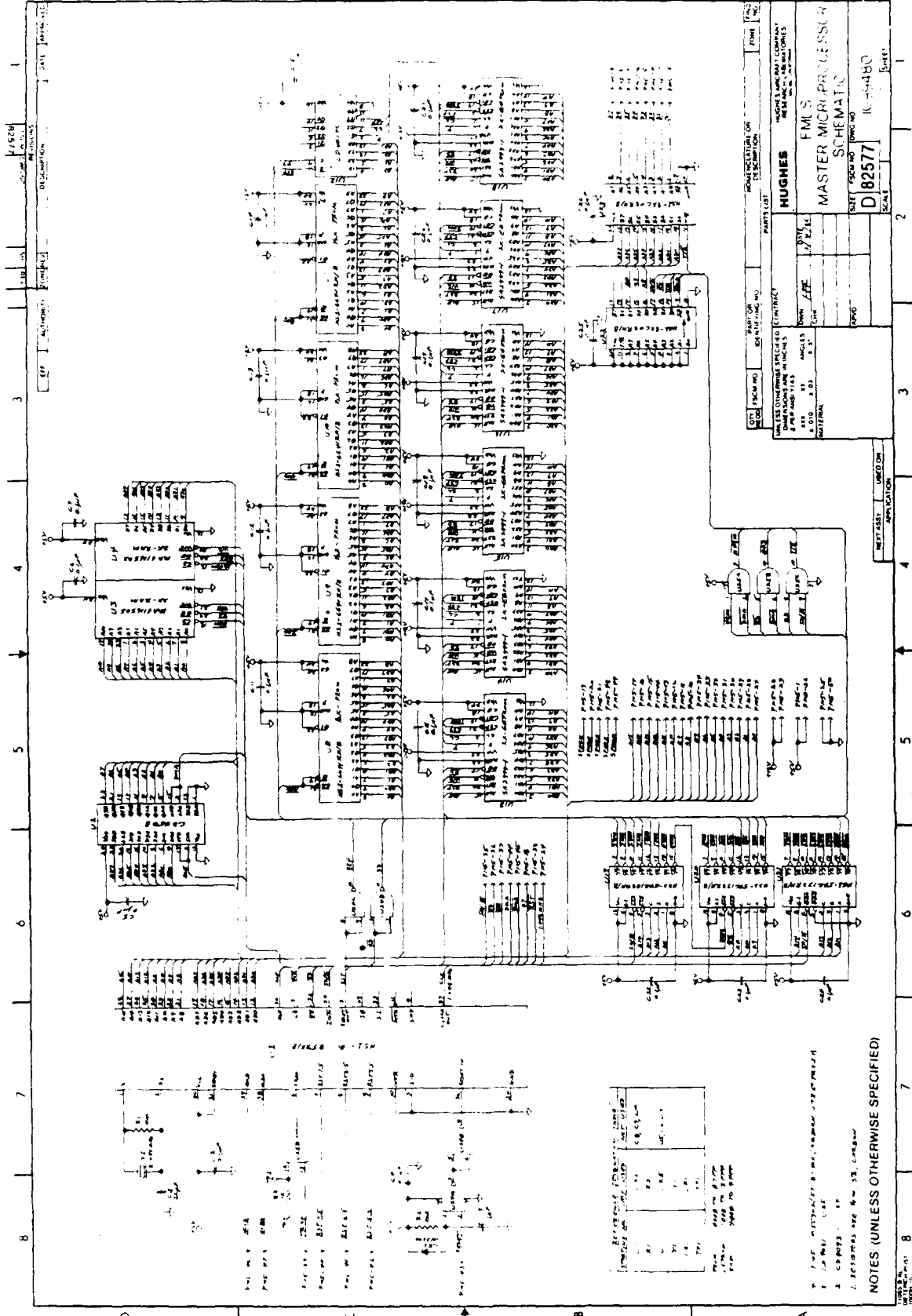
ESA, U58 is the ESA data input port, and U59 is an output port to the ESA for the data clock and to the master microprocessor for handshaking (ESA R/V).

I/O address decoding is provided by U134, U135, U136, and U137 of Figure 6-4. Output ports U132 and U133 are used for the digital commands to the ESA, U130 is the output port for turning the valves and inverters ON/OFF, and U131 is the output port for turning the sensors (ESA, SPMs, and TPM) ON/OFF. Counters U139, U140, and U141 divide the clock signal from the master microprocessor for timing purposes, including the 4-s interrupt and watchdog timer. The subroutine timer and latching-solonoid timer are U143 and U144, respectively, with U142 being the latch to turn them ON/OFF.

The analog-to-digital (A/D) converter and more I/O is shown in Figure 6-5. U80 and U81 are 16-channel analog multiplexers (total of 32 channels), U83 is a sample-and-hold amplifier, and AR10, U84, and U85 comprise the A/D converter. U86 is the input port for the digitized analog data, U87 starts the conversion process, and U88 stores the channel address for the analog multiplexers. U82 is an output port that turns the plasma-source power supplies ON/OFF and selects their operating setpoint.

Figure 6-6 shows the interface with the TPM and the command/telemetry interface with the spacecraft. U111, U112, U113, and U114 are the I/O ports that transfer commands and data between the TPM and the master microprocessor. Optical isolation with the spacecraft for the command/telemetry interface is provided by U100, U101, and U102. It is assumed that the optical isolation for the telemetry data line will be provided on the spacecraft end of the interface and that U119 is a line driver to drive that optical isolation. U103, U106, and U108 are edge-triggered D-type flip/flops to provide noise immunity for the incoming signals. U104 converts the serial command byte to parallel and U105 is the command input port. Flip/flops U107 and U110 and shift register U109 control the DMA timing which is shown in Figure 6-7. U115 is the parallel-to-serial telemetry shift register, U116 is the counter that selects the telemetry
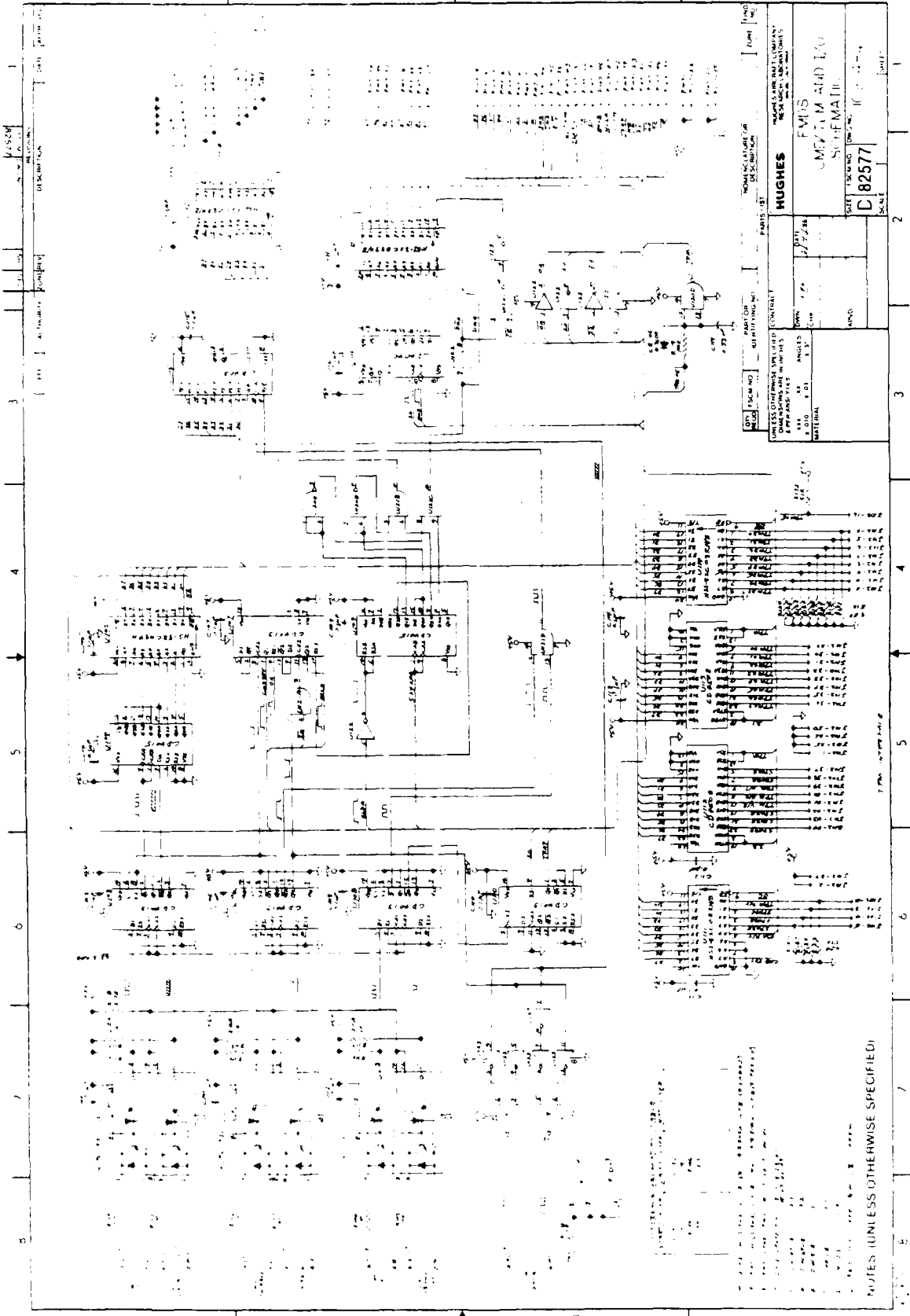
Figure 6-4. Schematic of the controller I/O circuitry.

Figure 6-5. Schematic of the analog-to-digital converter schematic.

Figure 6.6. Schematic of the command and telemetry circuitry.

Figure 6.7. Command and telemetry timing.
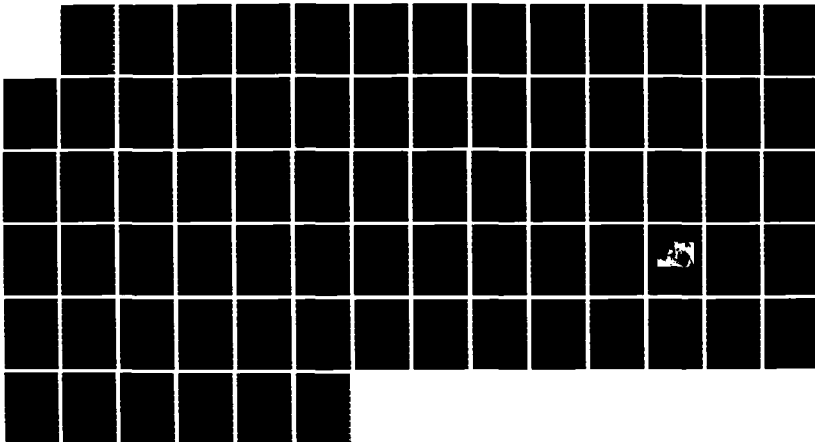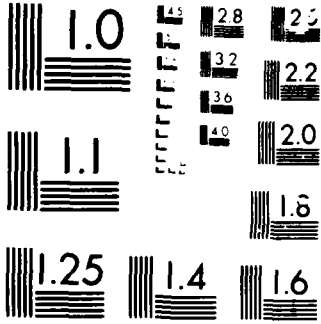
word for the DMA, and U118 is the port that forces the counter data onto the memory address bus. U117 is an input port for the SPM ranges, SPM sun sensors, and the ADC conversion complete (not CC) signal.

The command timing shown in Figure 6-7 is straightforward and involves a command-enable signal, a command clock, and the command data. The command-enable allows eight clock pulses to shift the eight data bits into the shift register. The clock can be either a continuous stream of pulses or an 8-bit burst. The trailing edge of the command-enable signal sets F/F U107A to indicate to the master microprocessor that a command has been received. U107A is reset by the master microprocessor after it has read the command. The commands that the FMDS will accept and the telemetry data it provides are listed in Appendix A.

The telemetry timing is more complex because of the DMA function. Whenever the spacecraft issues a frame-sync pulse, F/F U110A is set which interrupts the master microprocessor, causing it to load the DMA area of memory with a new set of telemetry data, provided the last set has all been sent. After updating the DMA memory, U110A is reset and a DMA cycle is initiated. F/F U107B is set which requests the bus from the master microprocessor. When the master microprocessor relinquishes the bus, shift register U109 is enabled which starts shifting "1s" down its outputs. These "1s" sucessively force the counter data into the address bus, clock the data in memory into the output shift register (U115), increment the DMA counter (U116), and reset F/F U107B which terminates the bus request, allowing the master microprocessor to resume operation. The first telemetry data word is now in the shift register and can be clocked out by the spacecraft at any time. When the present word is clocked out, the trailing edge of the telemetry enable signal will initiate another DMA cycle so that the next telemetry data word will be ready for the spacecraft.

The mechanical packaging of the controller will be on five PC boards which will be contained in a 4.3 in. x 6.0 in. x 5.5 in. box as shown in Figure 6 8.
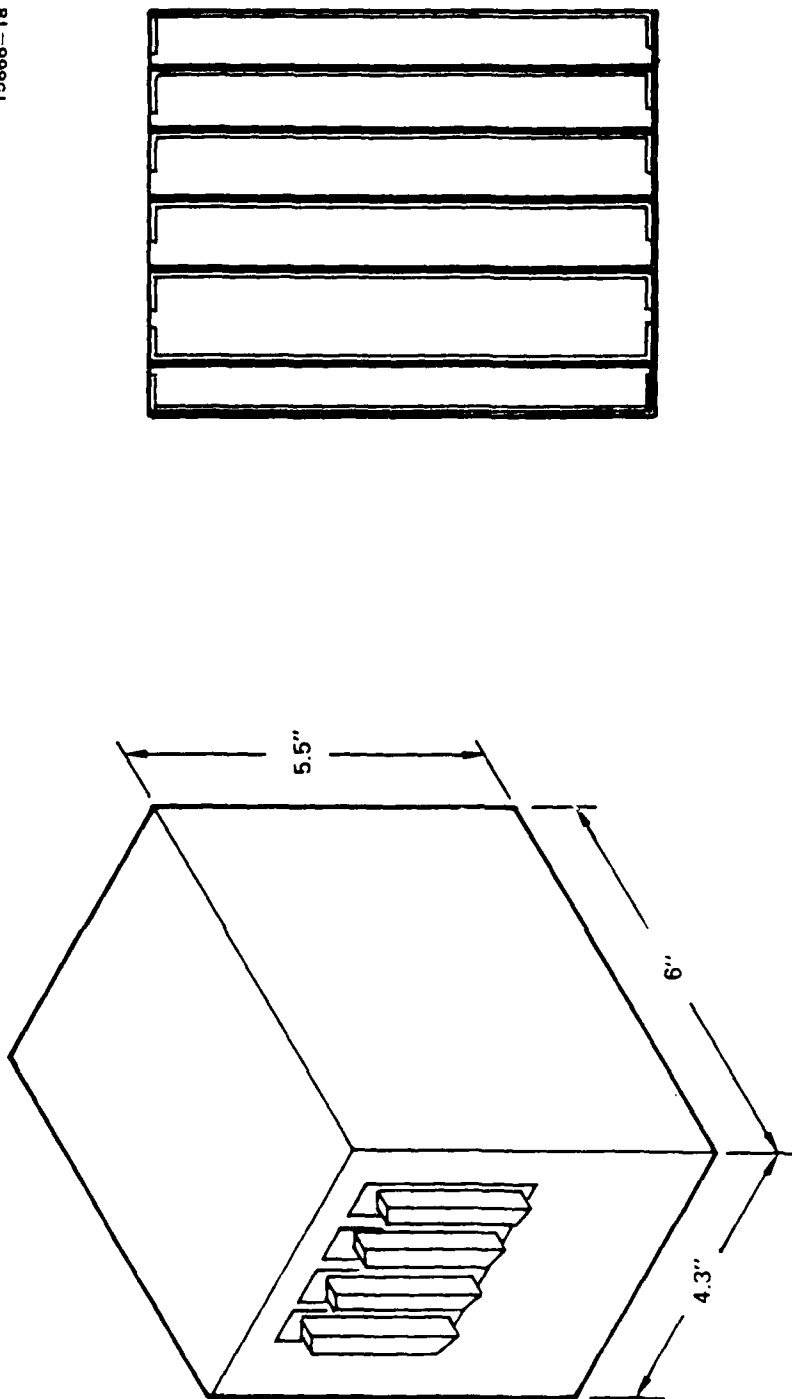
Figure 6-8. Mechanical packaging of the controller.

6.2 CONTROLLER SOFTWARE DESIGN

The software design is heavily modularized, consistent with
modern design practices. An "executive" routine is present,
which simply calls other modules in sequence. The advantage of
this approach is that individual modules can be altered, added,
deleted, or relocated with very little or very minor alteration
of the overall code. The software is realized in a machine-
intimate high-level language "C", but many portions are coded in
assembly language for additional speed and memory-use efficiency
requirements. A high-level language is used because it is
essentially self-documenting, while even well-documented assembly
coding is frequently impregnable and not maintainable.

The overall software architecture consists of the "Executive"
routine, shown in Figure 6-9, which is the controlling force of
the master microprocessor. This routine is called by the 4-s
interrupt (hardware implemented). Upon entering the routine the
4-s flag is checked and if it is set, this indicates that the
microprocessor did not have time to execute all of the executive
routine the last time before it was interrupted again by the 4-s
interrupt. This should not normally occur and if it does an
error flag is set. The "watchdog timer" is reset next (the
watchdog timer is implemented in hardware; if it is not reset at
least once every 16 s, it resets the entire system). The 4-s
flag is then set to indicate that we are in the executive
routine, after which all timers are decremented by 4 s. Several
subroutines are then executed to digitize the analog data,
service the TPM, and service the ESA microprocessor. A
subroutine timer exists which generates an interrupt and causes a
jump to the next subroutine if the present subroutine is not
completed in a preset period of time. This prevents the
microprocesor from becoming trapped in an endless loop by a
malfunctioning external device (A/D converter, TPM, or ESA
microprocessor). The digital data from the SPMs are read next
and a check is made to see if a command byte has been received.
If it has, then the command processor is called to input and
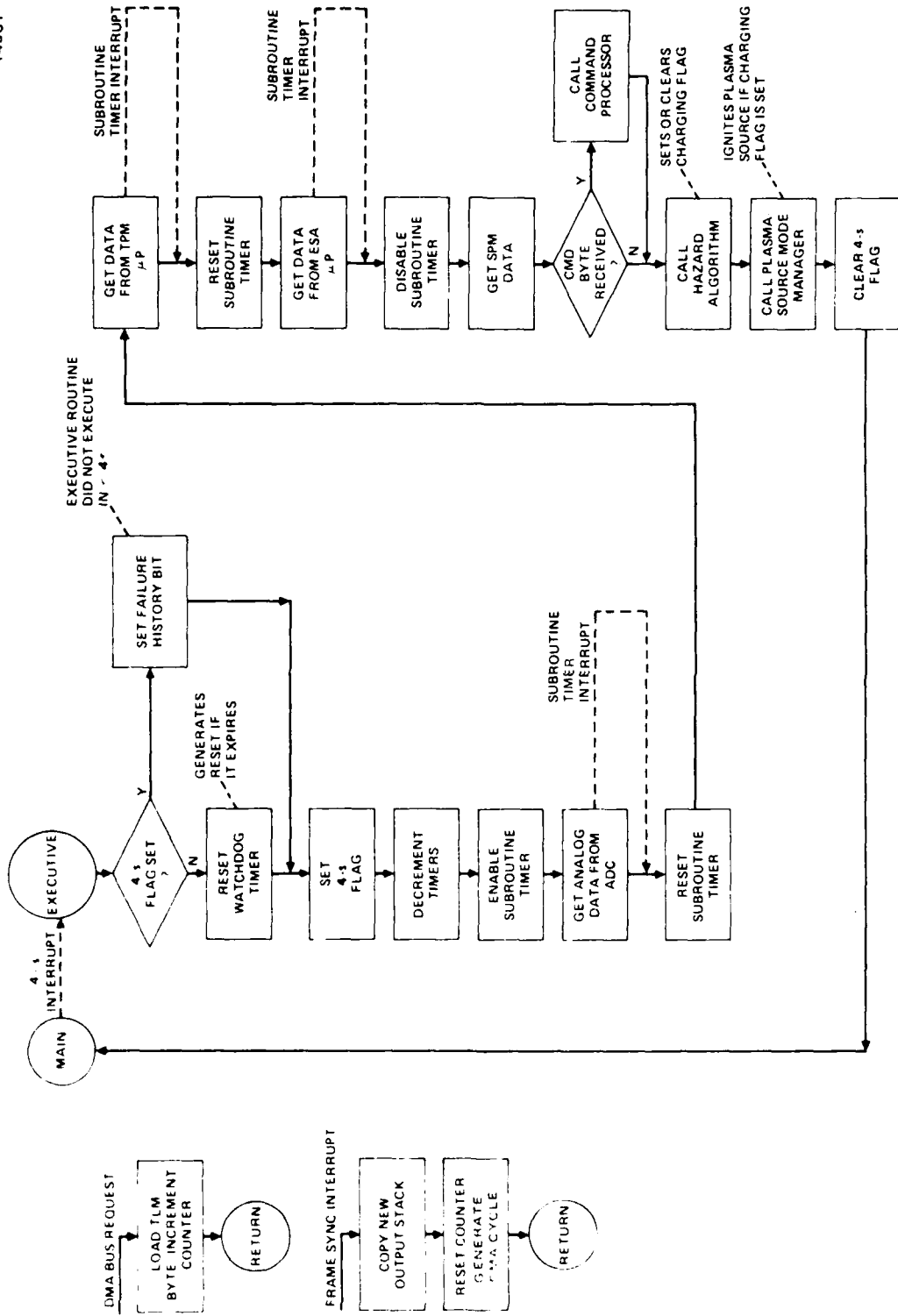
Figure 6-9. Software executive routine flowchart.

14961-4R3

process the command. The charging-hazard algorithm is executed next which determines whether or not the plasma source should be ON. This is followed by the routine to turn the plasma source ON and OFF and monitor its condition. Clearing of the 4-s flag allows the microprocessor to return to what it was doing when the 4-s interrupt occured.

The frame-sync interrupt shown in Figure 6-9 interrupts the microrocessor, causes it to copy a new telemetry data set into the DMA area of memory, resets the DMA counter, and initiates a DMA cycle before allowing the microprocessor to return to what it was doing. The DMA cycle consists of a DMA bus request, loading a telemetry byte into the telemetry shift register, incrementing the DMA counter, and return of the bus to the microprocessor.

The hazard routine flowchart is shown in Figure 6-10. It first initializes all charging flags to false and then checks to see if the ESA is active. If not, it moves on to the SPMs. However, if it is active it checks to see if new ESA spectra have been received. If not it moves on to the SPMs again. If new spectra have been received, it checks the ion-ESA data to see if the spacecraft potential is above the threshold level. If it is, it then checks for the sweep rate of the ESA. If the ESA is in the 16-s sweep, it requires two successive indications of charging before the flag is set. If the ESA is in the 8-s sweep, it requires three successive indications of charging before the flag is set, and if the ESA is in the 4 s or 2 s sweep it requires five successive indications. Any time that charging is not indicated, the algorithm resets k to 2, 3, or 5, depending on the ESA sweep. The algorithm then checks the electron ESA data; if it indicates that a charging environment is present, that the spacecraft is in eclipse (if the eclipse detection is enabled), and if the same requirements as for the ion ESA sweep time are met, then a flag is set.

The SPMs are checked next and if at least one of them indicates charging above the threshold level for three successive scans, then a flag is set. The TPM is the final sensor to be checked; if it indicates that any positive or negative pulses
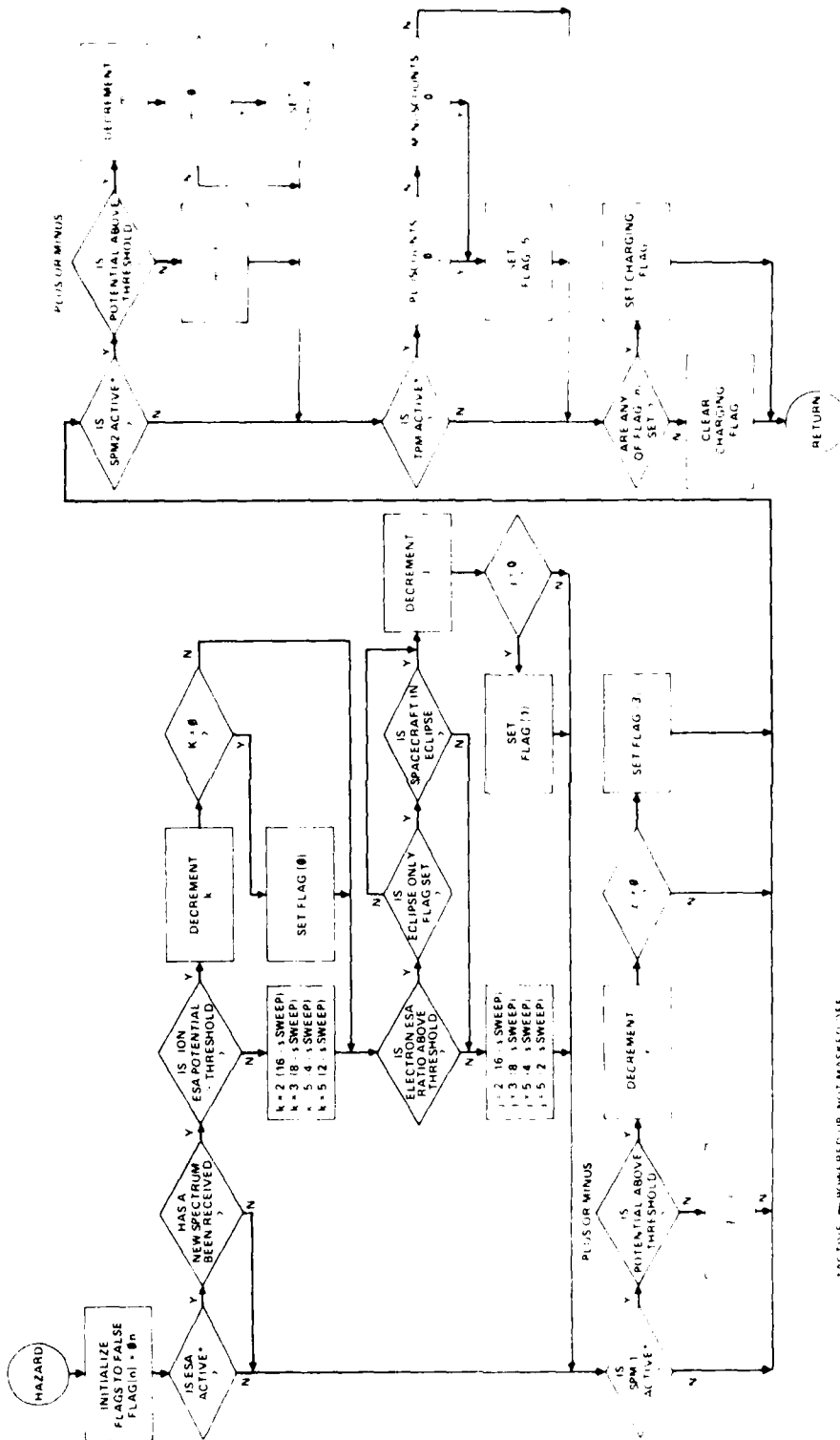
Figure 6-10. Software hazard routing flowchart.

have occured, then a flag is set. If any flags are set, then the charging flag will be set and the plasma source will be turned ON. If no flags are set, then the charging flag is cleared.

When the requirement for charging protection has passed, the software will maintain plasma-source operation until two conditions are satisfied: (1) when a preset timeout, set at the time of plasma source turn ON has expired, and (2) when the charging environment (as indicated by the electron ESA) has been absent for a predetermined period of time.

The second (or ESA) microprocessor performs a single function: it interprets the ion and electron energy spectra generated by the ESA. The ESA microprocessor inputs data from the ESA and stores it in memory. When a full spectrum has been input (16 channels), the processor begins execution of algorithms which determine if the net vechicle potential has exceeded a preset threshold and if a charging environment is present.

The algorithm for determining vehicle potential based on the ion-ESA data is shown in Figure 6-11. This "distribution-function-algorithm" (DFA)[4] was authored by Herb Cohen of AFGL and Stanley Spiegel of the University of Lowell. It examines adjacent ion-ESA energy channels to find an abrupt increase in ion counts from one channel to the next. The algorithm calculates the difference of counts between adjacent channels and determines whether this difference is both large enough and of adequate statistical significance. The sharp rise in count rate is assumed to result from the acceleration of ambient low-energy ions through the potential difference between the spacecraft and local space plasma. If this potential difference is V_S, then no space-potential ions can traverse the ESA when it is tuned to an energy lower than eV_S. This situation creates an ion energy spectrum which has a characteristically sharp edge below which there are (ideally) no ion counts (some counts are, however, found in the "impossible" region between energies of 0 and eV_S; these counts are probably due to spacecraft generated charges). The DFA seeks to identify the spectral edge at energy eV_S by looking for a large and statistically significant increase in count rate between adjacent channels.
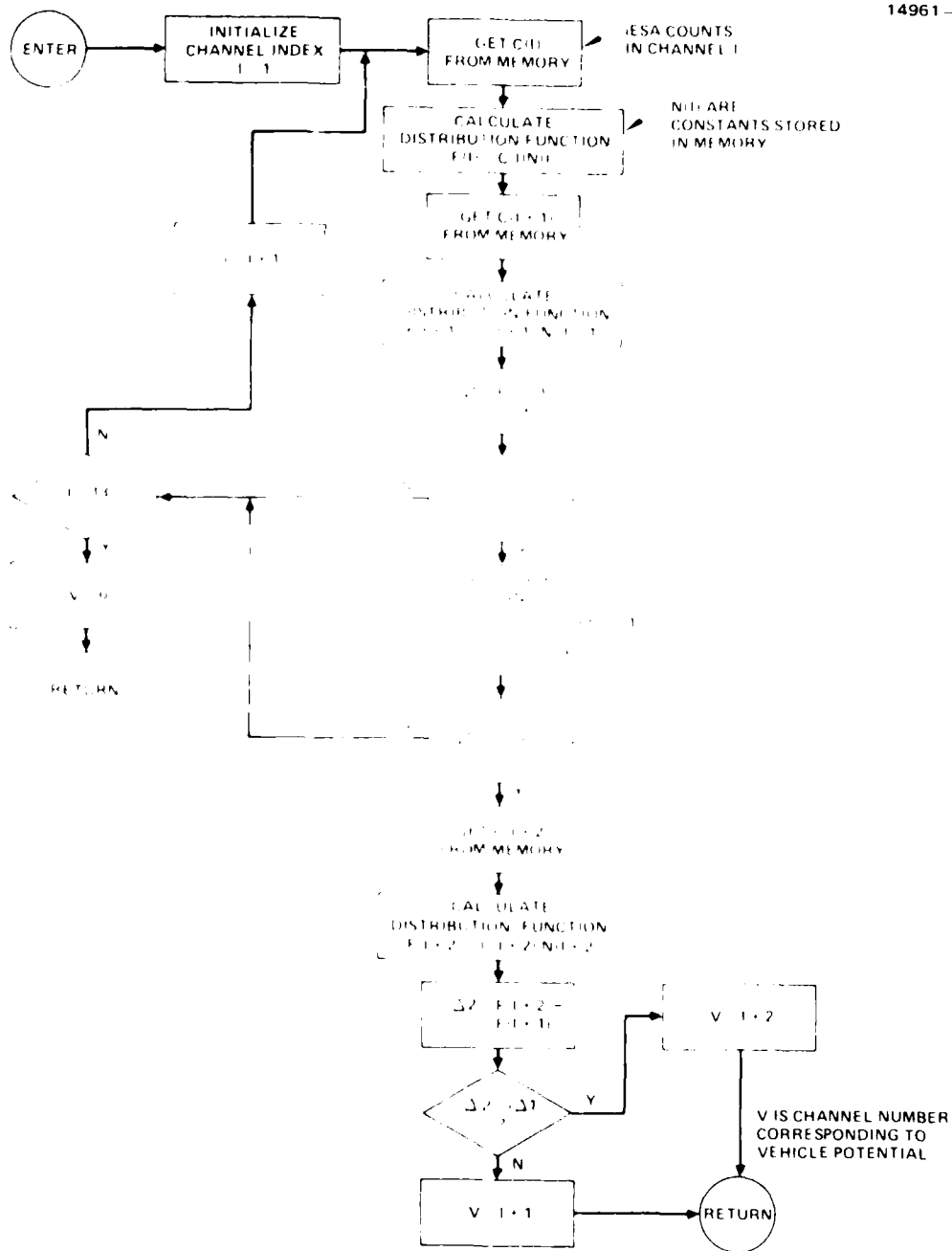
Figure 6-11. Flowchart of the distribution function algorithm (DFA).

The other algorithm which we considered seriously was a template-matching algorithm (TMA) which was implemented by preparing a number of templates--dummy spectra which have calculated edges and shapes corresponding to varying degrees of spacecraft charging. The TMA sequentially compares the actual ion-energy spectrum with each of the templates and produces a vechicle potential which corresponds to the closest match between a template and the actual spectrum.

These two algorithms were tested using SC-9 data which has been reformated into the FMDS channel widths and energy range. The DFA was found to be more accurate than the TMA on a spectrum-by-spectrum basis, as shown in Table 6-1. On a charging-event basis the DFA was found to determine charging above threshold 100% of the time. A few spectra might not agree, but the charging event was always detected. Two typical charging events and a comparison of the visual and DFA-determined vehicle potentials are shown in Figure 6-12. As can be seen from the figure, the DFA closely tracks the visual.

Table 6-1. Comparison of the DFA and TMA Ion ESA Algorithms

15866—17

SPECTRUM-BY-SPECTRUM

ALGORITHM	THRESHOLD ENERGY (eV)	VISUAL	AGREE	DISAGREE	MISS	ACCURACY
DFA	2000	873	760	79	113	87.1%
	1000	2025	1933	168	92	95.5%
	448	3020	2813	120	207	93.2%
	200	3819	3458	178	361	90.6%
TMA	1000	2025	1805	655	220	89.1%

VISUAL – NUMBER OF SPECTRA WHICH INDICATE CHARGING ABOVE THRESHOLD
       AS DETERMINED BY AFGL VISUAL INSPECTION OF AVAILABLE DATA.

AGREE – ALGORITHM AGREES WITH VISUAL.

DISAGREE – ALGORITHM INDICATES CHARGING ABOVE THRESHOLD WHEN
       VISUAL DOES NOT.

MISS – ALGORITHM DOESN'T INDICATE CHARGING ABOVE THRESHOLD WHEN
       VISUAL DOES.
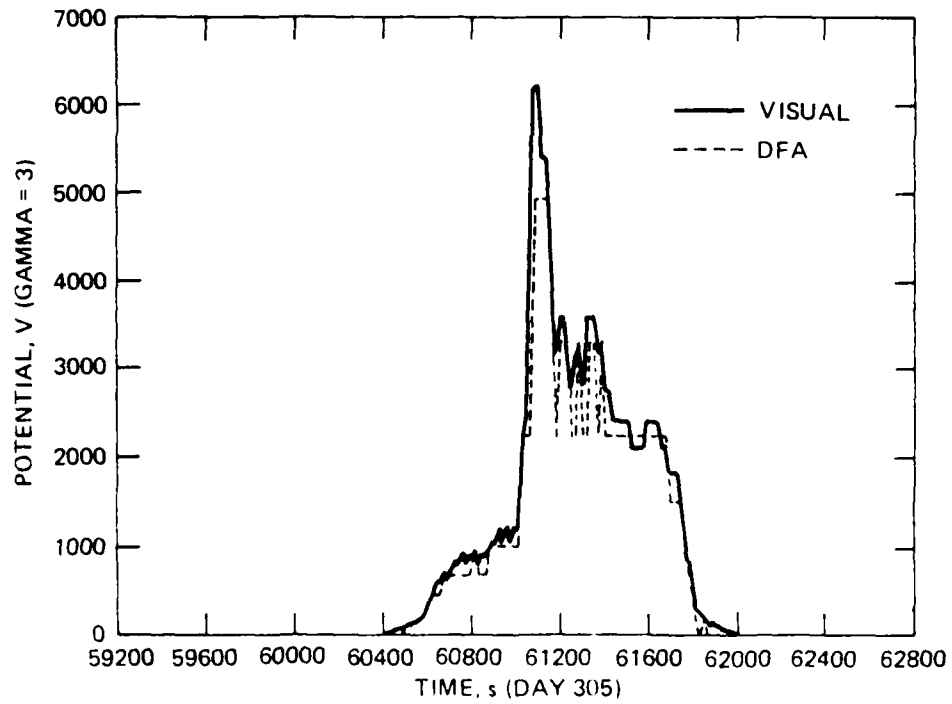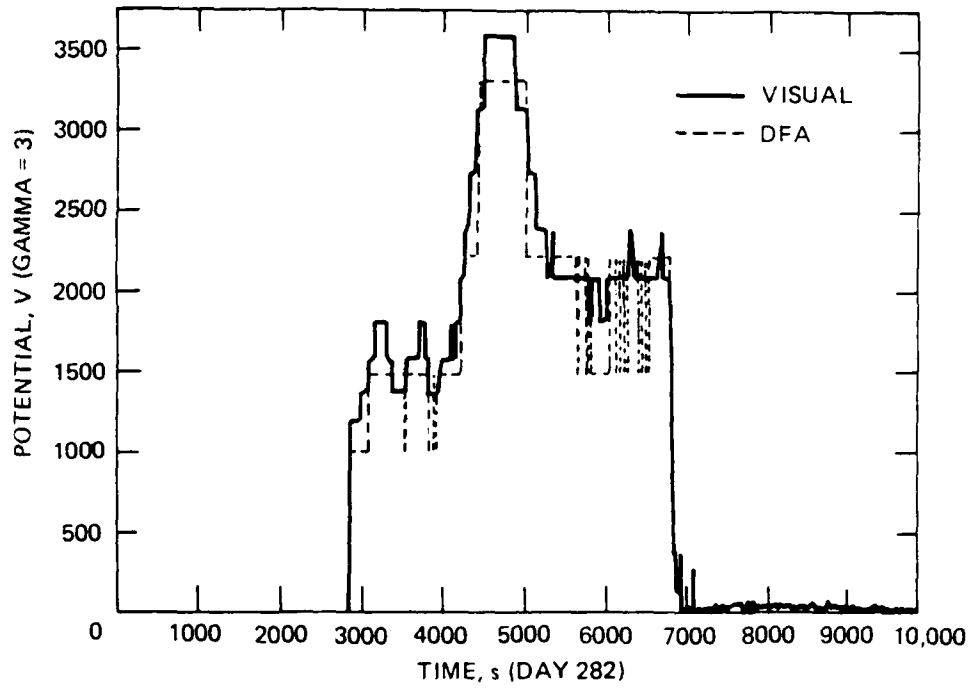
Figure 6-12. Comparison of the visual and
DFA determined vehicle potential.

The algorithm for interpreting the electron ESA-data is shown in Figure 6-13. It is a simple algorithm that compares the sum of the counts in the two highest energy channels with the sum of the counts in the lower energy channels (excluding the background channel). If the two highest energy channels contain more counts than the lower energy channels, then it is probable that a charging environment exists. This algorithm is based on results by Olsen,[5] but has been tested with only one day of SC-9 data. Further analysis is being performed to verify it with a larger SC-9 data set.

6.3 BREADBOARD TESTING

The controller and its software were debugged, tested, and modified as the complete FMDS system was being checked out and prepared for the breadboard demonstration. Modifications were made as their need was pointed out by the testing or when worthwhile improvements were uncovered. In general, it performed very well, as shown by the breadboard system test results presented in Section 8. Three notable exceptions are discussed below.

One of the major glitches encountered during the breadboard demonstration was loss of sync for the telemetry data and latchup of the command and telemetry UART in the controller. This problem resulted in abandoning the UART in favor of the conventional enable signal, clock signal, and data signal type of interface discussed in Section 6.1. We have used this type of interface before without the problems that were experienced with the UART.

The ion ESA algorithm that we wrote along the lines of Spiegel's Distribution Function Algorithm (DFA) called for subtracting the background channel counts from the other channels before looking for a statistically significant edge. Since the count in the background channel was equal to or larger than some of the other channels and the DFA returned a count of 1 for
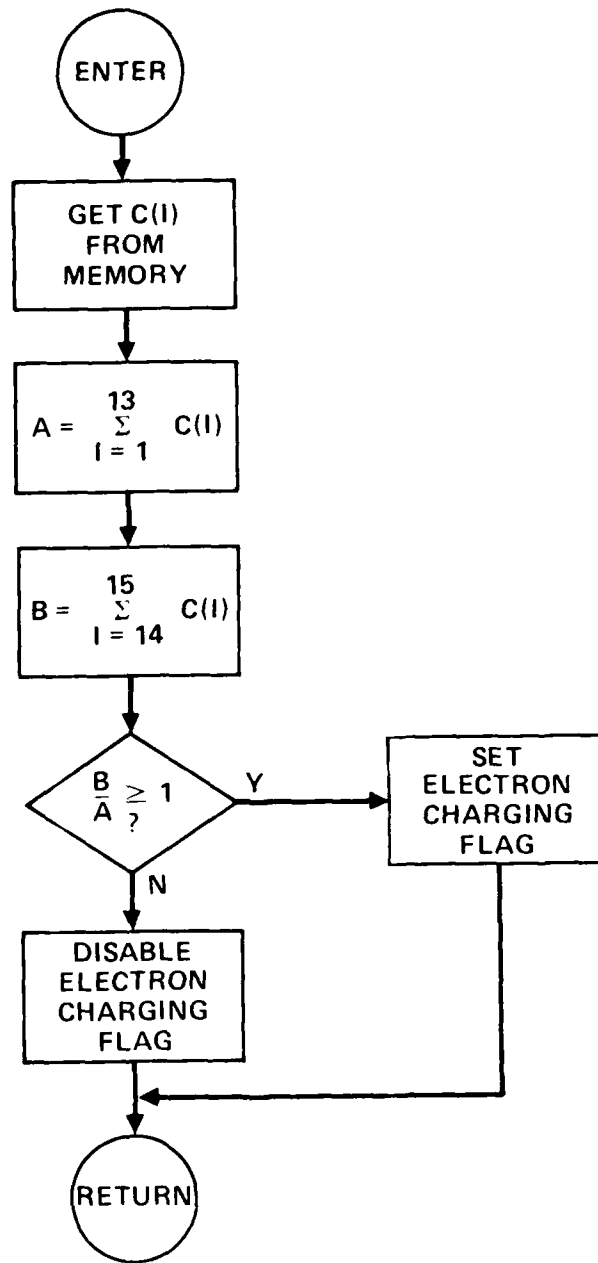
Figure 6-13. Flowchart of the electron ESA algorithm.

6-23

subtractions that were negative or zero, then going from 1 to 3 or 4 counts after the subtraction appeared to be statistically significant, when in reality there was no edge at that channel in the raw data. When the subtraction of the background channel was eliminated, the DFA determined the correct level of spacecraft charging.

During the breadboard demonstration the controller was operating at half the speed that is required. The slower cycle was used because it appeared that under worst case conditions (longest path through the software) there wasn't enough time to execute all of the software routines. The software is written in "C" and the compiler we are using contains some rather inefficient (timewise) subroutines particularly the I/O routines. We can substitute our own subroutines for those presently in the compiler, which will significantly speed up those portions of the software. We feel confident that the faster cycle time can be achieved in this manner. This was not done for the breadboard demonstration because of more pressing problems in getting ready for the demonstration.

SECTION 7

PLASMA SOURCE

The FMDS plasma source consists of three subsystems: the SPACECLAMP plasma generator, the power electronics required to operate and control the plasma generator, and the expellant storage and control assembly. The SPACECLAMP plasma generator has been developed under a Hughes IR&D project and this technology is being provided to the FMDS program for the flight plasma generator design. The following sections discuss the detailed designs of these components, along with test results.

7.1 PLASMA GENERATOR

The plasma generator is regarded as the major element of the system, since its design and operating characteristics determine the requirements for the other two elements (power supplies and feed system). The SPACECLAMP plasma generator has the general characteristics shown in Table 7-1.

The plasma generator (Figure 7-1) is a compact arrangement of a hollow-cathode, keeper and anode electrodes, a magnetic field, and a ground shield. Xenon gas flowing through the plasma generator is ionized by electron bombardment. The ionized gas flows out of the plasma generator, providing a low density ($\sim 10^{10}/cm^3$), inert-gas plasma which will netralize differential charge buildup between various surfaces of the spacecraft and will also form an electrically conducting "bridge" between the spacecraft and the natural space plasma.

A less than 1-s turn ON of the Plasma Generator is achieved by gas-burst ignition. Approximately 1000 V is applied between the keeper and the cathode, and then a burst of high-pressure gas (a few hundred Torr) is admitted to the cathode. The keeper voltage falls almost immediately to <20 V. We believe that the ignition process consists of the formation of an arc which runs on a small spot on the insert until the insert temperature is raised to the point of thermionic emission. At this point

Table 7-1. SPACECLAMP Plasma Generator Characteristics

14881-22R1

PARAMETER	VALUE	UNIT
EXPELLANT FLOW RATE	< 40	mA EQUIV
DISCHARGE VOLTAGE	< 40	V
DISCHARGE CURRENT	< 250	mA
KEEPER VOLTAGE	< 25	V
KEEPER CURRENT	< 400	mA
TOTAL POWER (RUN)	< 10	W
TOTAL POWER (ONE-TIME-ONLY CONDITIONING)	20	W
IGNITION TIME	< 1	S
EXPECTED LIFETIME	> 1200	HOURS
EXPECTED RESTART CAPABILITY	> 1000	STARTS
ION-EMISSION CURRENT (MAX)	> 1	mA

1 mA ION CURRENT

14821 1R6

OUTER SHIELD

ANODE

MAGNET RETAINER

KEEPER

CATHODE TIP

|B| = 830 G

GAS DIVERSION APERTURES IN KEEPER

TAPERED-TWO-METAL FOIL INSERT

SmCo₅ MAGNETS

CATHODE-KEEPER BAFFLE

CATHODE HEATER WITH RADIATION SHIELD

THIN-WALL CATHODE TUBE

DISCHARGE SUPPLY

CATHODE-HEATER SUPPLY

KEEPER SUPPLY

XENON FLOW 0.5 sccm
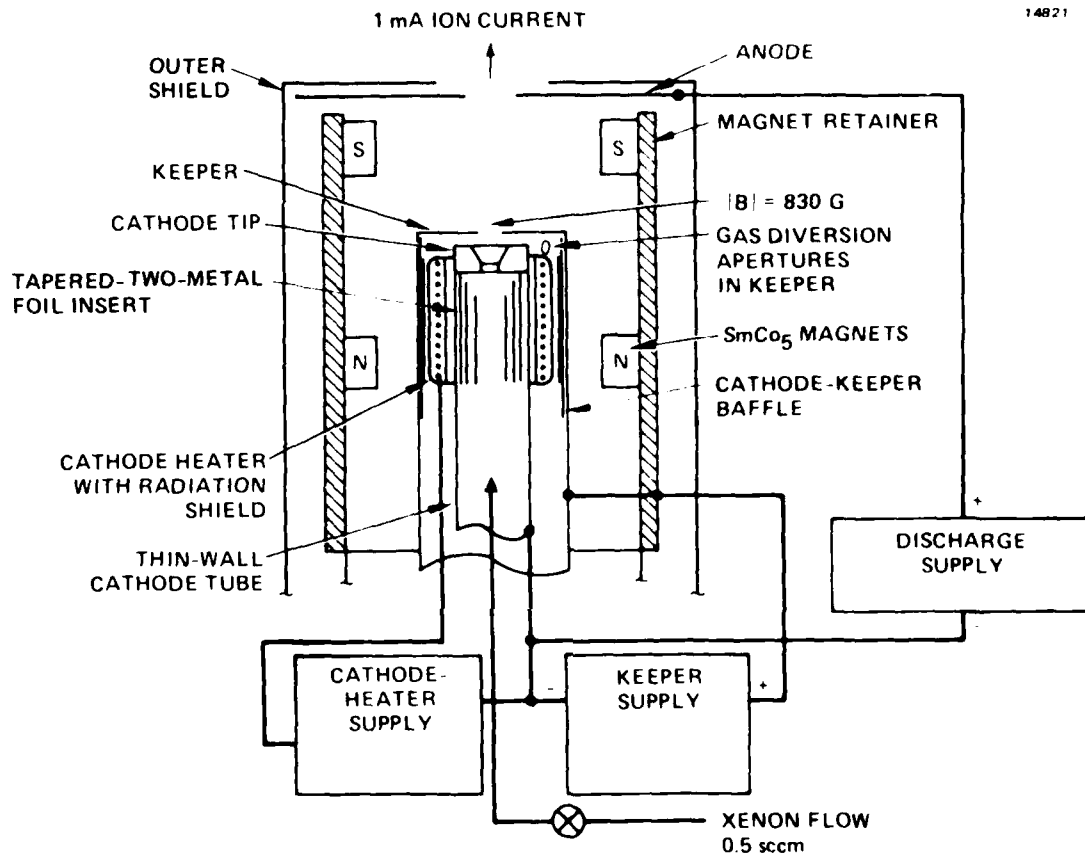
Figure 7 1.   Simple schematic of the plasma generator.

cathode operation undergoes a rapid transition to a low-voltage hollow-cathode mode. The total energy input during the high voltage portion of the ignition transient is about 0.25 J, which is nondestructive to the the insert. The gas pressure and flow settle out to the nominal 0.5 SCCM condition in ~60 s.

The rolled-foil insert consists of 0.013-mm (0.5-mil) thick rhenium foil with a sputter-deposited linear platinum grid deposited on one side. A Hughes proprietary emissive mix is sprayed on both sides of the foil to provide a low work function medium for electron emission. The rhenium foil is then rolled into a cylindrical structure for insertion into the cathode.

The flight design of the Plasma Generator is shown in Figure 7-2. It is designed as a hermetically sealed unit so that it can be evacuated (through the remove-before-launch cap) and operated during ground testing and spacecraft integration. The cathode, keeper, and anode are all electrically isolated from the outer shell so that the return current from the spacecraft can be measured.

7.2 EXPELLANT STORAGE AND CONTROL SYSTEM

The expellant feed and control system consists of the storage tank, valves, pressure regulator, flow impedance, and pressure transducers required to provide the source with gas-burst ignition and a steady state 0.5-SCCM flow rate (Figure 7-3). The storage tank is a Department of Transportation (DoT) approved pressure vessel (rated for transportation on commercial aircraft), with a volume of ~2 liters and containing 100 standard liters of xenon at a pressure of 5.5 MPa (800 psia). The tank is fitted with a pressure transducer (to indicate the quantity of remaining expellant) and a manually operated fill valve.

The xenon flows from the tank through the high pressure valve, which is intended to save the expellant if a slow downstream leak should develop, to the pressure regulator. The pressure regulator reduces the xenon pressure to a constant 69 kPa (10 psia). The 69 kPa is applied to the upstream side of

15866-15
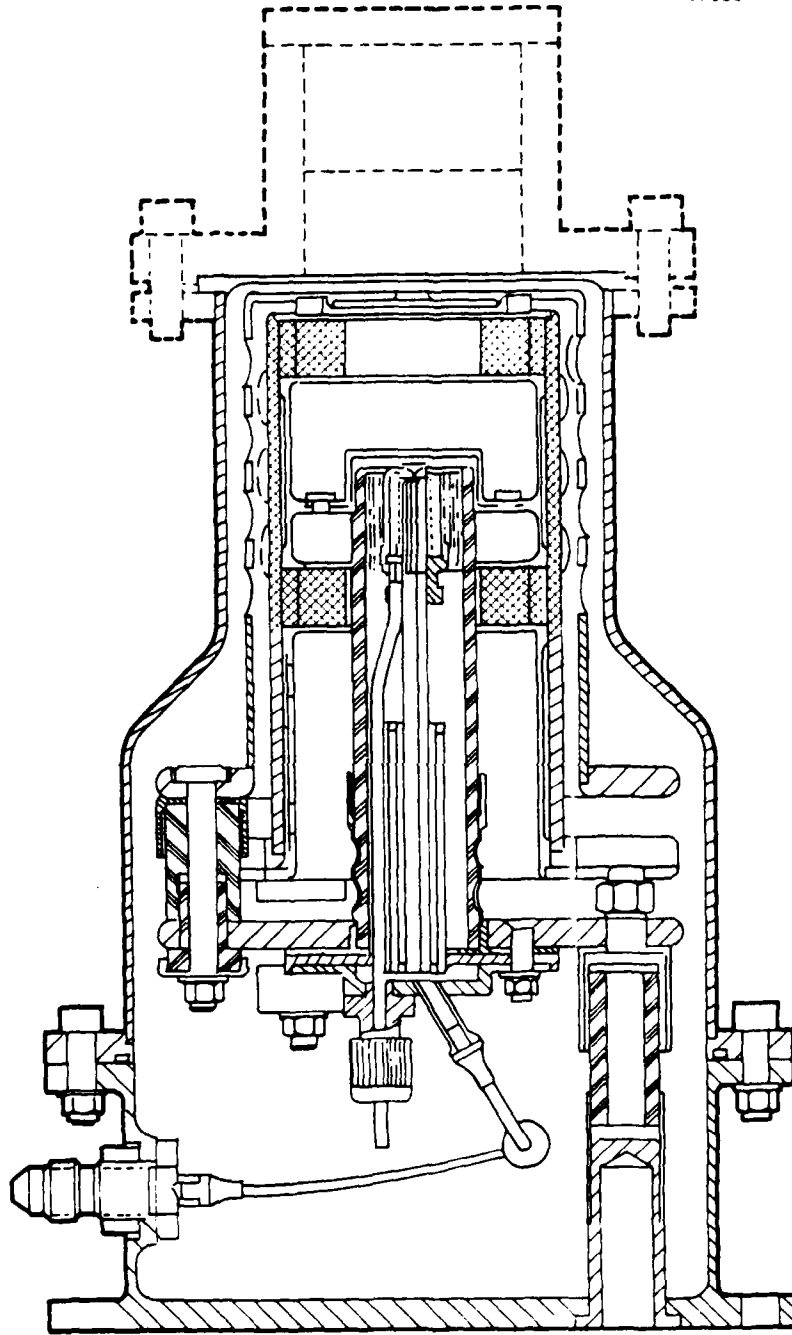
Figure 7 2.   Cross section of the flight plasma generator.
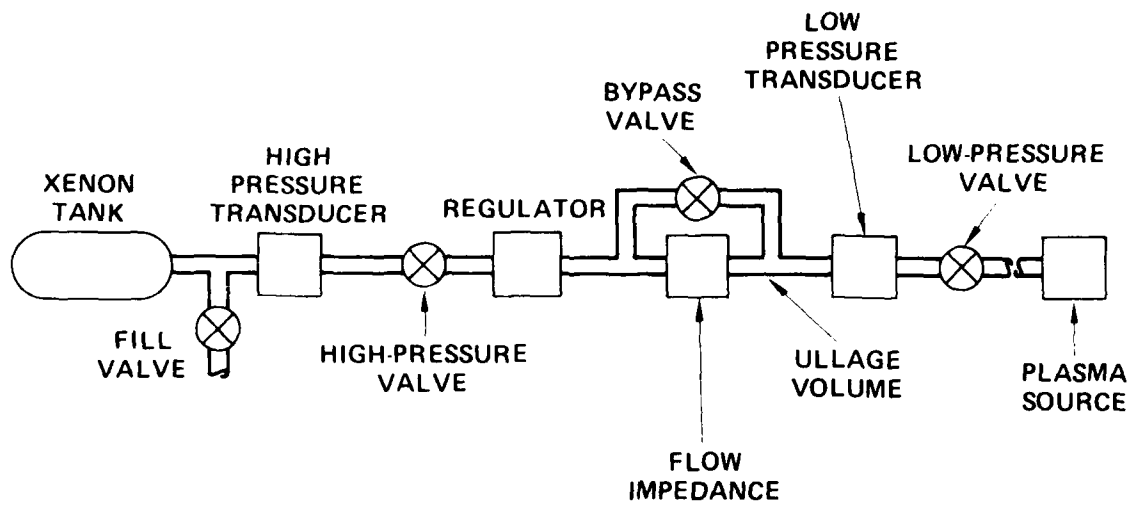
Figure 7-3. Block diagram of the expellant storage and feed system.

a constant flow impedance to maintain a steady state flow rate of
0.5 SCCM. The low-pressure valve is the valve that actually turns
the flow to the plasma generator ON/OFF.

The low pressure transducer measures the pressure in the
ullage volume and is used to indicate if the low-pressure valve
is open or closed. With the valve closed, the pressure in the
ullage volume builds up to 69 kPa which indicates that the valve
is closed. If the valve is open, then the pressure in the ullage
volume is approximately zero and indicates that the valve is
open. The ullage volume provides the burst of gas required for
gas-burst ignition and the bypass valve is used to quickly fill
this volume. The low-pressure valve and the bypass valve are
never both open at the same time.

The tank is removable from the remainder of the FMDS so that
it can be filled and/or transported separately. Sectional
drawings of the flight valves and flight pressure regulator are
shown in Figure 7-4 and 7-5, respectively. The same valve is
used for both the high pressure and low pressure portions of the
feed system.

7.3 PLASMA GENERATOR ELECTRONICS DESIGN

The plasma-generator electronics block diagram is shown in
Figure 7-6. It contains a discharge supply, keeper supply, and a
heater supply for operation of the plasma generator, a bipolar
log-electrometer to measure the emission from the plasma
generator (return current from the spacecraft), valve drivers for
the valves, and analog telemetry signal conditioning.

7.3.1 Power Supplies

The plasma generator power requirements are relatively low
(<20 W), which rules out the need for complex inverters in order
to obtain reasonable efficiencies. Therefore, half-wave flyback
inverters are used for all three power supplies. The half-wave
flyback inverter (Figure 7-7) is the simplest type of inverter
which provides isolation and high reliability while requiring a

1.19 DIA

IN

MACHINE PLUNGER
TO OBTAIN 018 · 024
STROKE

0.727
0.663

1.62

0.33

060
WITH ENDS
FLUSH (REF)

3.117
3.073
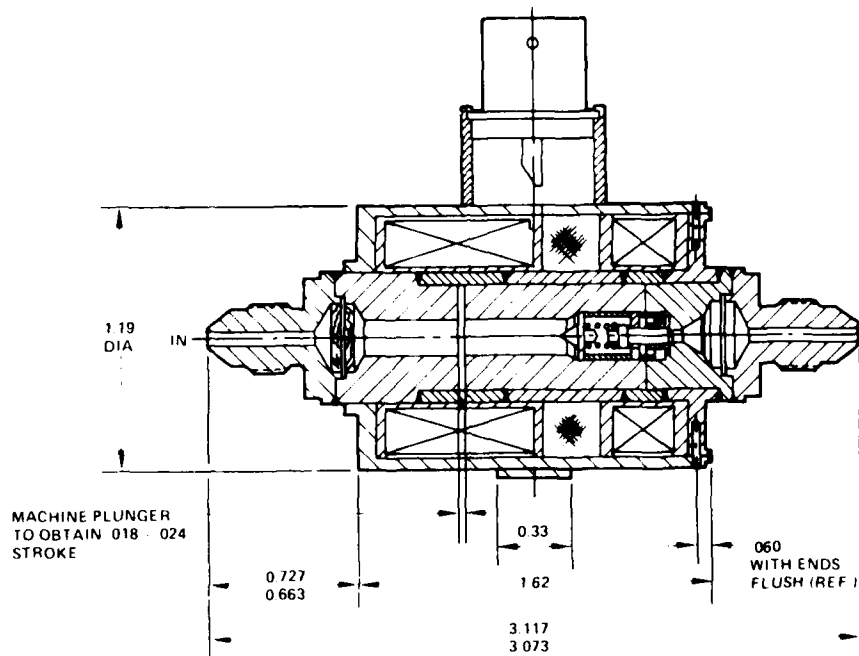
1   MEDIUM   PURE XENON GAS

2   PRESSURES
      OPERATING   10 psig TO 850 psig
      PROOF   1275 psig
      BURST   2125 psig

3   TEMPERATURES
      AMBIENT   OPERATING   40°C TO +71°C
                                              NON OPERATING   40°C TO +85°C

4   FLOW   020 DIA ESEO (MIN) (Cd   65)

5   LEAKAGE   INTERNAL 1.0 x 10^{-5} SCC/sec G He AT 0 TO 850 PSIA
                                              EXTERNAL 1.0 x 10^{-6} SCC/sec He AT 850 psig

6   POWER   30 W MAX AT 27.2 vdc AND 20°C
      VOLTAGE   24.8 TO 27.2 vdc
      DUTY   INTERMITTENT, 100 ms ON 100 ms OFF
      RESPONSE TIME (ELECTRICAL) AT 27 Vdc, 70°F AND 372 PSID
                                              OPENING   40 ms MINIMUM PULSE
                                              CLOSING   40 ms MINIMUM PULSE

7   FILTRATION   10 μm (NOMINAL)

8   WEIGHT   0.65 lb (CALCULATED)

9   MATERIALS IN CONTACT WITH MEDIA
    ST STL 302, 304, 304L AND 430 CHROME PLATE SEAL POLYIMIDE

10 INSULATION RESISTANCE   100 MΩ AT 500 Vdc

11 DIELECTRIC 500 VRMS (60 Hz) 1 min   5 mA MAX
                                              LEAKAGE

Figure 7.4.   Cross section of the flight valves.

DESIGN DATA

1.	MEDIA	XENON
2.	INLET PRESSURE	25 TO 850 psia
3.	REGULATED PRESSURE	5–15 psia (±10% OF SET POINT)
4.	FLOW	0.5 ssc/min AT FULL RANGE OF INLET PRESSURE
5.	PROOF PRESSURE	1200 psi
6.	BURST PRESSURE	2400 psi
7.	LEAKAGE:	
	INTERNAL	1×10^{-5} scc/s He MAX
	EXTERNAL	1×10^{-6} scc/s He MAX
8.	TEMPERATURE RANGE:	
	NON-OPERATING	-40°C TO +85°C
	OPERATING	-25°C TO +71°C
9.	WEIGHT, ESTIMATED	.32 lb

.209 DIA. THRU 2 MTG. HOLES

FILTER, 10 μm

1.38 DIA.

1.65

.75

.36
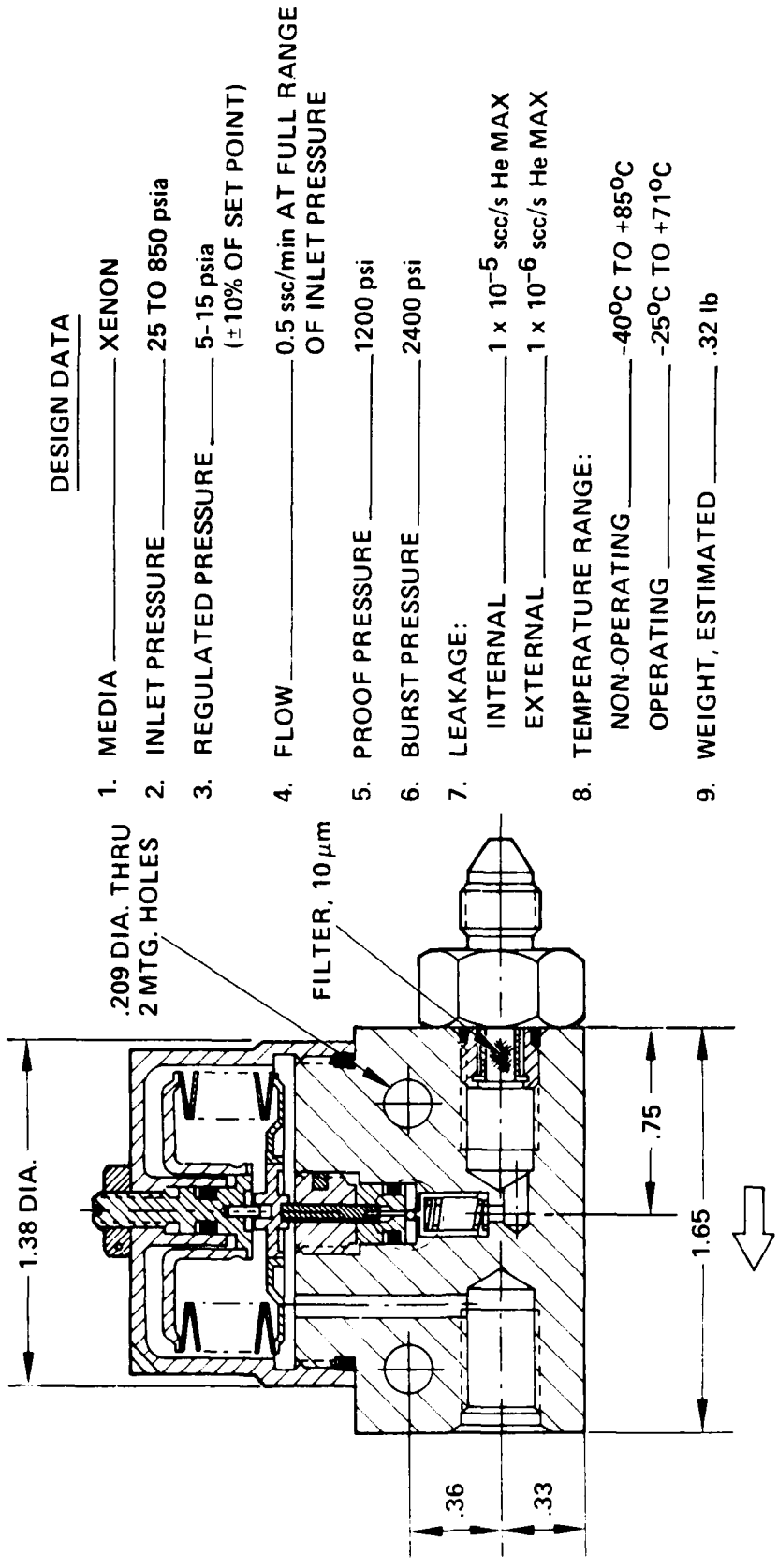
.33

Figure 7 5. Cross section of the flight pressure regulator.
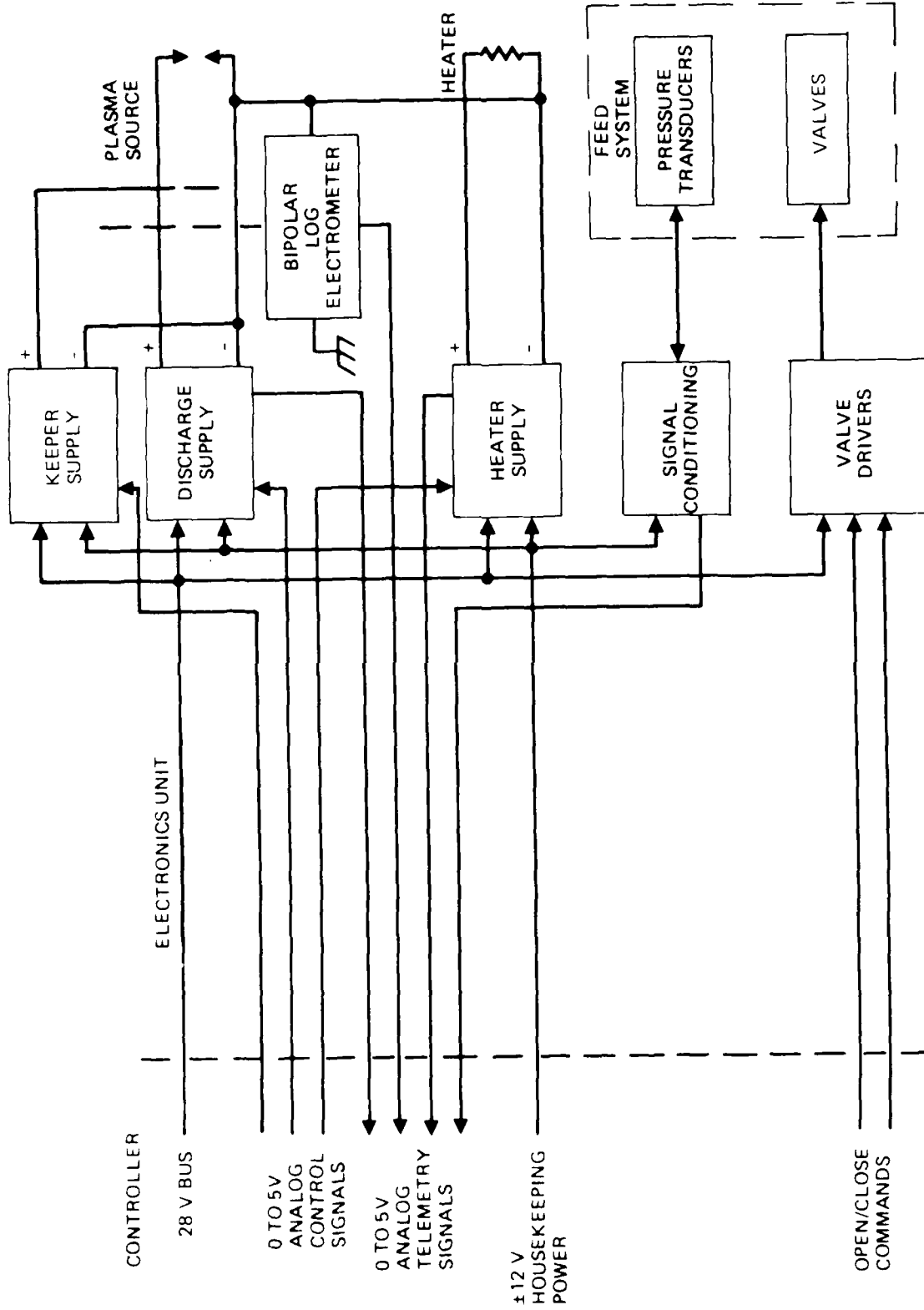
Figure 7-6 Block diagram of the plasma generator electronics.
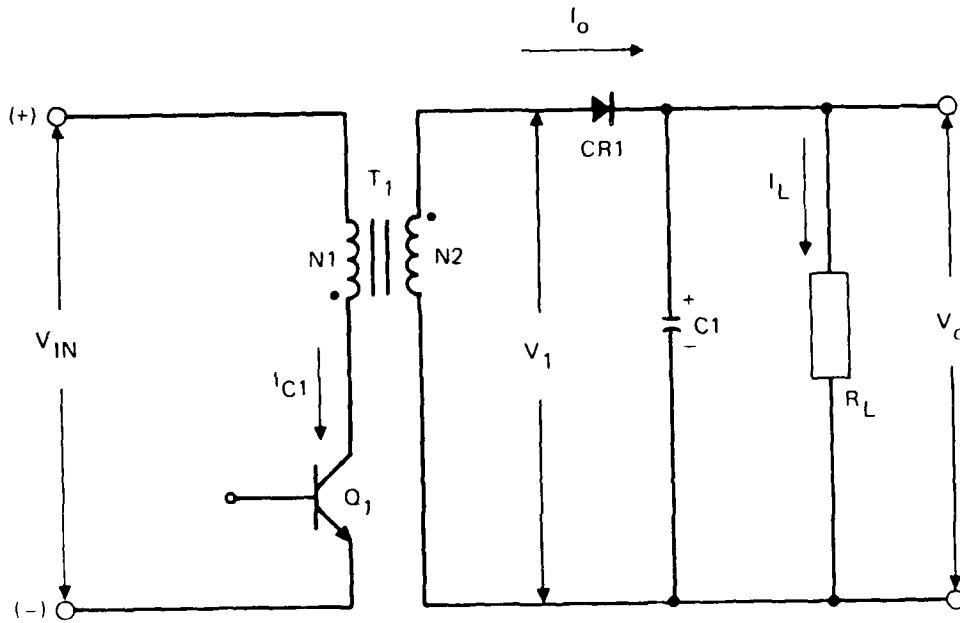
Figure 7-7. Simplified schematic of a half wave
flyback inverter.

minimum number of components. Since it operates in a current-source mode rather than a voltage-source mode, it exhibits inherent output short-circuit protection. Only four power-handling components are required:

- One transformer (T1)

- One transistor switch (Q1)

- One blocking diode (CR1)

- One filter capacitor (C1).

The flyback inverter functions by cyclically storing energy in the magnetic field of transformer T1 while Q1 is turned ON and then transferring this stored energy to T1's secondary through diode CR1 to the output filter (C1) and the load when Q1 is OFF. By varying the Q1 ON time, the amount of energy stored and transferred to the load in each cycle can be controlled or regulated in proportion to changes in input voltage, output load, or commanded setpoint.

The heater supply is shown schematically in Figure 7-8. The supply produces a maximum constant-current output of 7 V at 3 A and is controlled by an integrated circuit (U1) which is a pulse width-modulator (PWM). Regulation is accomplished by sensing the output current through T3 and U3 and feeding this signal back to the PWM. The output of U3 is also used to provide the current telemetry signal.

Optical isolation (U2) is used to isolate the output of U1 which is referenced to control-and-telemetry common from the gate of the switching MOSFET (Q1) which is referenced to input-power common. Q2, Q3, and Q4 interface the output of U2 with the gate of Q1. The peak current through Q1 is limited by sensing this current with T2 and feeding it back to the current limit input of U1.

The voltage telemetry is derived from a separate winding on the output transformer (T1D). A synchronous sample/hold circuit (Q6) is used to minimize the effects of the leading edge

Figure 7 8. Heater supply schematic.

transient spike. This telemetry voltage is also fed back to the PWM to limit the output voltage under open-circuit conditions.

The ON/OFF command and the setpoint command from the Controller are buffered and decoded by U4. The outputs of the U4 gates are open collector allowing them to function as normally open switches.

The discharge supply design shown in Figure 7-9 is very similar to the heater supply. It produces a constant-current output of up to 0.3 A at up to 40 V, and an open circuit output of 180 V. The output voltage is limited to 180 V via VR2, VR6, and U3 feeding back to U1. The voltage telemetry signal is not fed back to U1. The peak transient current to the plasma generator is limited to less than 2 A by way of Q7, Q8, and R42.

The keeper supply is similar to the discharge supply and is shown in Figure 7-10. It produces a constant-current output of up to 0.4 A at up to 30 V with an open circuit voltage of 1000 V. The 1000 V is produced by a second flyback stage (Q2, Q3, and T2) which automatically turns ON/OFF. If the output is open circuited, then the voltage on the drain of Q1 will flyback to greater than 75 V which will turn Q3 ON with CR7, R9, VR3, and VR1. When Q3 is ON it effectively grounds the source of Q2 allowing the high voltage stage to operate and produce the 1000 V output. As the output is loaded down, the flyback voltage on Q1 drops below 75 V, turning Q3 OFF and disabling the high voltage stage. Peak transient currents to the Plasma Generator are limited to 1 A from the 1000 V through R2 and to less than 2 A from the low voltage section through Q5, Q4, and R4. Under open-circuit conditions, Q5 turns ON, thereby turning Q4 OFF and placing R4 into the circuit. Approximately 1 min. after the Plasma Generator ignites, Q5 turns OFF which turns Q4 ON removing R4 from the circuit.

7.3.2 Bipolar Log Electrometer

The bipolar log electrometer measures currents in the ranges of -1 μA to -10 mA and 1 μA to 10 mA. It has a 0 to 5-V analog

Figure 7.9. Discharge supply schematic.

Figure 7-10. Keeper supply schematic.

telemetry output with zero-V out equal to -10 mA, 2.5-V out equal to -1 μA to 1 μA, and 5-V out equal to 10 mA.

Current is converted from being linear to being logarithmic with the base-emitter junction of a transistor (Q1A or Q2A of Figure 7-11) in the feedback loop of an operational amplifier (U1). Q1, Q3, and U3 are used for positive currents and Q2, Q4, and U2 are used for negative currents. Q1B (Q2B) and R12 (R27) provide temperature compensation for the circuit. Q3 (Q4) is a constant-current source that sets the low end of the logarithmic range (1 μA) while R13 (R10) sets the high end of the range (10 mA) by adjusting the gain of amplifier U3 (U2). The outputs of U3 and U2 are summed by amplifier U4 to provide the bipolar function.

7.4 BREADBOARD TEST RESULTS

During the FMDS breadboard testing we used a cylindrical Langmuir probe, which was 7.5 in. from the plasma source, to measure the plasma density. The electron density was measured by biasing the probe tip to collect electron current, which was then used to estimate the electron density. When the source was not biased relative to the vacuum chamber (simulating an uncharged condition) we measured an electron density of $1.5 \times 10^8/cm^3$ and an electron temperature of approximately 1.5 eV. When the source was biased to -30 V relative to the vacuum chamber to simulate charging conditions, the resultant net ion current was about 1 mA, and the electron density and temperature were about $9.5 \times 10^7/cm^3$ and 0.8 eV, respectively.

The net ion emission current from the plasma source was measured during ignition and at its throttled setpoints. The emission current was measured by biasing the plasma source 30 V positive relative to the vacuum chamber walls. A plot of net emission current versus bias voltage is shown in Figure 7-12 for the nominal operating point. Figure 7-13 shows a stripchart recording of the emission current during ignition. The emission current starts at 0.4 mA, falls to 0.1 mA at 5 s, increases to
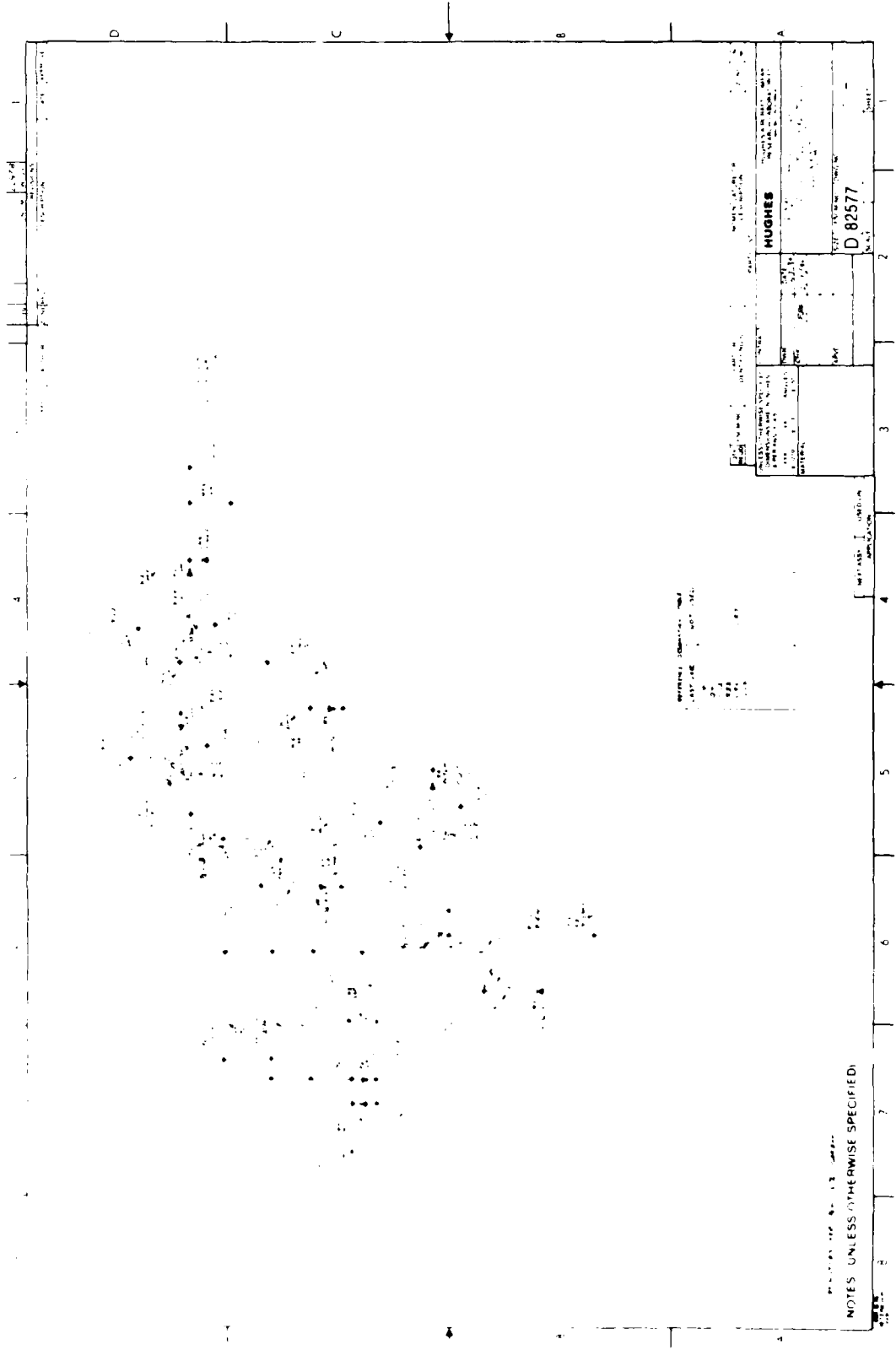
Figure 7-11. Schematic of the bipolar log electrometer.
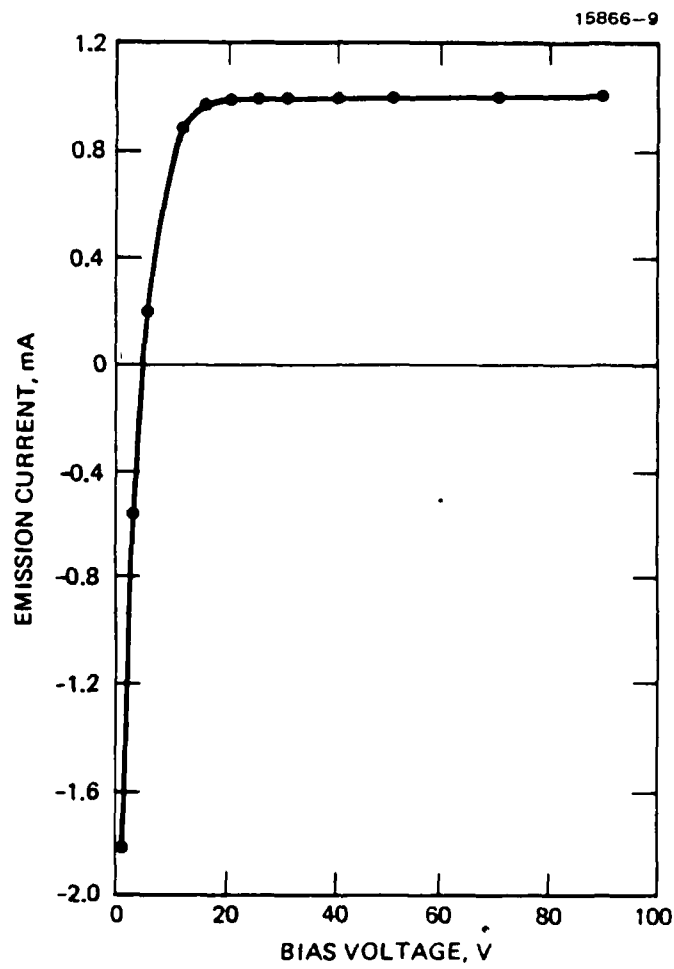
*Figure 7 12. Plasma source net emission current versus
bias voltage for the nominal operating point.*
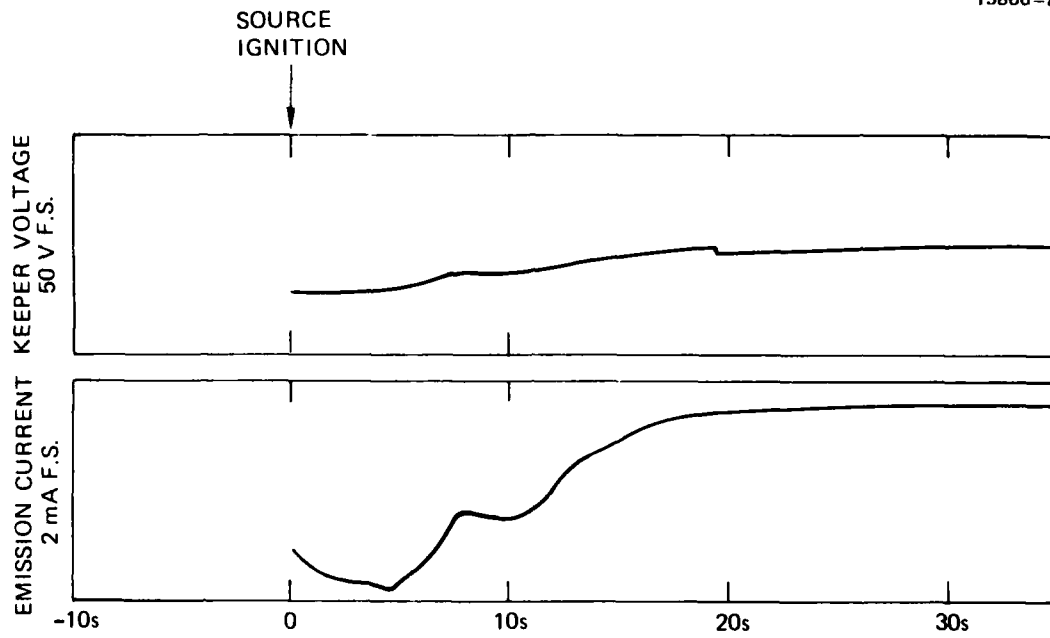
Figure 7 13. Plasma generator emission current during ignition.

0.8 mA at 8 s and finally steadies out at 1.8 mA after 20 s. The variation in emission current is the result of the pressure inside the source decreasing to its steady-state value after the gas-burst-ignition.

The stripchart recording in Figure 7-14 shows the emission current from the source for its various operating points. They are:

- 1.8 mA at setpoint 2 (nominal operating point)

- 0.84 mA at setpoint 1

- 0.80 mA at setpoint 0

- 0.45 mA at setpoint 2 with the discharge supply OFF

- 2.05 mA at setpoint 3.

For the plasma generator, ion emission as a function of discharge current for a keeper current of 250 mA is shown in Figure 7-15. Some optimization of the plasma source was performed between the breadboard data and the October 1 1985 data shown in Figure 7-15. This optimization was performed to improve the ignition and operating characteristics of the plasma generator and as a result of data collected during the breadboard demonstration. The optimization consisted of:

- Incorporating a ceramic insulator between the cathode and keeper and optimizing the ullage volume; these changes increase the interelectrode gas pressure to reliably produce the Paschen breakdown that initiates cathode ignition.

- Developing a new cathode-insert fabrication technique in which 0.051-mm-thick foil is used to space and thermally isolate different layers of the rolled-foil insert.

- Tapering the downstream edge of the insert, thereby exposing a greater number of layers of foil to the cathode plasma.

- Improving the discharge-chamber gas feed by providing several gas-diversion holes in the keeper (i.e., post-cathode gas diversion), result ng in increased ion emission from the source.

7-21

15866-7
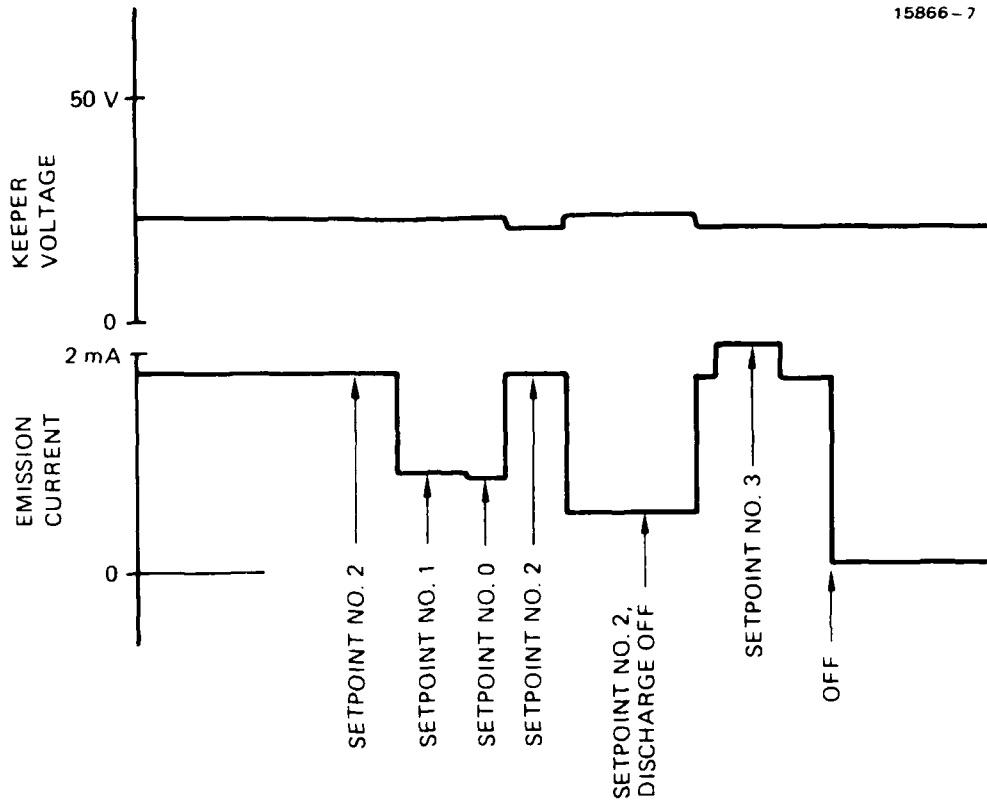
Figure 7-14. Plasma generator emission current at its various operating points.
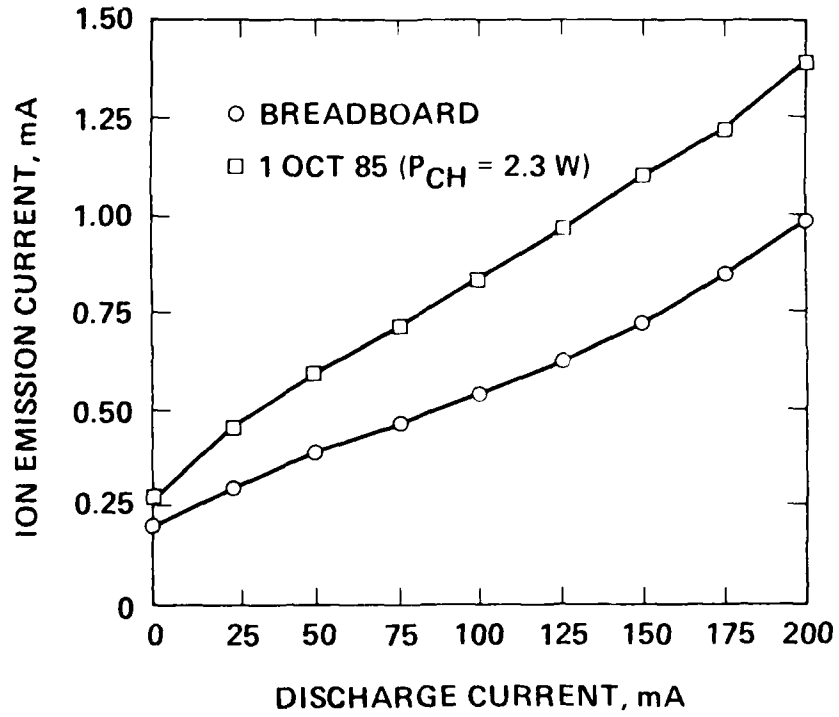
Figure 7-15. Plasma generator ion emission current as a function of discharge current.

- Installing a new current-limiting circuit in the keeper
  power supply to reduce the peak current delivered to the
  source during ignition; we have found that ignition
  currents greater than a few amperes lead to degraded
  source performance.

A prototype source was operated for a total of 730 h and 913
gas-burst ignitions as part of a lifetest. The lifetest was
terminated after the source operation became unreliable. Upon
disassembly of the source, we found that the cathode tube had
become brittle and fractured. We utilized SEM and EDAX
techniques to carefully examine the cathode, which consists of a
tantalum tube with a tungsten tip and the rolled-foil insert.
The elements found within the tube and in the neighborhood of the
fracture included aluminum, barium, copper, tantalum, rhenium,
and iron. The presence of each element can be explained by the
manufacturing techniques used to fabricate the cathode, except
for the iron which may have been residual contamination from the
SEM vacuum vessel. We concluded that foreign materials were not
introduced into the cathode, and that the fragile condition of
the tube was probably a result of a reaction between the emissive
mix on the rolled-foil insert and the tantalum cathode tube.

We also found that the 0.010-in.-diameter cathode orifice in
the tungsten tip had become partially occluded. However, since
we found only aluminum, copper, and tantalum within the orifice
and did not measure traces of rhenium or platinum, the occluding
material is probably not a remnant of the rolled-foil insert.

The brittle state of the cathode tube indicates that the
design of the plasma source should incorporate a cathode tube
assembly which is fabricated from an alternative material, one
which is less subject to becoming brittle than tantalum.
Therefore the design has been changed to 50/50 molybdenum-
rhenium, a material that has shown greater resistance to becoming
brittle in testing by Hughes under a NASA-LeRC ion propulsion
contract (NAS 3 22474).

Another lifetest will be performed to demonstrate the required source performance of over 1200 h of operation and 1000 gas-burst ignitions. The test will utilize the plasma generator which was part of the FMDS breadboard demonstration, a new cathode employing moly-rhenium, flight-type power supplies, and a flight regulator (set to 69 kPa) in the xenon feed system. Prior to performing the lifetest, we will correct the less-than-ideal gas-burst ignition properties of the source observed during the breadboard demonstration by optimizing the keeper and discharge power supply load lines.

SECTION 8

SYSTEM DESIGN

The FMDS is designed as a self-contained system. This approach minimizes the interfaces with the satellite and makes the FMDS more attractive as a "housekeeping" function that performs the task of keeping the satellite in a neutral charge state. The command-and-telemetry interfaces are accommodated through the controller and the power interface is accommodated through the plasma-source electronics box. This enables single types of command, telemetry, and power interfaces with the satellite. Any differences in command and/or telemetry format required by the sensors or the plasma source are provided by the controller and not the satellite. All of the components of the FMDS are mounted on a flat plate, as discussed in Section 2-1. This flat plate is the mechanical and thermal interface with the satellite.

The SPACECLAMP plasma generator for the FMDS turns ON in 1 s or less once the power supplies have been turned ON and the gas valve opened; therefore the response time of the FMDS (the time-span from the satellite reaching the threshold level selected as the critical charging level until low energy plasma is emitted) is mainly determined by the sensor response times and the time required for the controller to process the appropriate algorithms.

The controller operates on a 4-s cycle and will turn ON the plasma-generator power supplies during the same cycle that charging is detected. The gas valve, however, will not be opened until the next cycle and therefore it will actually take from 4 to 8 s from the time that an algorithm determines that charging is present until the plasma generator is turned ON. The ion ESA has sweep times of 2, 4, 8, and 16 s, and the algorithm associated with it requires from 2 to 5 sweeps to reliably detect charging. Therefore, if the ESA is set to the 16-s sweep, the 30-s response time is not feasible (by ~8 s). If the ESA is set

to the 2-s, 4-s, or 8-s sweep, the 30-s response time is met (see Table 8-1). The SPM responds almost immediately and its algorithm is very simple; therefore, the response time associated with this instrument is 3 cycles plus the plasma generator turn-ON time or a maximum of 20 s. The TPM also responds immediately and one detected arc sets the charging flag. Therefore the TPM response time is a maximum of 8 s. In general, if the ESA is swept at 8 s or less, the 30-s response time requirement is met.

8.1 ELECTRICAL DESIGN

Since the exact vehicle and/or satellite on which the FMDS will be flown is not known, the exact power, command, and telemetry interfaces are not known. Therefore, we have designed interfaces for the case we consider to be standard and reasonable.

The primary power return, the command return, and the telemetry return are all isolated from the case and from each other by at least one megohm, which allows the satellite to have a "single ground-point" grounding scheme and prevents the satellite structure from being used as an intentional current carrying conductor. The ground-return-isolation scheme is shown in Figure 8-1.

Table 8-1. Estimated Response Times of the FMDS for the Various Charging Sensors

15866-6 R1

CHARGING SENSOR	ESTIMATED RESPONSE TIME, S
ESA (2-S SWEEP)	<28
ESA (4-S SWEEP)	<28
ESA (8-S SWEEP)	<32
ESA (16-S SWEEP)	<38
SPM	<20
TPM	<8
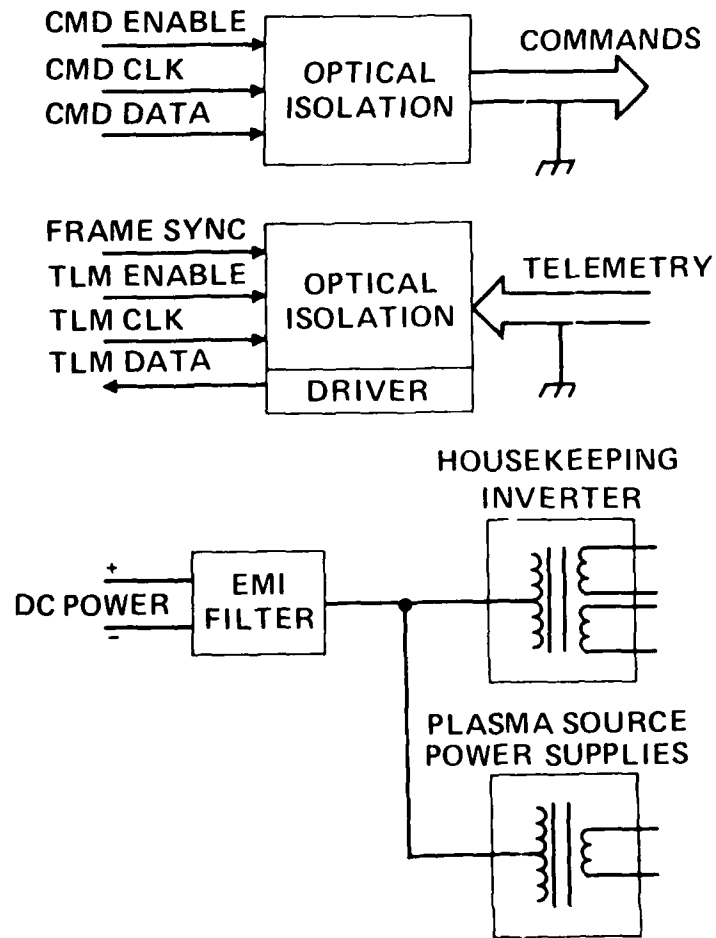
Figure 8 1. Ground return isolation scheme for the FMDS.

The design for the 28-V power-input isolation regulator is shown in Figure 8-2. This regulator provides transformer isolation between the 28-V spacecraft bus and the FMDS electronics and regulated housekeeping power (±5 V, ±12 V, 28 V) to the sensors and plasma generator electronics. Primary power for the plasma generator power supplies is taken directly from the spacecraft bus with isolation provided by the individual inverter output transformers. Relays are provided to turn the power to the sensors and the plasma source ON/OFF by means of commands from the controller.

The regulator consists of three basic sections as shown in the block diagram of Figure 8-2: (1) A pulse-width-modulated (PWM) step-down preregulator which provides a constant 20-V input to the inverter section and (2) a current-fed, square-wave-inverter section which chops the 20-V power at a 40-kHz rate and provides power to (3) multiple secondary output windings.

The current-fed, push-pull, square-wave converter provides all the characteristics required of this isolation regulator:

- Transformer isolation between input power and output power

- Multiple output capability

- Good cross regulation between outputs

- Minimum complexity.

In addition, this configuration minimizes the high power stresses imposed on the switching elements during switching intervals by placing a filter choke in the input power line where it can limit the current through the transformer and the switching elements. It also prevents damage resulting from unbalanced dc currents and effectively turns the converter into a current source which aids in maintaining stable operation over a wide operating range. Minimum complexity is achieved by using one choke in the primary which current feeds all outputs in parallel. Since each secondary winding drives its load directly
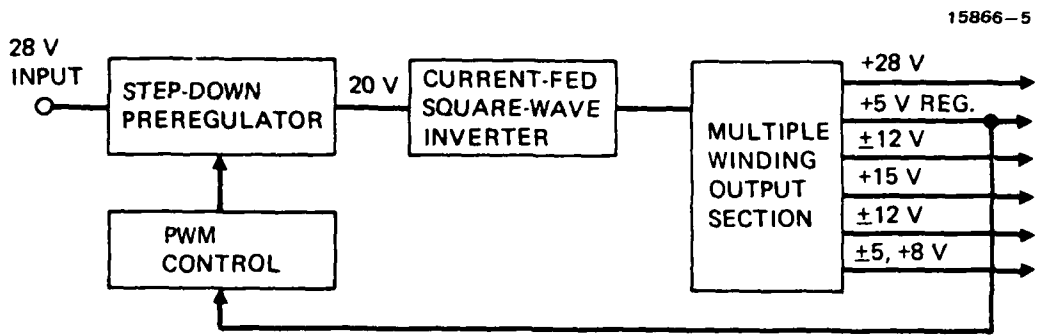
Figure 8 2. 28 V power input isolation
regulator block diagram.

(without a choke), cross coupling between outputs is very tight, resulting in excellent cross regulation. To achieve good cross regulation, however, it is necessary to maintain a continuous, low impedance across the primary winding which dictates driving the primary winding at maximum duty cycle (50% each side) at all times. This requirement precludes using PWM for output regulation. Instead, the step-down converter must be used to regulate the voltage to the current-fed converter, which in turn regulates all secondaries in parallel.

A schematic of the regulation inverter is shown in Figure 8-3. The pulse-width-modulator integrated circuit, U1, controls the step-down converter to regulate the 5 Vdc for the controller. All other housekeeping voltages track this regulated voltage. Q4 is the switching MOSFET that alternately connects L1 to common or to the +28 V (via CR1), thereby controlling the average current flowing in L1. L1 is then the current source that feeds the output inverter which is comprised of Q2, Q3, and T3. Q2 and Q3 are alternately switched ON/OFF by flip-flop U2, which is synchronized to U1. Startup power is applied to U1 and U2 through Q1; then the circuit is bootstraped with R19 and CR3 to provide higher efficiency.

To minimize high frequency EMI radiation from power-distribution lines, all rectification and filtering is performed within the regulator subsystem. Only dc power is distributed to the subsystems. Ground returns internal to the FMDS are connected to its case in a manner consistent with minimizing EMI and avoiding internal ground loops. The plasma source must be referenced to the satellite frame (through the emission-current detector to the FMDS mounting plate) for proper operation.

An input filter is provided for the spacecraft bus and is designed to meet the requirements of MIL-STD-461B and MIL-STD-1541. The filter, shown in Figure 8-4, is a two-stage LC filter and feeds all of the FMDS inverters. Its calculated attenuation characteristics are shown in Figure 8-5.

Figure 8.3. Schematic of the input isolation (housekeeping) inverter.

Figure 8-4. FMDS input Filter Schematic.
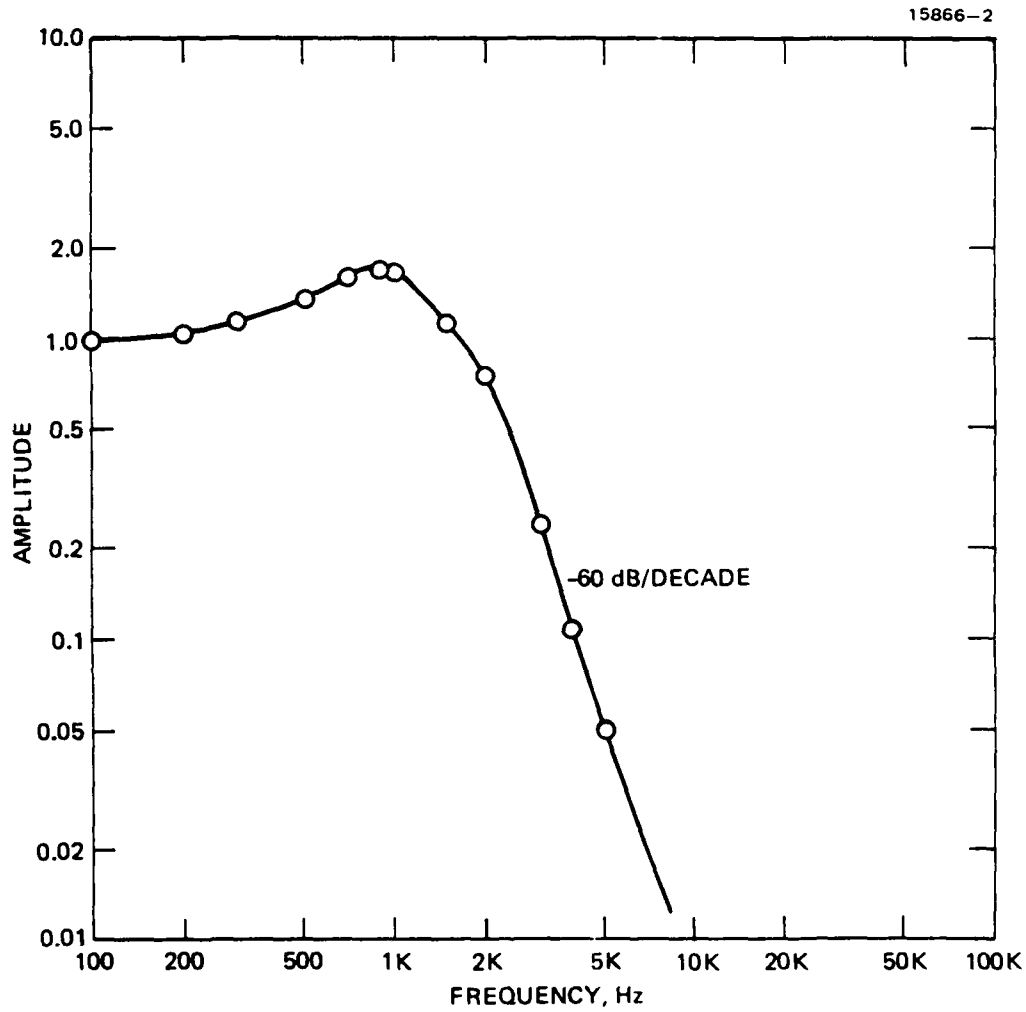
Figure 8-5.   Attenuation characteristics of the input filter.

8.2 COMMANDS AND TELEMETRY

All commands and telemetry to and from the FMDS are in the
form of serial digital signals. Ground isolation of digital
signals is easily performed with optical isolators, while ground
isolation of analog signals is a much more complicated process.
The use of serial digital signals (as opposed to parallel digital
signals) and multiplexing the commands or telemetry words
sequentially over the same wires significantly simplifies the
command and telemetry interfaces with the spacecraft. The
command interface requires three lines (an enable, a clock, and a
data line) and the telemetry interface requires four lines (an
enable, a clock, a data, and a frame-sync line).

Typical optical isolation and driver circuits are shown in
Figure 8-6. The telemetry data line requires optical isolation
on the spacecraft end, while the other six lines have their
optical isolation on the FMDS end. Futher details of the command
and telemetry interface were presented in Section 6.1 and a
listing of the commands and telemetry words are provided in
Appendix A.

15866-1

OPTICAL ISOLATION CIRCUIT
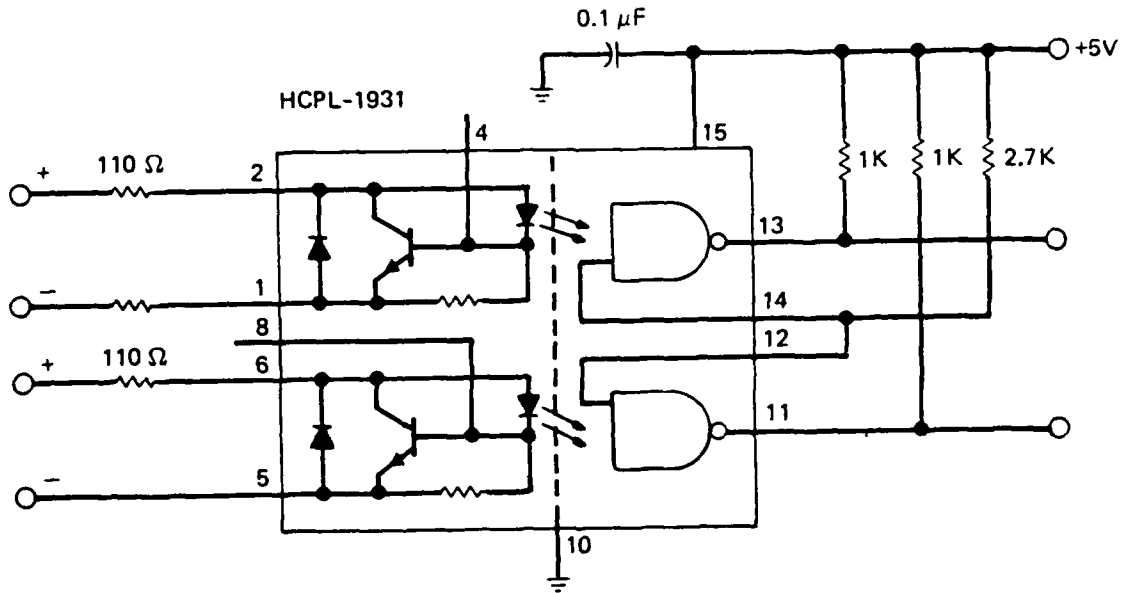
DRIVER CIRCUIT
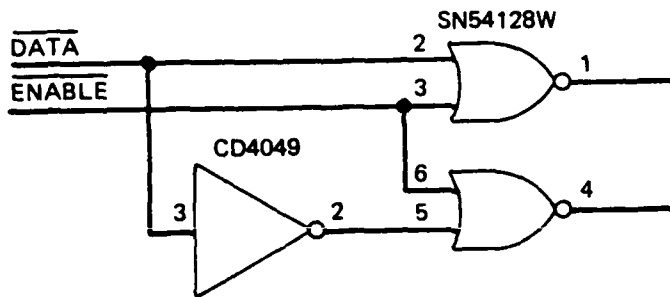
Figure 8 6. *Typical optical isolation and driver circuits for digital signals.*

SECTION 9

BREADBOARD DEMONSTRATION RESULTS

There were two demonstrations of the breadboard hardware at
Hughes Research Laboratories (HRL) during 1985. The first
demonstration was held on April 9, 10, and 11 with
representatives of the USAF Geophysics Laboratory (AFGL). The
design of the breadboard system was reviewed and a limited
demonstration of the hardware was performed for AFGL. The second
demonstration was held on May 29 and 30 and featured the full
capabilities of the breadboard FMDS system.

The plasma source and sensors are shown mounted on the test
fixture in Figure 9-1. An aluminum plate was mounted flush with
the plasma source and sensors to simulate the cover of FMDS
(Figure 2-2). This aluminum plate was then covered with 5-mil
Kapton to simulate thermal blankets covering the FMDS.

The test facility for breadboard testing is shown in Figure
9-2. The FMDS plasma source and sensors are mounted on a plate
inside the vacuum chamber, while most of the electronics are
mounted on a plate outside the vacuum chamber. The two plates
are connected with an 8-in. aluminum tube and mounted to the
chamber with a G-10 glass/epoxy flange. The aluminum tube
shields the interconnect wires between the sensors and the
electronics and the G-10 flange allows the entire FMDS to charge
or be biased 20 kV relative to facility ground. The facility
contains an electron gun, proton source, and UV source to
simulate the space environment, and a Faraday cup and Langmuir
probe for diagnostic measurements of the simulated environment
and the plasma from the plasma source. The dielectric target is
designed to charge up and create arcs for the TPM to detect.

9-1
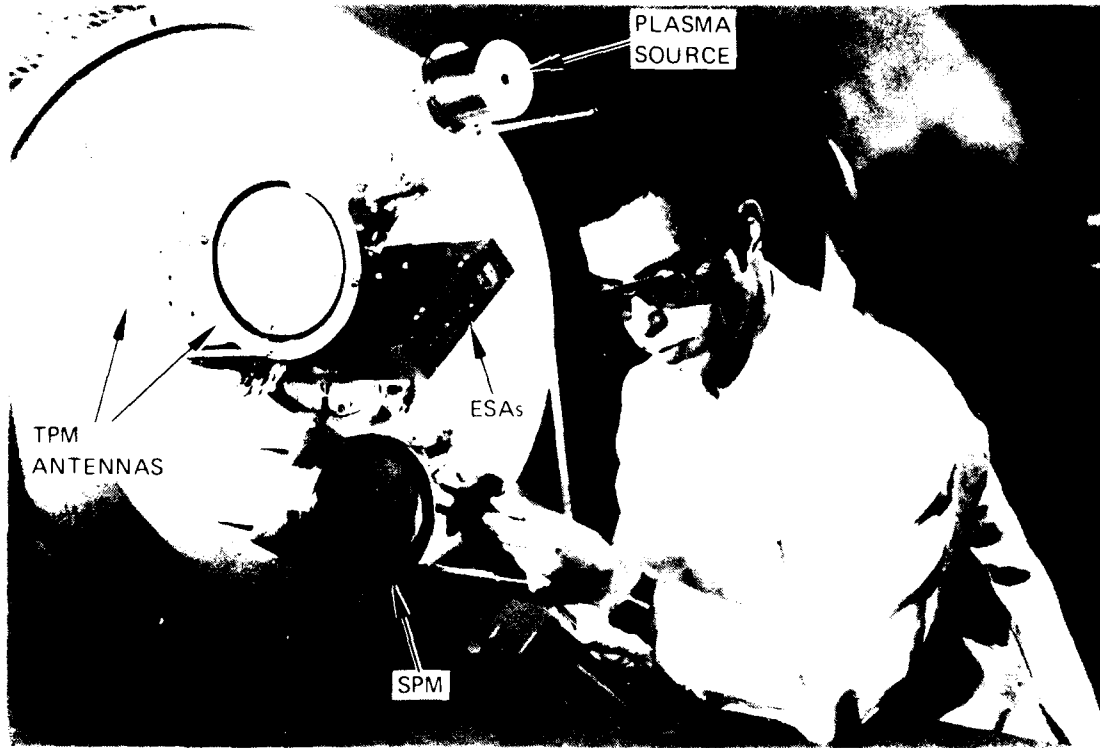
Figure 9-1. *FMDS breadboard plasma source and sensors mounted on the test fixture.*
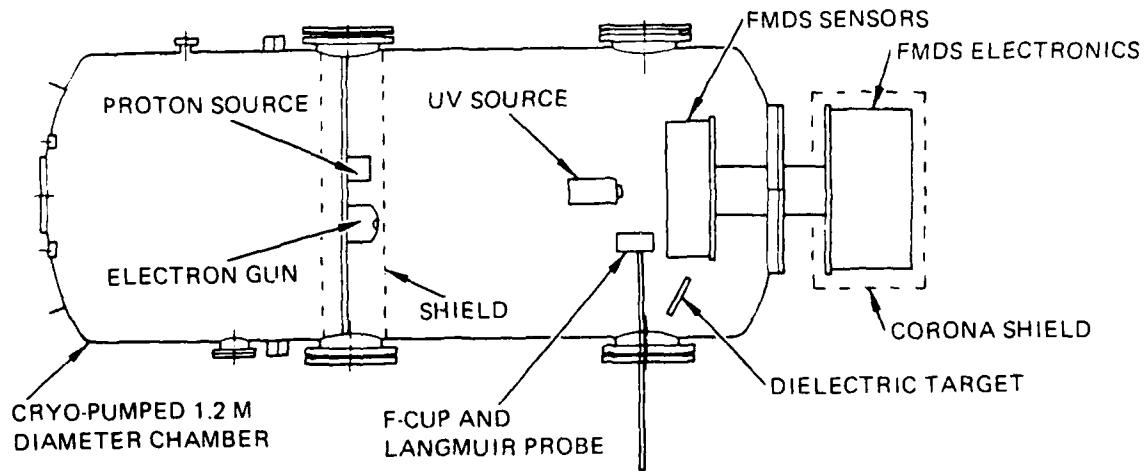
Figure 9 2. Test facility for testing the FMDS.

9.1 TEST SEQUENCES

The first demonstration of the FMDS breadboard consisted of the following sequence of events:

(1) Plasma source in operation

(2) Detection of protons by the ESA

(3) Single command turn-OFF and ullage fill of the plasma source

(4) Detection of differential charging by the SPM

(5) Simulation of spacecraft charging to -2.5 kV

(6) Single command turn-ON of the plasma source and discharge of the simulated spacecraft

(7) Turn-OFF of the plasma source and recharge of the simulated spacecraft.

The second demonstration consisted of the following sequence which demonstrated all of the FMDS capabilities.

1. Demonstration of plasma source

<1s ignition

Steady state emission current

Emission current during ignition

- Throttled operation

- Emission current at throttled setpoints.

2. Demonstration of ESA Operation

- Operation of sun sensor

Detection of ions

- Detection of electrons

- Ion ESA algorithm

Electron ESA algorithm.

3. Demonstration of SPM Operation

- Charge Kapton front surface with E-gun

- Turn ON UV source with e-gun ON; front surface discharges

- Resetting of the SPM using UV and grounding relay.

4. Demonstration of TPM Operation

- Inject pulses of known amplitude, polarity, width, and repetition rate; correlate with telemetry

- Produce arcs and detect with TPM

- Reverse antennas; TPM does not detect the arcs.

5. Demonstration of Controller

- Output telemetry

- Commands

- Setting of charging flags

- Masking of charging flags

- Change charging-flag threshold level

- Controller turn-ON of Plasma Source

- Controller turn-OFF of Plasma Source

- Manual control of Plasma Source.

6. Demonstration of System

- Plasma within 30 s of threshold level

- Charge entire FMDS; detect charging with ion-ESA; auto turn-ON of plasma source; FMDS discharge

- Detect high-energy electrons with electron ESA; auto turn-ON of plasma source; plasma source stays ON until high energy electrons disappear

- Charge the SPM; detect charging; auto turn-ON of plasma source; SPM discharge

9-3

- Generate arcs; detect arcs with TPM; auto turn-ON of plasma source; elimination of arcs

- Activate all sensors; see which one turns the plasma source ON.

9.2 DEMONSTRATION TEST RESULTS

The first demonstration was very short (30 min) and demonstrated the seven items listed above. This demonstration served to show the basic capabilities of the FMDS and the test facility.

The system was operated in an autonomous manner for the second demonstration to show that it can autonomously detect spacecraft charging and turn ON its plasma source to negate that charging. Many of the test results from this demonstration have been discussed previously in the sections on the individual instruments. The other significant results of this demonstration are discussed below.

The ion ESA and its algorithm were tested by charging the entire FMDS negatively with respect to facility ground (spacecraft frame charging) using the electron gun while protons were present in the chamber. The sharp increase in the proton spectra moved to higher energy channels as the FMDS charged more negative. When the peak moved past the threshold charging level as determined by the ion-ESA algorithm, the plasma source was automatically turned ON. Upon ignition of the plasma source, the FMDS potential immediately returned to facility ground potential.

The electron ESA and its algorithm were tested by increasing the energy of the electron beam until the sum of the counts in the two highest energy channels of the electron ESA exceeded the sum of the counts in the lower energy channels. This indicated that a charging environment was present; and the plasma source was automatically turned ON to prevent charging from occurring. The plasma source remained ON until after the simulated charging environment was removed and the plasma source preset ON time had expired. Both requirements had to be met before the plasma source would turn OFF.

The Kapton surface on the SPM was charged negatively (differential charging) using the electron beam and when the charging exceeded the threshold level the plasma source was automatically turned ON. The differential charge on the SPM was immediately removed and the SPM remained uncharged as long as the plasma source was ON. The UV source was also used to remove the charge from the SPM, indicating that the SPM could be re-zeroed during sunlight conditions. The UV source removed the charge with the electron gun ON or OFF.

The TPM was tested by charging Kapton surfaces inside the vacuum chamber using the electron beam until they arced to other surfaces or ground. The first arc was detected by the TPM and the plasma source was automatically turned ON. No further arcing was observed since the Kapton surfaces cannot charge with the plasma from the plasma source present. As discussed in Section 5, when the TPM antennas were reversed so that the internal antenna saw higher amplitude signals than the external antenna, the plasma source was not automatically turned ON.

The controller was tested by having it automatically control the FMDS as the other tests were being performed. The ability to mask instruments, change threshold levels, and manually control the plasma source by remote commands was also demonstrated during this testing.

The above tests were conducted with only one sensor activated at a time. Then all sensors were activated and the electron gun turned ON to see which sensor would respond fastest. With the FMDS system floating from facility ground, the ion ESA activated the plasma source as expected (spacecraft frame charging). With the FMDS floating, frame charging occurs much faster than differential charging; therefore, the SPM did not see a differential charge before the ESA activatd the plasma source. The SPM activated the plasma source (differential charging) when the FMDS system was connected to facility ground. Under these conditions the ESA never sees a shift in the ion spectra because

the FMDS frame cannot charge; however, differential charging does quickly occur, and therefore, the SPM activated the plasma source. In both cases there was not time for dielectric surfaces to charge to high enough potentials for arcs to occur, and therefore, the TPM did not activate the plasma source.

SECTION 10

CONCLUSIONS

The viability of the Flight Model Discharge System (FMDS) concept has been demonstrated by the successful fabrication and testing of a breadboard system. The testing revealed no hardware or software technology or scientific issues that will prevent the FMDS from achieving its ultimate goal of providing autonomous control of spacecraft charging.

REFERENCES

1. D.J. McComas and S.J. Bame, "Channel multiplier compatible materials and lifetime tests," Rev. of Scientific Instr. 55, No. 4, 463-467 (April 1984).

2. H. Rosenbauer, "Remarks on the qualification of continuous channel electron multipliers (CEMs) for use as detectors in long term space flight missions," (unpublished).

3. J.C. Sturman, "Development and design of three monitoring instruments for spacecraft charging," NASA Technical Paper 1800, 1981.

4. S.L. Spiegel and H.A. Cohen, "Real time, automatic vehicle potential determination from ESA measurements, Part 2: The distribution function algorithm," AFGL-TR-85-0103(II). ADA162072

5. R.C. Olsen, "A threshold effect for spacecraft charging," Jour. Geophy. Res. 88, No. A1, 493-499, (January 1, 1983).

APPENDIX A

FMDS COMMANDS AND TELEMETRY

The commands that can be sent to the FMDS by the ground support equipment or the spacecraft are as follows:

Command Number
(Hexadecimal)

Command 00 - Spare

Command 01 - Set Plasma Source Mode

       Enter Selection 1 to 6

       1.....Auto Mode

       2.....OFF Mode

       3.....ON Mode

       4.....Cathode Conditioning Mode

       5.....Manual Mode

       6.....Exit Routine

Command 02 - Set ESA CEM Gains

       Enter Lower Nybble - <O> To <F>

       Enter Upper Nybble - <O> To <F>

       Is The Above Data Correct <Y> or <N>

       Want To Exit <Y> or <N>

Command 03 - Set ESA Sweep Time

        Enter Selection 1 to 7

        1.....2-Second Sweep

        2.....4-Second Sweep

        3.....8-Second Sweep

        4....16-Second Sweep

        5.....Photo Diode Enable

        6.....Photo Diode Disable

        7.....Exit Routine

        Want Another Selection <Y> or <N>

Command 04 - Over Temperature Masks

        Enter Selection 1 to 6

        1.....Plasma Source Temperature Sensor #1

        2.....Plasma Source Temperature Sensor #2

        3.....ESA Electronics

        4.....TPM Electronics

        5.....

        6.....Exit Routine

        Enter <S> For Set or <C> For Clear

        Set/Clear Another Mask <Y> or <N>

Command 05 - Spare

Command 06 - Spare

Command 07 - Set Output Telemetry Start Byte

        Enter Number of Stack Pointer - <0> to <169>

Command 08 - Manual Valve Control

   Enter Selection 1 to 9

   1.....Main Power ON

   2.....Main Power OFF

   3.....Valve 1 ON

   4.....Valve 1 OFF

   5.....Valve 2 ON

   6.....Valve 2 OFF

   7.....Valve 3 ON

   8.....Valve 3 OFF

   9.....Exit Routine

   Want Another Selection <Y> or <N>

Command 09 - Manual Power-Relay Control

   Enter Selection 1 to 7

   1.....SPM ON

   2.....SPM OFF

   3.....ESA ON

   4.....ESA OFF

   5.....TPM ON

   6.....TPM OFF

   7.....Exit Routine

   Want Another Selection <Y> or <N>

Command OA - Plasma Source Manual Control

> Enter Selection 1 to 6
>
> > 1.....Discharge ON/OFF - <N> or <F>
> >
> > 2.....Cathode Heater ON/OFF - <N> or <F>
> >
> > 3.....Cathode Heater Setpoint - <O> to <3>
> >
> > 4.....Discharge Setpoint - <O> to <3>
> >
> > 5.....Keeper ON/OFF - <N> or <F>
> >
> > 6.....Exit Routine
>
> Make Another Change <Y> or <N>

Command OB - Set Emission-Current Limit

Command OC - Spare

Command OD - Set Cathode Heater Parameters

> Enter Selection 1 to 5
>
> > 1.....Enable Hardstart
> >
> > 2.....Disable Hardstart
> >
> > 3.....Set Heater Ignition Setpoint - <O> to <3>
> >
> > 4.....Set Heater Run Setpoint - <O> to <3>
> >
> > 5.....Exit Routine
>
> Want To Enable Run Setpoint During
>
> > Hardstart <Y> or <N>
>
> Want Another Selection <Y> or <N>

Command OE - Enable/Disable High-Pressure Valve Cycling

> Enter Selection 1 to 3
>
> > 1.....Valve Opened And Closed
> >
> > > For Each Source Operation
> >
> > 2.....Valve Unaffected During
> >
> > > Source Operation
> >
> > 3.....Exit Routine

Command OF - Set Plasma-Source Timeout

        Enter Selection 1 to 5

        1......5 min

        2.....10 min

        3.....30 min

        4.....60 min

        5.....Exit Routine

Command 10 - Set Charging Threshold

        Enter Selection 1 to 5

        1......200 V

        2......500 V

        3.....1000 V

        4.....2000 V

        5.....Exit Routine

Command 11 - Mask Instruments In Hazard Algorithm

        Enter Selection 1 to 6

        1.....Mask I ESA

        2.....Mask E ESA

        3.....Mask TPM

        4.....Mask SPM 1

        5.....Mask SPM 2

        6.....Exit Routine

        Want Another Selection <Y> or <N>

Command 12 - EEPROM Write: TPM

Command 13 - Eclipse Detect Enable/Disable

                Enter Selection 1 to 3

                ESA Triggers Plasma Source Whenever

                1.....Storm Imminent

                2.....Eclipse Only

                3.....Exit Routine

Command 14 - Clear Command Error

                Sending Clear Command

Command 15 - EEPROM Write: Master Microprocessor

Command 16 - Set TPM Parameters

                Want To Set The Threshold <Y> or <N>

                Enter <P> To Set Positive or <N> To Set Negative

                Enter TPM Threshold 0 to 255

                Want To Change Threshold Again <Y> or <N>

                Want To Set The Gain <Y> or <N>

                Enter <I> To Set Internal Or <E> To Set External

                Enter <H> To Set Gain High Or <L> To Set Gain Low

                Want To Change Gain Again <Y> or <N>

                Is The Above Data Correct <Y> or <N>

                Want To Exit <Y> or <N>

Command 17 - EEPROM Write: ESA Microprocessor

There are 170 telemetry bytes that are available from the FMDS. These telemetry bytes in the order they appear in the output telemetry stack are listed below:

Order In TLM
Stack (Decimal)

0	System Status Word
1	Charging Flag
2	Plasma-Source-On Flag
3	Plasma-Source Mode
4	Ion-ESA Vehicle Potential
5	Electron-ESA Charging Flag
6	SPM Range And Sun Sensor
7	SPM-1
8	SPM-2
9	TPM Positive Counts
10	TPM Negative counts
11	Emission Current
12	Last Command Byte
13	Discharge Voltage
14	Discharge Current
15	Keeper Voltage
16	Keeper Current
17	Cathode-Heater Voltage
18	Cathode-Heater Current
19	Pressure 1
20	Pressure 2
21	ESA Channel 0 Status Byte 1

22	ESA Channel 0 Status Byte 2
23	ESA Channel 0 Ion High Byte
24	ESA Channel 0 Ion Low Byte
25	ESA Channel 0 Electron High Byte
26	ESA Channel 0 Electron Low Byte
27	ESA Channel 1 Status Byte 1
28	ESA Channel 1 Status Byte 2
29	ESA Channel 1 Ion High Byte
30	ESA Channel 1 Ion Low Byte
31	ESA Channel 1 Electron High Byte
32	ESA Channel 1 Electron Low Byte
33	ESA Channel 2 Status Byte 1
34	ESA Channel 2 Status Byte 2
35	ESA Channel 2 Ion High Byte
36	ESA Channel 2 Ion Low Byte
37	ESA Channel 2 Electron High Byte
38	ESA Channel 2 Electron Low Byte
39	ESA Channel 3 Status Byte 1
40	ESA Channel 3 Status Byte 2
41	ESA Channel 3 Ion High Byte
42	ESA Channel 3 Ion Low Byte
43	ESA Channel 3 Electron High Byte
44	ESA Channel 3 Electron Low Byte
45	ESA Channel 4 Status Byte 1
46	ESA Channel 4 Status Byte 2
47	ESA Channel 4 Ion High Byte
48	ESA Channel 4 Ion Low Byte

49	ESA Channel 4 Electron High Byte
50	ESA Channel 4 Electron Low Byte
51	ESA Channel 5 Status Byte 1
52	ESA Channel 5 Status Byte 2
53	ESA Channel 5 Ion High Byte
54	ESA Channel 5 Ion Low Byte
55	ESA Channel 5 Electron High Byte
56	ESA Channel 5 Electron Low Byte
57	ESA Channel 6 Status Byte 1
58	ESA Channel 6 Status Byte 2
59	ESA Channel 6 Ion High Byte
60	ESA Channel 6 Ion Low Byte
61	ESA Channel 6 Electron High Byte
62	ESA Channel 6 Electron Low Byte
63	ESA Channel 7 Status Byte 1
64	ESA Channel 7 Status Byte 2
65	ESA Channel 7 Ion High Byte
66	ESA Channel 7 Ion Low Byte
67	ESA Channel 7 Electron High Byte
68	ESA Channel 7 Electron Low Byte
69	ESA Channel 8 Status Byte 1
70	ESA Channel 8 Status Byte 2
71	ESA Channel 8 Ion High Byte
72	ESA Channel 8 Ion Low Byte
73	ESA Channel 8 Electron High Byte
74	ESA Channel 8 Electron Low Byte
75	ESA Channel 9 Status Byte 1

76	ESA Channel 9 Status Byte 2
77	ESA Channel 9 Ion High Byte
78	ESA Channel 9 Ion Low Byte
79	ESA Channel 9 Electron High Byte
80	ESA Channel 9 Electron Low Byte
81	ESA Channel 10 Status Byte 1
82	ESA Channel 10 Status Byte 2
83	ESA Channel 10 Ion High Byte
84	ESA Channel 10 Ion Low Byte
85	ESA Channel 10 Electron High Byte
86	ESA Channel 10 Electron Low Byte
87	ESA Channel 11 Status Byte 1
88	ESA Channel 11 Status Byte 2
89	ESA Channel 11 Ion High Byte
90	ESA Channel 11 Ion Low Byte
91	ESA Channel 11 Electron High Byte
92	ESA Channel 11 Electron Low Byte
93	ESA Channel 12 Status Byte 1
94	ESA Channel 12 Status Byte 2
95	ESA Channel 12 Ion High Byte
96	ESA Channel 12 Ion Low Byte
97	ESA Channel 12 Electron High Byte
98	ESA Channel 12 Electron Low Byte
99	ESA Channel 13 Status Byte 1
100	ESA Channel 13 Status Byte 2
101	ESA Channel 13 Ion High Byte
102	ESA Channel 13 Ion Low Byte

103	ESA Channel 13 Electron High Byte
104	ESA Channel 13 Electron Low Byte
105	ESA Channel 14 Status Byte 1
106	ESA Channel 14 Status Byte 2
107	ESA Channel 14 Ion High Byte
108	ESA Channel 14 Ion Low Byte
109	ESA Channel 14 Electron High Byte
110	ESA Channel 14 Electron Low Byte
111	ESA Channel 15 Status Byte 1
112	ESA Channel 15 Status Byte 2
113	ESA Channel 15 Ion High Byte
114	ESA Channel 15 Ion Low Byte
115	ESA Channel 15 Electron High Byte
116	ESA Channel 15 Electron Low Byte
117	TPM - Amplitude Highest External Positive Pulse
118	TPM - Amplitude Highest External Negative Pulse
119	TPM - Width Highest External Positive Pulse
120	TPM - Width Highest External Negative Pulse
121	TPM - Amplitude Widest External Positive Pulse
122	TPM - Amplitude Widest External Negative Pulse
123	TPM - Width Widest External Positive Pulse
124	TPM - Width Widest External Negative Pulse
125	TPM - Amplitude Internal Pulse Corresponding 117
126	TPM - Amplitude Internal pulse Corresponding 118
127	TPM - Amplitude Internal Pulse Corresponding 121
128	TPM - Amplitude Internal Pulse Corresponding 122
129	TPM Relay Status

130	+28 V Power Input Voltage
131	+5 V Housekeeping Voltage
132	+12 V Housekeeping Voltage
133	+28 V Power Input Current
134	PPU Temperature 1
135	PPU Temperature 2
136	ESA +5 V Housekeeping Voltage
137	ESA +10 V Reference
138	ESA Electron-CEM Bias
139	ESA Ion-CEM Bias
140	ESA Temperature
141	ESA Sweep Voltage
142	ESA High Voltage (±50, ±300, ±500)
143	ESA +10 V Housekeeping Voltage
144	Ion Hazard Count Low Byte
145	Ion Hazard Count High Byte
146	Electron Hazard Count Low Byte
147	Electron Hazard Count High Byte
148	SPM 1 Hazard Count Low Byte
149	SPM 1 Hazard Count High Byte
150	SPM 2 Hazard Count Low Byte
151	SPM 2 Hazard Count High Byte
152	TPM Hazard Count Low Byte
153	TPM Hazard Count High Byte
154	Source Ignitions Low Byte
155	Source Ignitions High Byte
156	Bit Flip Count Low Byte

157	Bit Flip Count High Byte
158	Over Temperature Flag
159	Power Relay Status
160	Ion-ESA Caused Ignitions Low Byte
161	Ion-ESA Caused Ignitions High Byte
162	Electron-ESA Caused Ignitions Low Byte
163	Electron-ESA Caused Ignitions High Byte
164	SPM 1 Caused Ignitions Low Byte
165	SPM 1 Caused Ignitions High Byte
166	SPM 2 Caused Ignitions Low Byte
167	SPM 2 Caused Ignitions High Byte
168	TPM Caused Ignitions Low Byte
169	TPM Caused Ignitions High Byte

END
DTIC
8-86